R592 | 2019 – Frankfurt am Main

Engineering Guide

Engineering Guide for Assessment of Creep Crack Initiation on Components by Two-Criteria-Diagram

Engineering Guide

Engineering Guide for Assessment of Creep Crack Initiation on Components by Two-Criteria-Diagram

Engineering Guide

Engineering Guide for Assessment of Creep Crack Initiation on Components by Two-Criteria-Diagram

Authors: Dr. Jürgen Ewald [1]
Dr. Shilun Sheng [2]
Dipl.-Ing. Henning Almstedt [2]
Dr. Falk Müller [3]
Dr. Andreas Klenk [4]
Dr. Alfred Scholz [5]
Dr. Alexander Hobt [6]

[1] Independent Expert, formerly Siemens AG, Mülheim
[2] Siemens AG, Gas and Power, Mülheim/Ruhr
[3] Zentrum für Konstruktionswerkstoffe – State Materials Testing Institute Darmstadt (MPA) and Chair and Institute for Materials Technology (IfW), Technische Universität Darmstadt
[4] Materials Testing Institute (MPA), University Stuttgart
[5] formerly Zentrum für Konstruktionswerkstoffe – State Materials Testing Institute Darmstadt (MPA) and Chair and Institute for Materials Technology (IfW), Technische Universität Darmstadt
[6] formerly Materials Testing Institute (MPA), University Stuttgart

Preface

The engineering guide for assessment of crack initiation behavior at higher temperatures consists of following 3 parts:

- Part A - Influence of creep deformation capability on the tolerable defect size for components for which no creep crack initiation occurs,
- Part B - Description of crack initiation in creep ductile materials by Two-Criteria-Diagram (2CD),
- Part C - Consideration of the influence of the creep deformation capability on the shape of the Two-Criteria-Diagram.

In 1985 [1.1], [1.2] a Two-Criteria-Diagram (2CD) for assessment of creep crack initiation of pre-existing defects in creep ductile materials (i.e. no notch weakening materials) was proposed and the application of this 2CD for ferritic materials was proven meanwhile.

This diagram distinguishes between two main damage modes: Ligament damage (small initial defect sizes, dominant nominal stress in the ligament) and Crack tip damage (large initial defect size, low stresses in the ligament). If both damage modes have influence a mixed mode damage area was determined. In 1999 an extension of the 2CD for the consideration of slow load changes in addition to constant load was proposed [1.3], [1.4]. Subsequently in 2003 the influence of the creep deformation capability of the shape of the Two-Criteria–Diagram in the crack tip damage area was elaborated [1.5].

In recent time in the frame of a German research program [1.6] the expected influence of different creep deformation capabilities (uniform rupture elongations) in the Ligament damage area was proved and quantified. This means, that depending on the rupture ductility and the nominal stress in a component (for example nominal stress of 1 % strain in the far field of the defective component area) for distinct initial defect sizes, crack initiation does not occur. This makes a fracture mechanical approach unnecessary for these defects.

These newly developed results helped to better define the border lines for creep crack initiation of the 2CD in the area of the Ligament damage mode. The shape of the 2CD was adjusted and called now 2CD15.

Reference

[1.1] Ewald, J.; K.-H. Keienburg: A Two Criteria Diagram for creep crack initiation, Int. Conf. on Creep, Tokyo, pp. 173-178, 14-18 April (1986).

[1.2] Ewald, J.; K.-H. Keienburg, K. Maile: Estimation of manufacturing defects in the creep range. Nucl. Eng. and Design, Vol. 87, pp. 389/98 (1985).

[1.3] Ewald, J.; S. Sheng, A. Klenk, G. Schellenberg: Engineering guide to assessment of creep crack initiation on components by Two-Criteria-Diagram, 2. Int. HIDA Conf.-Stuttgart, 4-6 Oct. 2000, paper S5-2.

[1.4] Granacher, J., F. Müller, A. Klenk, G. Schellenberg, J. Ewald: Creep fatigue crack behaviour of two power plant steels, 2. Int. HIDA-Conference, Stuttgart, 4-6 Oct. 2000, paper S4-2.

[1.5] Ewald, J.: Zwei-Kriterien-Diagramm für Kriechrisseinleitung - Berücksichtigung des Kriechverformungsvermögens, 26. Vortragsveranstaltung "Langzeitverhalten warmfester Stähle und Hochtemperaturwerkstoffe" (AGW), VDEh, Düsseldorf 28.11.2003, Tagungsband, S. 87-97.

[1.6] Roos, E.; A. Hobt, A. Klenk, M. Oechsner, C. Berger, T. Mao, F. Müller, A. Scholz: Bewertung von Bauteilen mit Fehlstellen in Abhängigkeit vom Kriechverformungsvermögen, AVIF-Vorhaben A252, Abschlussbericht, FVV Frühjahrstagung, Tagungsband, Bad Neuenahr 2011.

Contents

1 Acknowledgement

The authors acknowledge to the input of all researchers from Institut für Werkstoffkunde (IfW, Institute for Materials Technology), Technische Universität Darmstadt, Head: Prof. Dr.-Ing. Christina Berger, resp. today Prof. Dr.-Ing. Matthias Oechsner and from Materialprüfungsanstalt (MPA, Materials Testing Institute), Universität Stuttgart, Head: Prof. Dr.-Ing. Eberhard Roos, resp. today Prof. Dr.-Ing. Stefan Weihe who performed and supported the research in the programs listed in Table 1.1.

These research studies were conducted since 1984. Hence the results of the booklet in hand is the summary of 30 years systematic research work of the German "High Temperature Creep-Crack-Behavior Group", W14, of the German "Forschungsvereinigung Warmfeste Stähle und Hochtemperaturwerkstoffe (FVWHT)". The authors appreciate the contribution of the members of the German working group W14 as well as the financial support of the research by "Forschungskuratorium Maschinenbau Frankfurt" (FKM), the "Forschungsvereinigung der Arbeitsgemeinschaft der Eisen und Metall verarbeitenden Industrie" ("Research Association of the Working Group of the Iron and Metal-Processing Industry", AVIF) and the "Arbeitsgemeinschaft industrieller Forschungsvereinigungen" ("German Federation of Industrial Research Associations", AiF).

Table 1.1: Research programs of the German High Temperature Crack Behaviour Group

Project No.	Project duration	Subject	Research institute/ person in charge	
			IfW Darmstadt	MPA Stuttgart
AiF 6038	1984 - 1988	Kriechrisseinleitung und Kriechrisswachstum warmfester Kraftwerksbaustähle unter Berücksichtigung des Größeneinflusses	R. Tscheuschner	W. Eckert
AiF 7251	1987 - 1992	Rissverhalten warmfester Kraftwerksbaustähle im Kriech- und Kriechermüdungsbereich	R. Tscheuschner	W. Eckert
AVIF A48	1991 - 1995	Anwendungsorientierte Auswertung von Kriechrissdaten an warmfester Stählen	T. S. Mao	J. Bareiß
AVIF A78	1994 - 1999	Kriechrissverhalten ausgewählter Kraftwerksstähle in erweitertem, praxisnahem Parameterbereich	J. Kostenko	G. Schellenberg
AiF 10395	1995 - 1999	Rissverhalten typischer warmfester Kraftwerksbaustähle im Kriechermüdungsbereich	M. Tramer	G. Schellenberg
AVIF A127	1998 - 2001	Hochtemperaturrissverhalten der neuen 600 °C-Stähle für Wellen und Gehäuse von Dampfturbinen	F. Müller	W. Stadtmüller
AiF 11722N	1998 - 2002	Einfluss inerter Atmosphäre auf das Rissverhalten warmfester Stähle im Kriech- und Kriechermüdungsbereich	F. Müller	G. Schellenberg
AiF 12308N	1999 - 2003	Rissverhalten von Nickelbasiswerkstoffen unter überlagerter Kriech- und Kriechermüdungsbeanspruchung	F. Müller B. Petrovski	M. Machalowska T. Gengenbach
AiF 12687N	2000 - 2003	Anwendbarkeit von Bruchmechanikkonzepten auf Kriechrisseinleitung und Kriechrisswachstum von niedriglegiertem Stahlguss im praxisrelevanten Beanspruchungsbereich	F. Müller	C. Weichert
AVIF A141	1999 - 2002	Berechnung von Risseinleitung und Rissfortschritt in Hochtemperaturbauteilen	T. S. Mao	T. Gengenbach

1 Acknowledgement

Project No.	Project duration	Subject	Research institute/ person in charge	
			IfW Darmstadt	MPA Stuttgart
AVIF A178	2002 - 2005	Kriech- und Kriechermüdungsrissverhalten moderner Kraftwerksstähle im Langzeitbereich	F. Müller	M. Machalowska
AVIF A202	2003 - 2004	Programmgestützte fortschrittliche Kriech- und Kriechermüdungsrissbeschreibung für typische langzeitbeanspruchte Kraftwerksbauteile	F. Müller	M. Machalowska
AiF 14609N	2006 - 2008	Absicherung von Konzepten zur Beschreibung des Rissverhaltens der Legierungen Inconel 706, Inconel 718 und IN-738 LC unter überlagerter Beanspruchung	F. Müller	M. Speicher
AiF 15626N	2008 - 2009	Rissverhalten von Nickelbasis-Gusslegierungen mit unterschiedlicher Kornstruktur	J.-M. Rudnig	M. Speicher
AVIF A252	2008 - 2010	Bewertung von Bauteilen mit Fehlstellen in Abhängigkeit vom Kriechverformungsvermögen	F. Müller, T. S. Mao	A. Hobt
AiF 17195N	2011 - 2013	Bewertung des Rissverhaltens von Fehlstellen hochtemperaturbeanspruchter Schaufeln aus Nickelbasis-Gusslegierungen	C. Baumann	M. Speicher C. Kohler
AVIF A277	2012 - 2015	Ermittlung des Einflusses von Spannungsgradienten auf das Kriech- und Kriechermüdungsrissverhalten	T. S. Mao	A. Hobt
AVIF A300	2016 - 2019	Bewertung von Fehlergrößen bei Schweißverbindungen in Kraftwerken unter flexibler Fahrweise	T. S. Mao	T. Bender
AiF 19226N	2016 - 2019	Simulation des Rissverhaltens von grobkörnigen Nickellegierungen bei hohen Temperaturen	L. Wöllmann	M. Speicher C. Kohler

2 Part A - Influence of creep deformation capability on the tolerable defect size for components for which no creep crack initiation occurs

2.1 Introduction

Experience has shown that materials with sufficient creep rupture ductility, A_u, can tolerate smaller defects without creep crack initiation over the lifetime in an else defect free component. Components of creep brittle material tolerate nearly no defects.

Usually the defect size in semi-finished products depends on the NDT tolerance levels. These levels were laid down on an empirical base and not on fracture mechanic considerations. Only in high loaded components (such as turbine rotors and casings) the tolerable defect size is elaborated on safety analysis.

Hence it was the aim of the research project "ductility" [2.1], to determine, depending on the rupture ductility, A_u, a limit depth of a defect, a_{th}, which does not initiate a creep crack for a required operating time under the component`s strain resp. stress in the far field.

The following suggestion had to be scrutinized: A fracture mechanic calculation can be renounced, if the (static) creep-crack-initiation time, t_i, is equal or longer than the time to reach 1 % creep strain, t_{p1}, in the undamaged far field (ligament) of a component[1], Figure 2.1.

$$t_i \geq t_{p1} \; . \tag{2.1}$$

The strain restriction in the far field (1 % for pressure containing components, or even 0.2 % or 0.5 % creep strain in (turbine) machinery parts) is related to usual design practice. Thus, limited by this creep loading, there exists a threshold value of defect size a_{th} for non-initiation during the operation time depending on the creep rupture ductility of the material.

The evaluations should result in a matrix which shows, depending on the materials rupture ductility, A_u:

- the tolerable threshold crack length a_{th},
- a belonging plastic limit length L_{pl}, resp. a technical stress distribution length, X,
- minimum width/ligament of the component, W-a.

2.2 Numerical Assessment Method

As explained above, creep crack initiation depends on the creep rupture ductility of the material. To determine the crack size threshold value a_{th} an approach based on FE-calculations (modified Garofalo equation by IfW Darmstadt resp. Graham-Walles by MPA-Stuttgart) has been carried out and the results have been compared with test data in creep range up to 30,000 h of different specimens [2.1].

The applied finite element model includes a detailed meshing of the crack tip area as shown in Figure 2.2 to account for the effect of creep ductility, an approach has been developed calculating the creep strain, $\varepsilon_{c,q_{min}}$, at the position of the maximum multi-axiality (q_{min}) as a characteristic point (see q_{min} in Figure 2.2). When this creep strain reaches the local creep deformation capacity, creep crack initiation is postulated.

The quotient q according to [2.2] is given by the ratio of von Mises equivalent stress σ_{vM} to hydrostatic stress σ_h

[1] Having reached the designated 1 % creep strain in the far field/ligament, a defect with just the tolerable threshold depth a_{th} has consumed the available creep deformation capacity of the material (maximum blunting, largest plastic zone, creep crack initiation) near crack tip.

$$q = \frac{\sigma_{vM}}{\sqrt{3}\cdot\sigma_h}. \qquad (2.2)$$

To consider the effect of multi-axiality, the calculated creep strain $\varepsilon_{c,q_{min}}$, is modified by the Cocks & Ashby factor [2.3] to determine an equivalent creep damage strain ε^*_{ref}. The parameter ε^*_{ref} is finally compared with data from uniaxial creep tests ε_{gl}. The value ε_{gl} is determined as the uniform (rupture) elongation from uniaxial creep tests. This strain must be used because the creep rupture ductility A_u is a specimen dependent strain value, which can only be used to compare the ductility of small size specimen to each other. Components of larger size can only be assessed by the uniform rupture ductility ε_{gl}, which is the only size independent uniaxial creep ductility value for small and large size bodies. The importance to use the uniform stress is recently summarized in [2.4].

The uniform rupture ductility of uniaxial test bars is estimated assuming constant volume according to Figure 2.3. The uniform rupture ductility is always smaller than the rupture ductility A_u, because it represents only the uniform elongation before upset of necking. Usually from creep tests only the rupture ductility A_u is reported. Therefore, a conversion diagram to demonstrate the relationship between uniform elongation ε_{gl} and creep rupture ductility A_u was created, Figure 2.4.

Another point which needs consideration when comparing the experimental data with the calculated crack initiation times deals with the crack initiation criteria, which was defined here as Δa_i = 0.1 mm. This is deviating from the normal procedure in Germany, where an "engineering crack initiation criterion" with Δa_i = 0.5 mm is preferably applied, which includes a certain (small) amount of crack growth. The consideration of the latter would have complicated the numerical evaluation.

The results of the calculation in Figure 2.5 support the presumption that cracks tend to grow when the reference strain at the position q_{min} has been reached. The calculated multi-axial reference strains of the specimen at this position for the time t_i are in the narrow scatter range of the uniaxial uniform elongation ε_{gl}, Figure 2.5. The analytically predicted reference strain at initiation time t_i for the tests is in good accordance with the curve for uniform strain.

Based on the above-mentioned method a_{th}-values for different times of 10,000 h, 30,000 h, 100,000 h, and 200,000 h corresponding to a given limited ligament creep strain of 0.2 %, 0.5 %, and 1.0 % can be determined by an iteration process as shown in Figure 2.6. The FE-calculations were mainly done at MPA-Stuttgart but they were supported by parallel FE computations at material 30CrMoNiV4-11/AMA and with a specific analytical method developed by IfW Darmstadt [2.1].

2.3 Materials

The investigation was carried out with the materials data of three earlier intensively investigated turbine steels. They have differing rupture elongations values and characteristics:

- 28CrMoNiV4-9/AGB, a brittle (due to special heat treatment) 1%CrMoV-steel with $A_{u,min} \approx 5$ % at 550 °C, Figure 2.7,
- 30CrMoNiV4-11/AMA, an as specified 1%CrMoV-steel with $A_{u,min} \approx 8$ % at 550 °C, Figure 2.8,
- X12CrMoWVNbN10-1-1/1A, a 10%Cr-steel at 600 °C, with continuous high creep rupture elongation, $A_{u,min} \approx 20$ %, Figure 2.9.

2.4 Results

2.4.1 Threshold Crack-Depth

Figure 2.10 shows the threshold crack depth a_{th} in dependence of creep rupture ductility A_u, resulting from the FE-calculations for material 30CrMoNiV4-11/AMA at 550 °C. The a_{th}-values decrease with time due to the time wise lowering rupture elongation. This is plausible, because blunting up to crack initiation and size of the plastic (stress redistribution) zone than become smaller.

Figure 2.11 shows a_{th}-values of all three materials with differing rupture ductilities A_u at typical ligament strain values of 0.2 %, 0.5 %, 1 %. In case of the brittle 1%CrMoV-steel, AGB, a measurable a_{th}-value could only be evaluated for a ligament strain of 0.8 %.

From these results it can be derived that the A_u-a_{th}-relationships of this evaluation are applicable for other ferritic/bainitic- and martensitic-steels with similar microstructure. Figure 2.11 includes three points with far field strain of 1 %, for which the increase of the a_{th}-value from Δa_i = 0.1 mm to Δa_i = 0.5 mm can be seen. This shows the conservatism of the evaluated a_{th}-values based on Δa_i = 0.1 mm. The threshold values for Δa_i = 0.5 mm lie in the range of the larger a_{th}-values for 0.5 % far field strain.

2.4.2 Plastic limit length, stress distribution length

Plastic limit length und stress redistribution zone both are distances behind the crack tip. The plastic limit length L_{pl} at the time of crack initiation is derived from the calculated point of intersection of the redistributed primary stress with the rupture stress, see Figure 2.12. The plastic limit length L_{pl} contains twice the intersection radius r_{pl}: $L_{pl} = 2\cdot(r_{pl} - r_{plo})$, where $2\cdot r_{plo}$ is the elastic portion of the limit length. As shown in Figure 2.13 the limit length increases with enlarging rupture elongation. This result was expected from considerations.

The plastic limit length gives an idea how deep the zone of intense stress redistribution behind the crack tip is. But from Figure 2.12 it derives that the inhomogeneous stress behind the crack tip needs larger distance to subside to the level of the gross nominal stress in the far field. This distance can be nominated as technical stress distribution length X. This understanding is important for components with smaller wall thickness, for they need a minimum load carrying width W. In this case X must be always smaller than W-a:

$$X < W\text{-}a \; . \tag{2.3}$$

The values for X were estimated to

$$X = 0.5\cdot A_u \tag{2.4}$$

with X in mm, A_u in % and are shown also in Figure 2.13. (The estimation is based on evaluations of round, notched specimens with different notch depth and diameters from materials with different rupture elongations [2.5].)

2.4.3 Gross nominal stress in the far field and von Mises equivalent stress near far field

The prior defined criteria (2.1) for the determination of the threshold crack length used the nominal (net) stress within the ligament and not the components gross nominal stress in the far field. This is no problem in case of large scale components, because the a_{th}-values are not too big. But according to Figure 2.14 there is a certain increase of the gross nominal stress within the stress distribution length X, which must carry the free cut load of the crack plane.

To estimate, whether this must be taken into consideration, the mean von Mises equivalent stress (mean σ_{vM}) of the multi-axial constraint-situation in the limit length L_{pl} (Figure 2.13) was compared with the belonging gross nominal stress σ_n in the far field. A few calculations for

validation purposes on DENT specimen (a_{th} ≈ 0.5 mm on 30CrMoNiV4-11/AMA, a_{th} ≈ 0.9 mm for X12CrMoWVNbN10-1-1/1A) gave similar stress levels, $\sigma_n \approx \sigma_{vMmean}$, so this needs no special consideration.

2.5 Recommended values / relationships for practical application

Table 2.1 and Figure 2.11 contain the summarized results of the FE-calculations of this research program [2.1] at different DENT-specimen. According to Figure 2.11 the a_{th}-values for 1 % ligament/far field strain (based on Δa_i = 0.1 mm) are relatively low. Under consideration that the available long-term data for crack initiation are based on the Δa_i = 0.5 mm initiation criteria, the use of the values from Table 2.1 and Figure 2.11 would be relatively conservative. Moreover, the calculated a_{th}-values for Δa_i = 0.5 mm and 1 % ligament strain were larger and had nearly the size of values with 0.5 % ligament strain, see Figure 2.11 and Figure 2.15. Therefore, it is proposed to apply an empirically fixed mean crack initiation threshold value for 1 % ligament strain as:

$$\bar{a}_{th} = 0.1 \cdot A_u \tag{2.5}$$

with $\bar{a}_{th}$ in mm and A_u in %.

This newly defined mean value covers the calculated data points and lies just below the a_{th} curve for 0.5 % ligament strain. The a_{th}-curves for 0.5 % and 0.2 % ligament strain allow no change/improvement, because the number of calculations is scars und the creep data on which the calculation is based are far wider extrapolated than for 1 % creep strain.

Table 2.2 summarizes for 1 % far field strain the relationships laid down between the rupture elongation A_u and

- the mean $\bar{a}_{th}$ values for 1 % ligament strain as
  $\bar{a}_{th} = 0.1 \cdot A_u$ for A_u = 5 % - 20 %, > 20 % -> const.
- the technical stress distribution length X, as
  $X = 0.5 \cdot A_u$ for A_u = 5 % - 20 %, > 20 % -> const.
- the width of the minimum wall thickness resp. ligament width (W) behind a crack tip, (W-a) ≥ X.

Another condition is a minimum total wall thickness: W_{min} ≥ 15 mm. This condition assures a certain lateral constraint at the crack tip and a sufficient ligament width (W-a) for 1 % far field strain.

a_{th}-values for 0.2 % and 0.5 % far field strain must be taken from Figure 2.15. Moreover, it should be pointed out, that all calculations were carried out on DENT specimen of different size and shape (W = 6 mm - 80 mm; B = 9 mm - 60 mm; a/W ≈ 0.01 - 0.3, a_o = 0.3 mm - 6 mm). For small cracks in round surface grooves the a_{th}-values cannot be applied. Such situations should be evaluated with the Two-Criteria-Diagram for crack initiation, see Part B.

2.6 Note

- Often the course of the creep rupture ductility vs. the time is not constant, but decreases, in these cases the lowest values must be used.

- The results from this research project were evaluated for pure static loading conditions. But from a research project[2] [2.6] and own consideration it can be postulated, that for creep ductile materials (A_u >≈ 8 %) slow load changes (t_h >≈ 0.35 h) indicate no cyclic crack growth.

2.7 Conclusions - Part A

The postulated dependence of creep rupture ductility A_u (which means basically dependent on the uniform rupture elongation) to the tolerable crack initiation threshold depth a_{th} was numerically quantified for DENT specimen. This means that depending on the height of the far field strain ε_{lig} and the creep rupture ductility A_u, there exist tolerable time independent defect sizes which do not initiate creep cracking. In case of other loading/size situations the tolerable DENT-specific a_{th}-values must be transformed to the other shapes and sizes.

This can be done in the following way: The a_{th}-values in Table 2.2 are valid for DENT-specimen, which together with its far field stress σ_n have a certain $K_{I\,id}/\sigma_n$-ratio, which points it in the "no crack area" of the Two-Criteria-Diagram (see Part B). A component with the same far field stress but different crack shape must have a $K_{I\,id}$-value, which leads to the same $K_{I\,id}/\sigma_n$-ratio and thus to the same position within the no crack area of the Two-Criteria Diagram[3].

Such tolerable defect sizes in creep ductile material (no notch weakening, A_u ≈> 8 % materials) are larger than normal non-metallic inclusions [2.4] and - in accordance with our experience - obviously of most of the UT-tolerance levels of semi products. To know whether such UT-tolerance levels are too conservative more specific evaluations are needed.

[2] D15-specimen from 30CrMoNiV4-11/AMA with crack depth of ≈ 1.5 mm and hold/shut down time of 0.32 h and 3.2 h showed no crack initiation until reaching the static 1 % creep strain limit with their upper stress (test duration ≈ 1,000 h).

[3] See in detail Part B: $K_{I\,id}$ is the fictitious elastic initial stress intensity, which for a far field stress $R_{p1/t/T}$ is $K_{I\,id} = R_{p1/t/T}\cdot\sqrt{\pi\cdot a}\cdot y$, for DENT -> y=1.122 (nearly independent of a/W) -> $K_{I\,id}/R_{p1} = \sqrt{\pi\cdot a}\cdot y$ -> a_{th} varies with y of another geometrical situation.

2.8 References - Part A

[2.1] Roos, E.; A. Hobt, A. Klenk, M. Oechsner, C. Berger, T. Mao, F. Müller, A. Scholz: Bewertung von Bauteilen mit Fehlstellen in Abhängigkeit vom Kriechverformungsvermögen, AVIF-Vorhaben A 252, Abschlussbericht FVV Frühjahrstagung Bad Neuenahr 2011.

[2.2] Clausmeyer, H.; K. Kußmaul, E. Roos: Influence of Stress State on the failure behaviour of cracked components made of steel, Appl. Mech. Rev. Vol. 44, 2nd February 1991 ASME.

[2.3] Cocks, A.; F. Ashby: Intergranular fracture during power-law creep under multiaxial stress, Metal Science, 395-401, 1980.

[2.4] Ewald, J.; T.-U. Kern: The role of the Material Parameter "Uniform Elongation"; 4th Int. ECCC Conference, Sept 10-14, 2017.

[2.5] Berger, C.; J. Granacher, T. Mao: Vergleichende Ermittlung des Zeitstandverhaltens bauteilähnlicher Rundkerbproben, Forschungsvorhaben DFG KI 300/54-1 und 2, Schlussbericht, Inst. f. Werkstoffkunde, TU-Darmstadt, 26.02.1999.

[2.6] Schellenberg, G.: Diss. MPA-Stuttgart, Techn.-wiss. Bericht, Heft 03-1 (2003): Beschreibung des Risswachstumsverhaltens von warmfesten Stählen unter Kriechermüdungsbeanspruchung.

2.9 Tables and figures - Part A

Table 2.1: Summary of results from Figure 2.11

Material	**Creep rupture ductility A_u**	**ε_{lig} = 1 %**		**ε_{lig} = 0.5 %**	**ε_{lig} = 1 % a_{th} / mm**
		a_{th} / mm	**$2(r_{pl}-r_{pl0})$ / mm**	**a_{th} / mm**	**Δa_i = 0.5 mm**
AGB/1%CrMoV	≈ 5 %	0.3*)	≈ 1*)	0.7	0.9
AMA/1%CrMoV	≈ 8 %	0.4	1.5	2	1.5
	≈ 12 %	0.5	2	2.5	-
	≈ 15 %	0.8	3	3	-
1A/10%CrMoWV	≈ 20 - 25%	1	4	3.5	3.3
	Δa_i = 0.1 mm				Δa_i = 0.5 mm

*) ε_{lig} = 0.8 % due to low A_u-values

Table 2.2: Recommended values for practical application to avoid creep crack initiation

Values for application (low alloyed ferritic steels and 10-12 % CrMo(W)V-steels, at 500 °C - 600 °C) (a_{th} evaluated with DENT-specimen with large ligament W, see section 2.5)			
Creep rupture elongation A_u	Crack threshold to avoid CCI a_{th} / mm	redistribution length X / mm	Boundary conditions
			ligament strain 1 %
5 – 20 %	$\bar{a}_{th} = 0.1 \cdot A_u$	X = 0.5 A_u	min. ligament width: W-a > X
> 20 %	$\bar{a}_{th}$ = 2 mm	X = 10 mm	mean wall thickness: W = s ≥ 15 mm,
	Fig. 2.15	Fig. 2.13	Surface notches with small radii r /mm and additional small cracks with depth a_{th} must be valued with the 2CD15 with $K_{Iid} = f(r+ a_{th})$

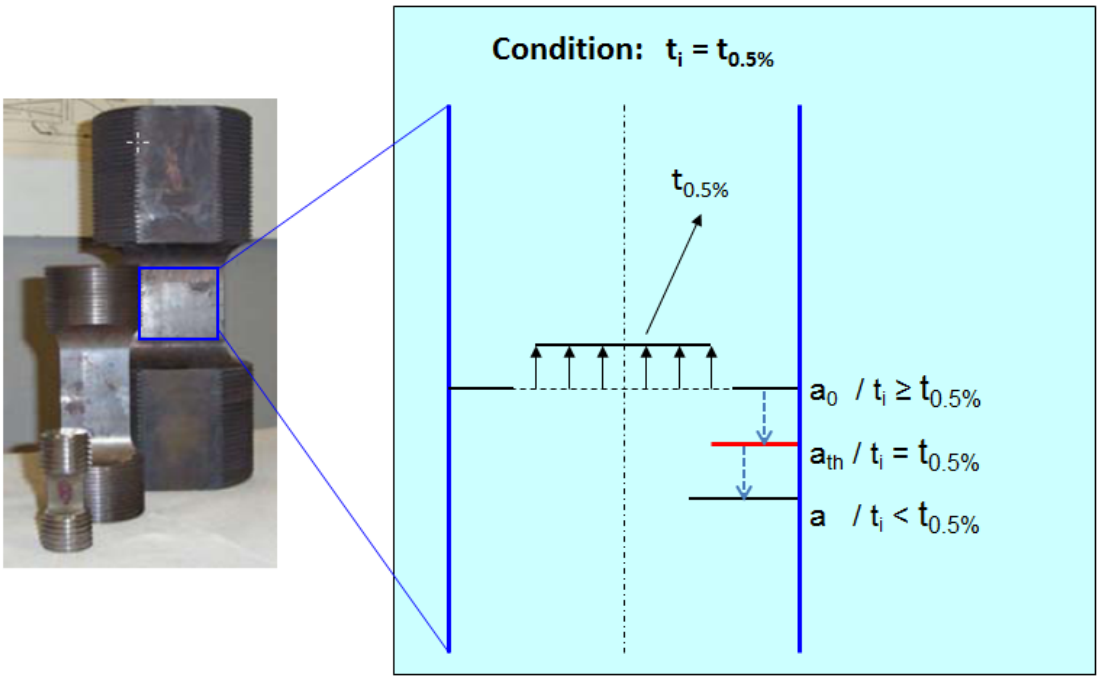

Figure 2.1: Definition of a_{th} for DENT specimen values to avoid creep crack initiation (ε_{lig} = 0.5% → $t_{0.5\%}$)

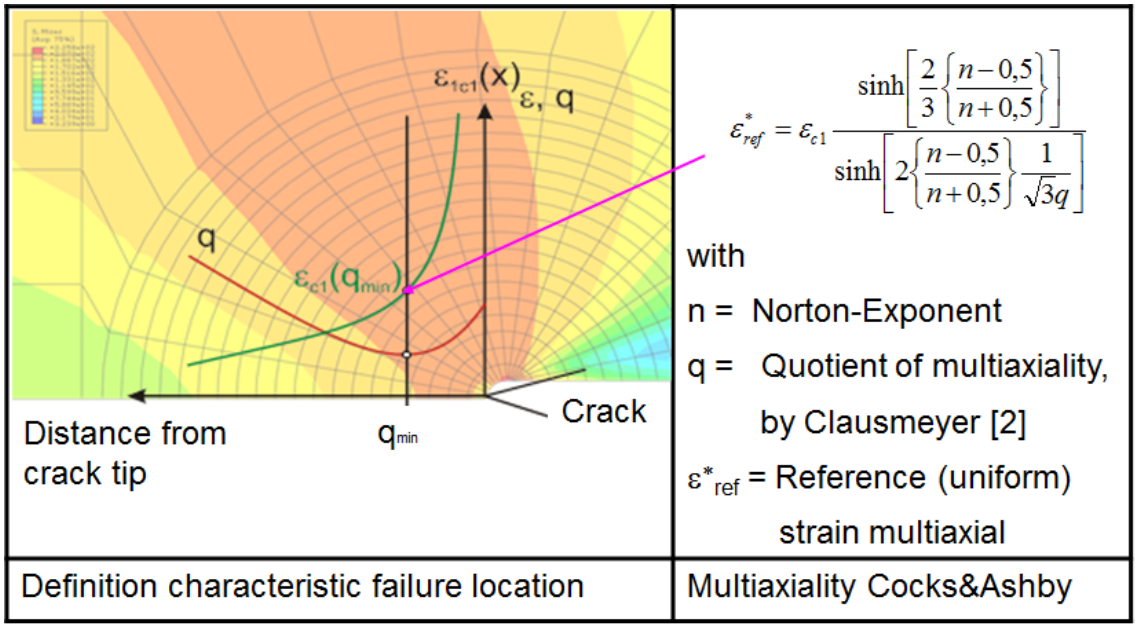

Figure 2.2: Definition of crack initiation criteria

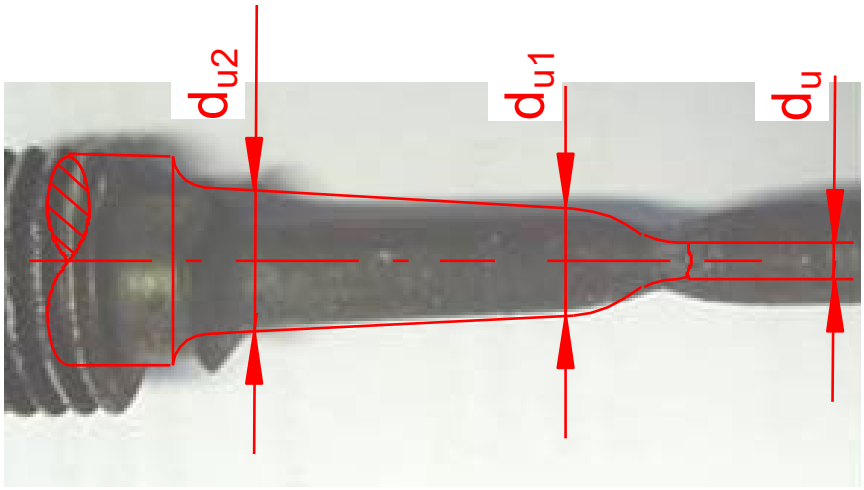

$$\varepsilon_{gl} = \left[\frac{d_o}{(d_{u1}+d_{u2})/2}\right]^2 - 1$$

Figure 2.3: Determination of uniform creep strain for uniaxial tests

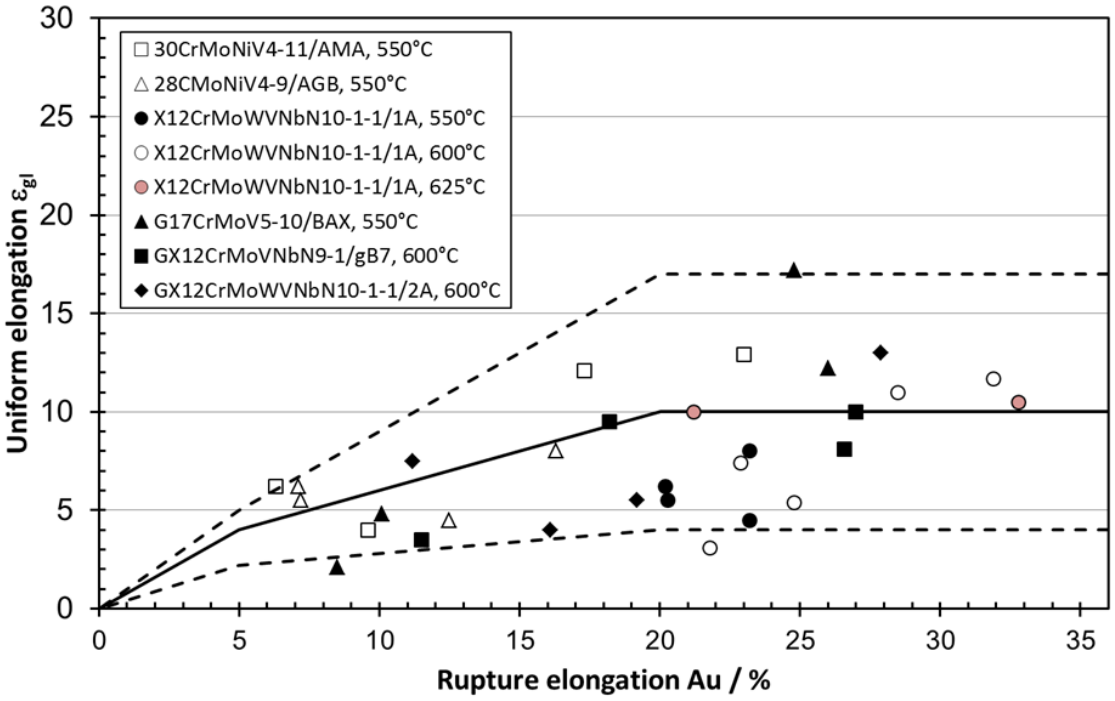

Figure 2.4: Relationship of uniform vs. rupture elongation ($l = 5 \cdot d_o$)

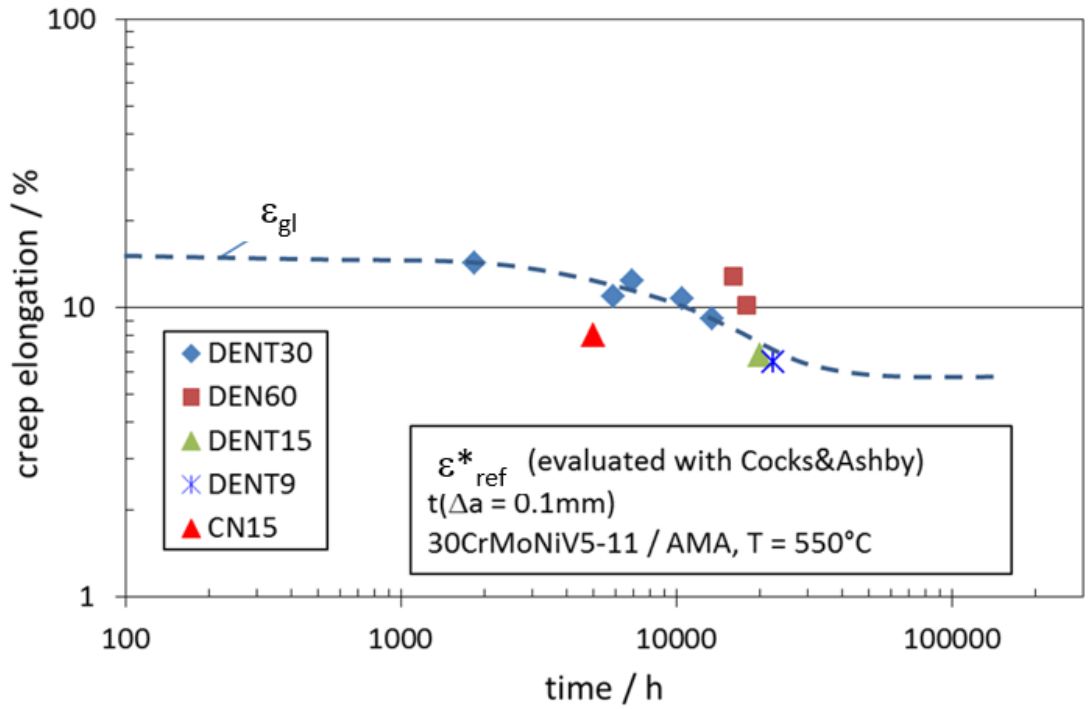

Figure 2.5: Assessment of creep strain ε^*_{ref} at q_{min} of experimental, data at unset of creep crack initiation (Δa_i = 0.1 mm), compared with uniform elongation ε_{gl} of the material 30CrMoNiV4-11/AMA, T = 550 °C

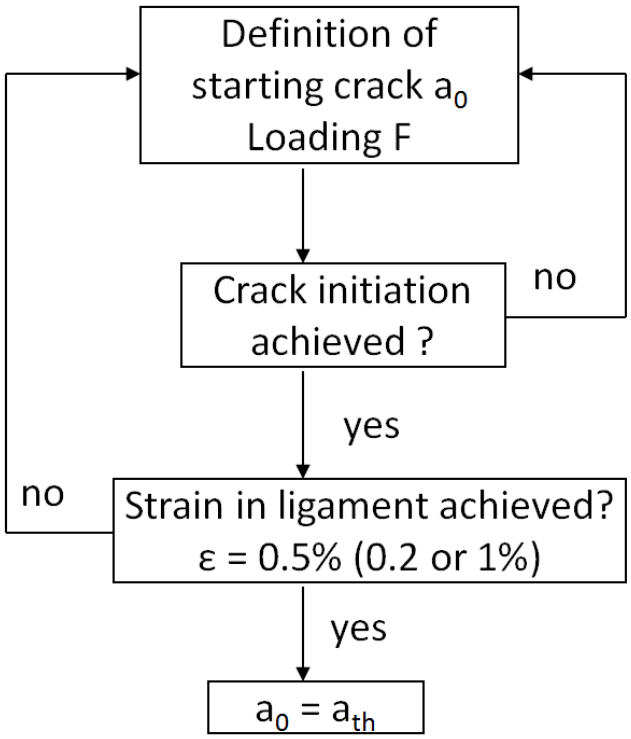

Figure 2.6: Iteration for determination of a_{th}

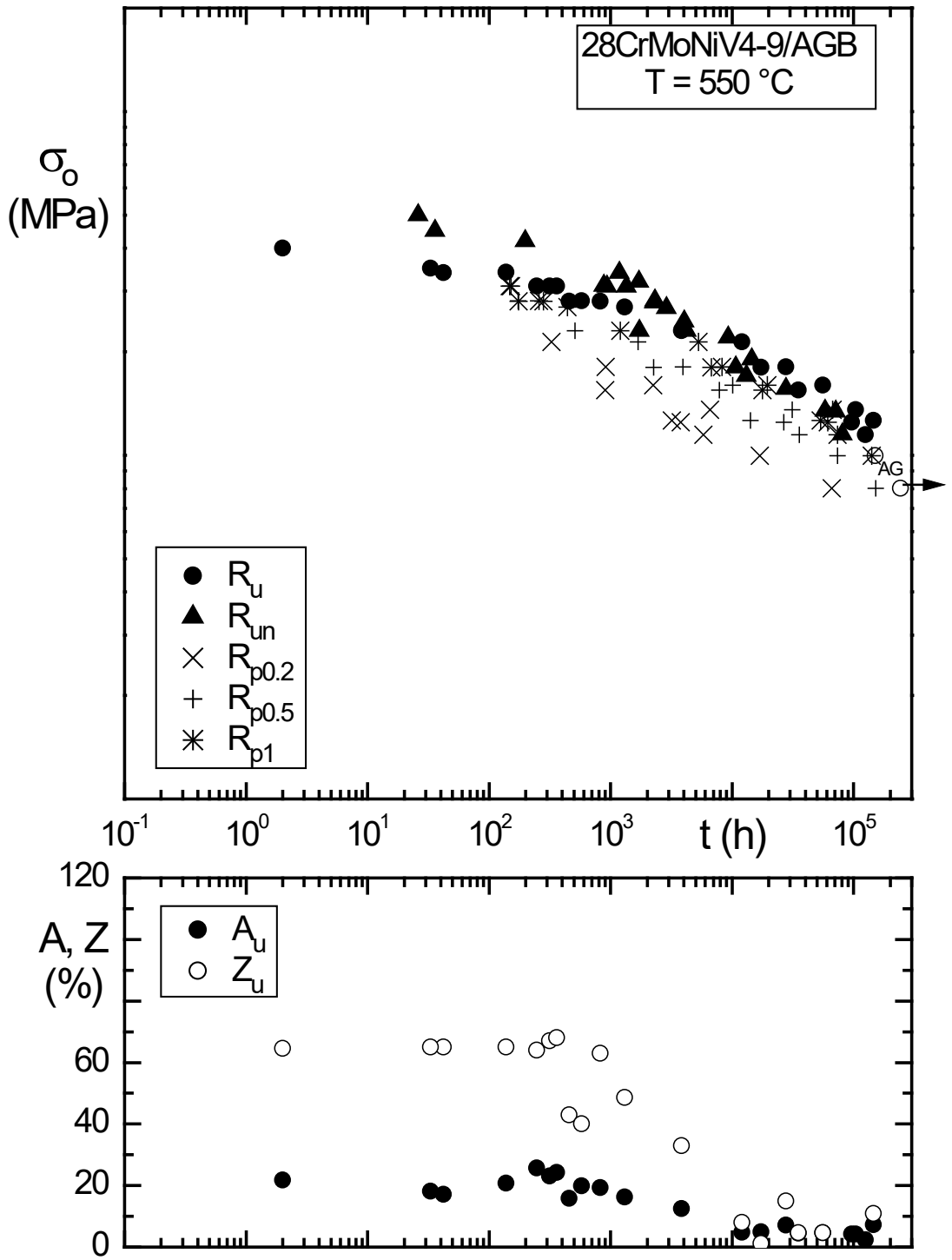

Figure 2.7: Creep rupture properties, 28CrMoNiV4-9/AGB, T = 550 °C

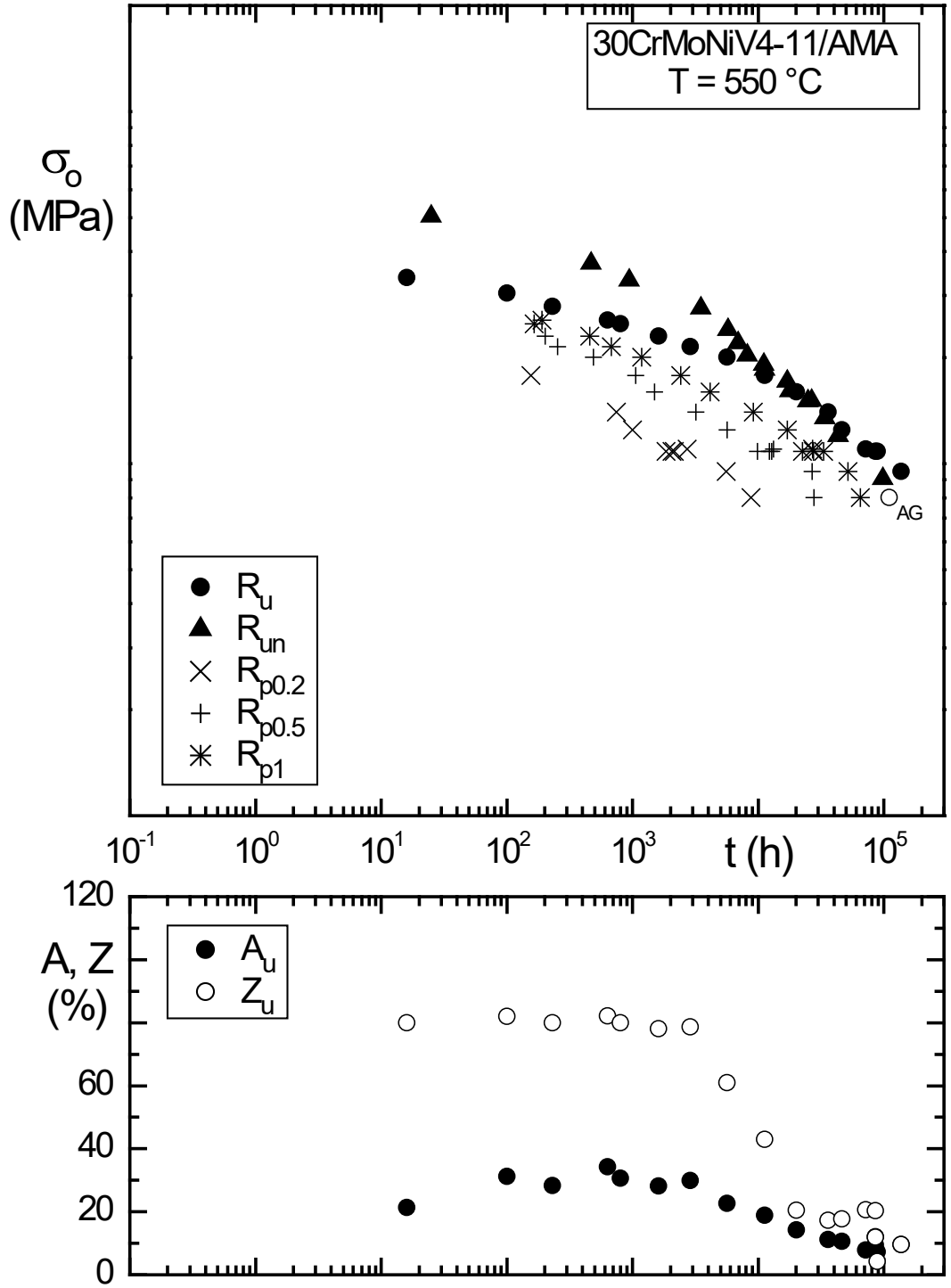

Figure 2.8: Creep rupture properties, 30CrMoNiV4-11/AMA, T = 550 °C

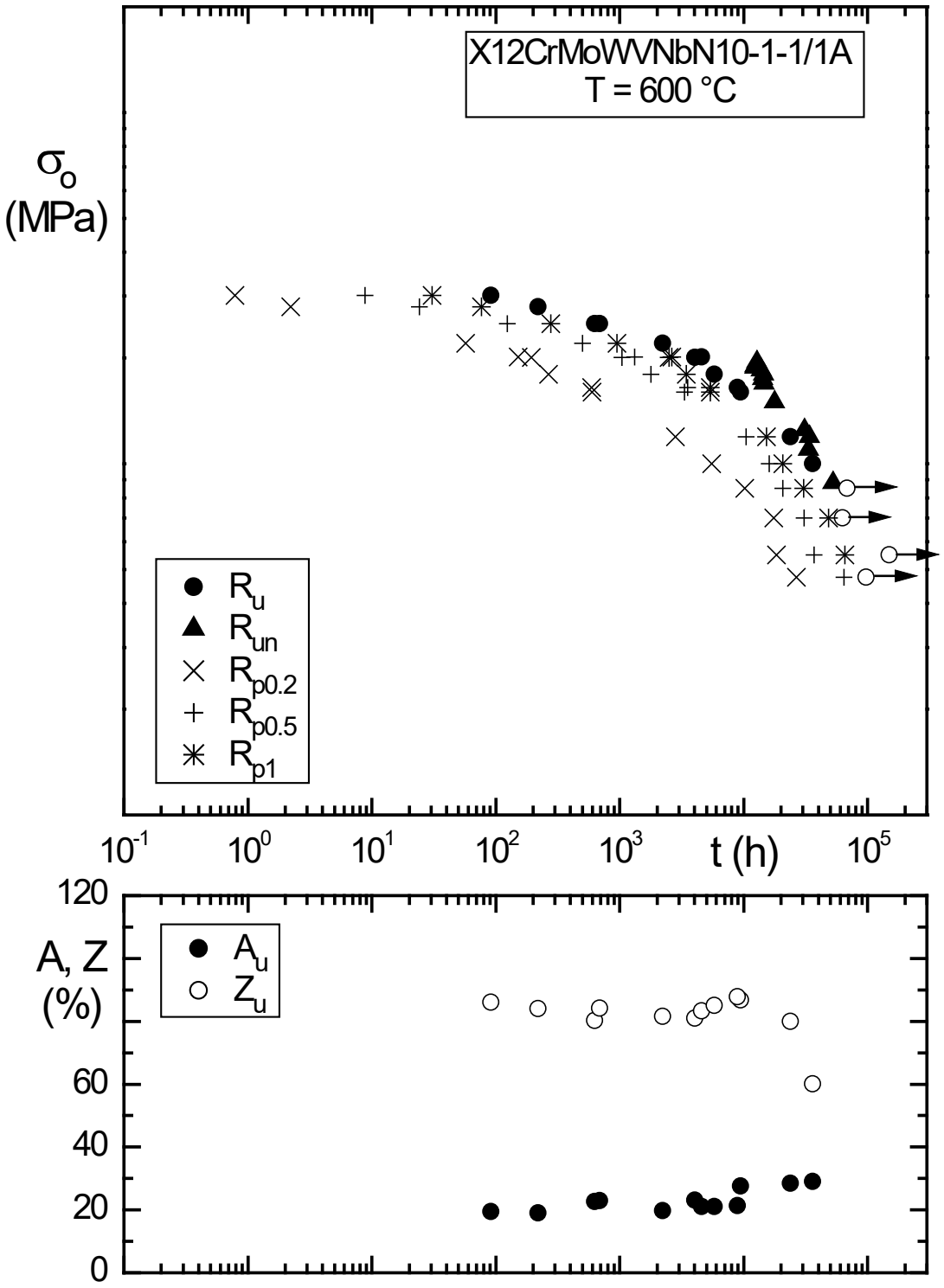

Figure 2.9: Creep rupture properties, X12CrMoWVNbN10-1-1/1A, T = 600 °C

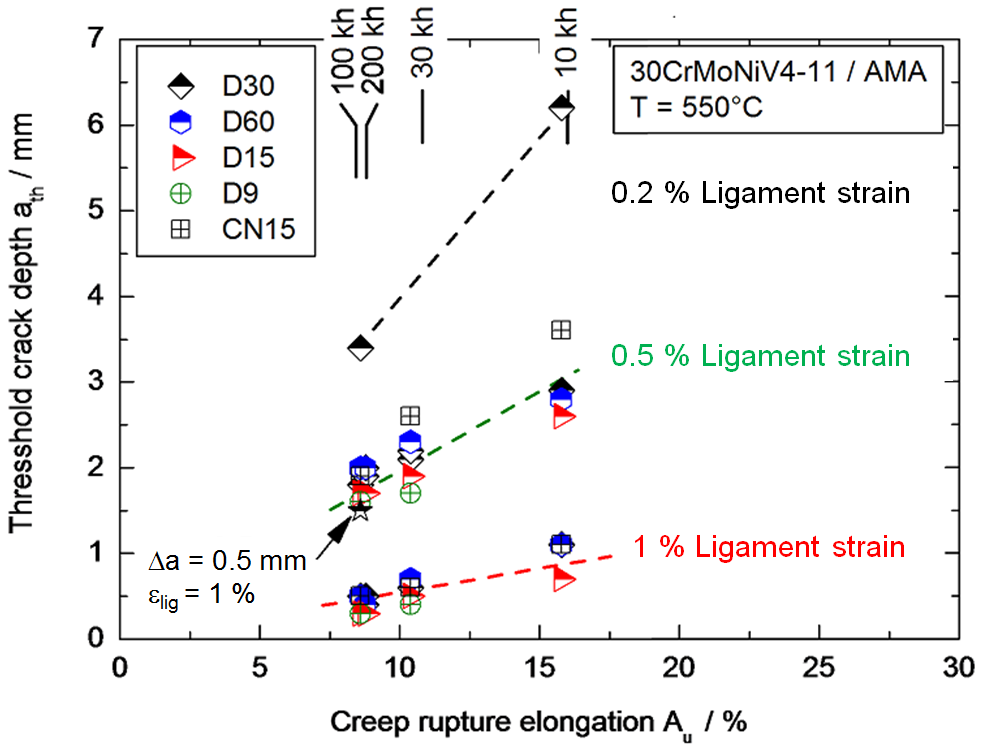

Figure 2.10: Crack initiation size a_{th} in dependence on rupture elongation A_u of 30CrMoNiV4-11/AMA, T = 550 °C

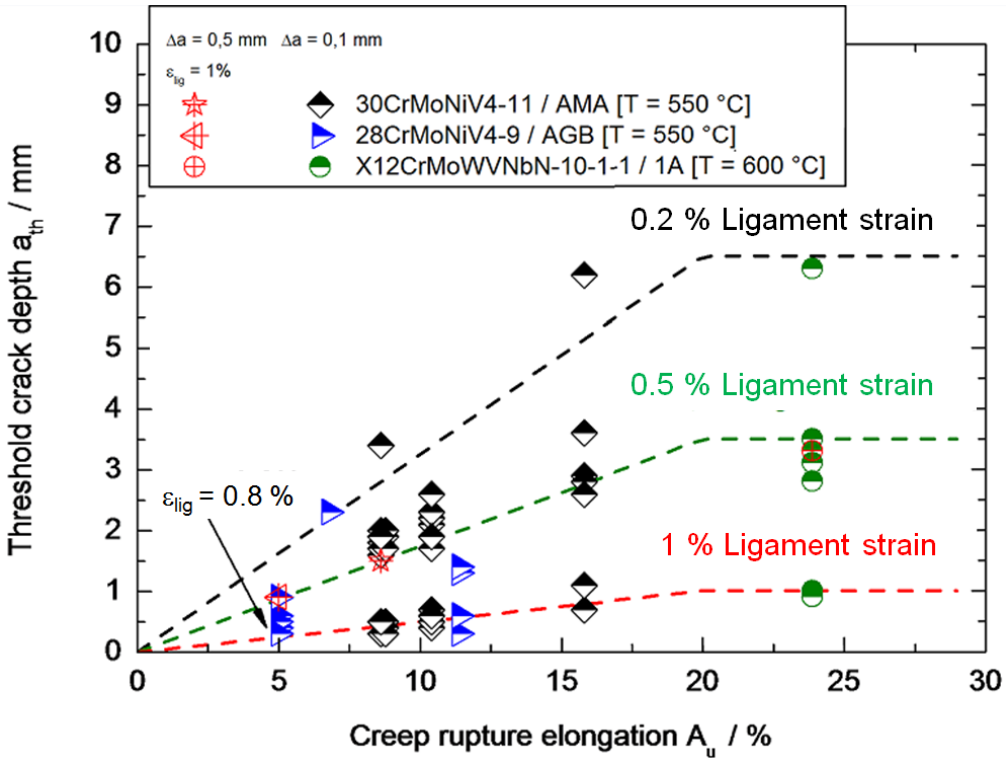

Figure 2.11: Creep crack initiation size a_{th} in dependence on rupture elongation, Δa_i = 0.1 mm and 0.5 mm

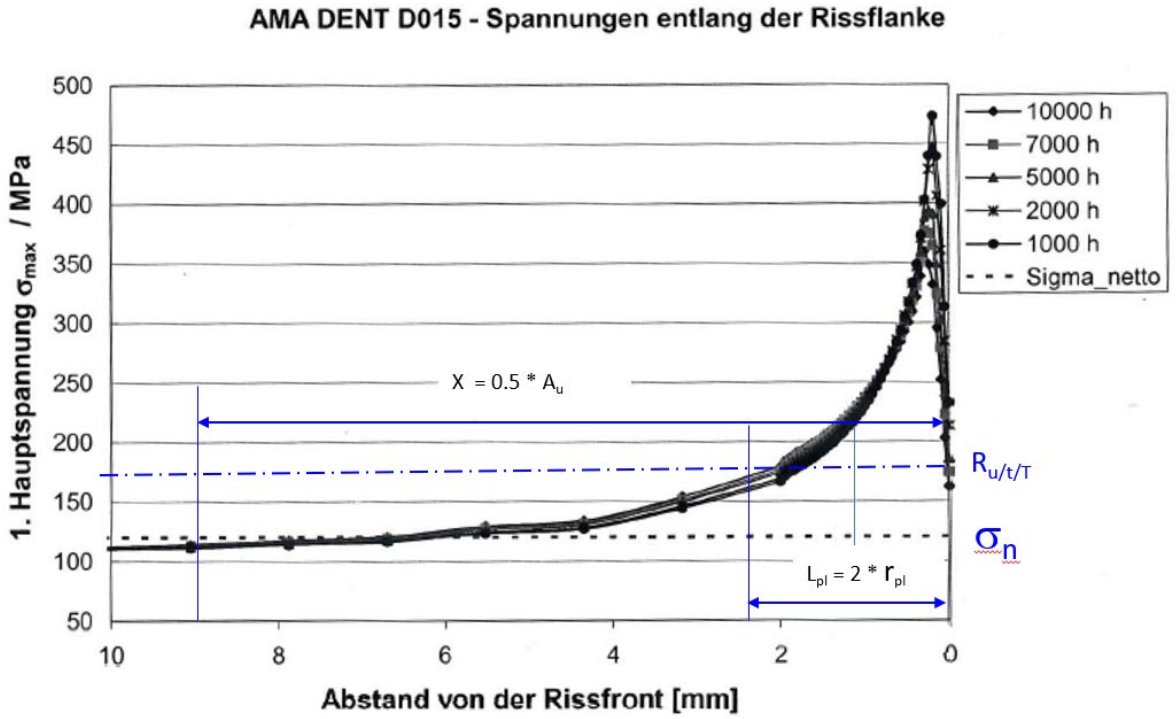

Figure 2.12: Determination of limit length, $L_{pl} = 2 \cdot r_{pl}$ from intersection of primary stress σ_1 with rupture stress $R_{u/t/T}$, both at crack initiation time t_i, and techn. stress redistribution length $X = 0.5 \cdot A_u$ (DENT)

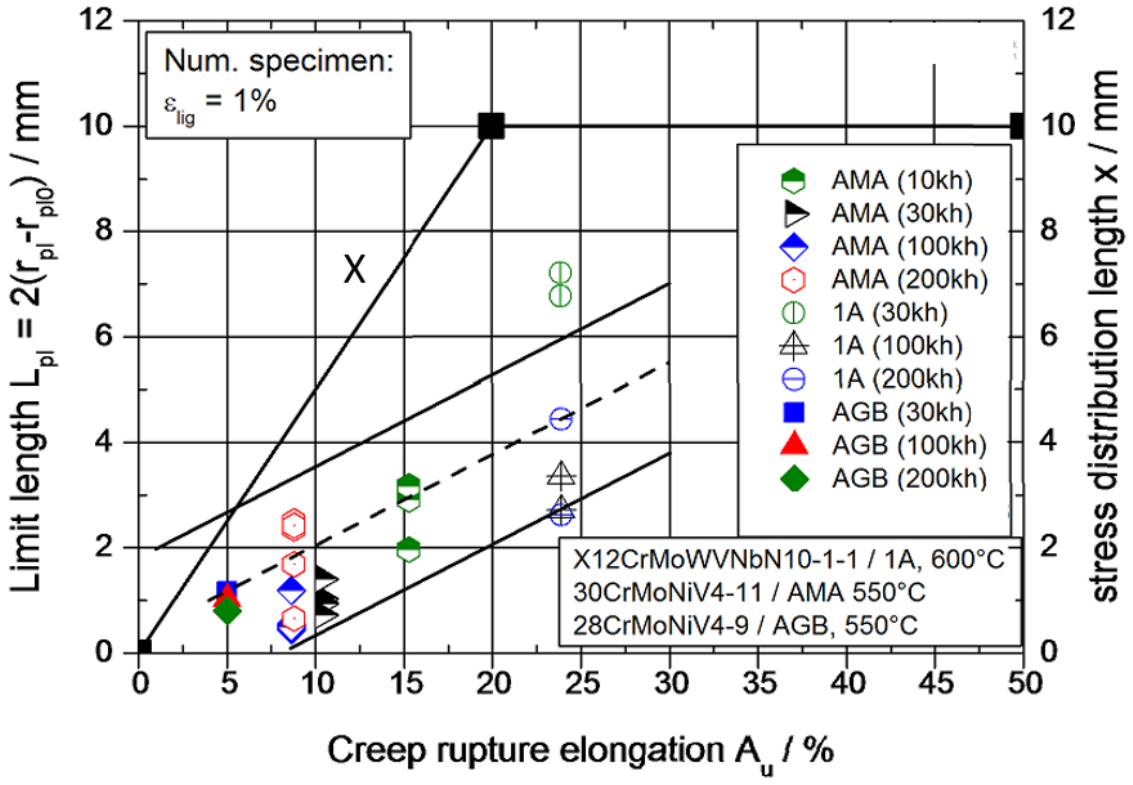

Figure 2.13: Limit length L_{pl} and stress redistribution length X for 1 % ligament strain (DENT specimen)

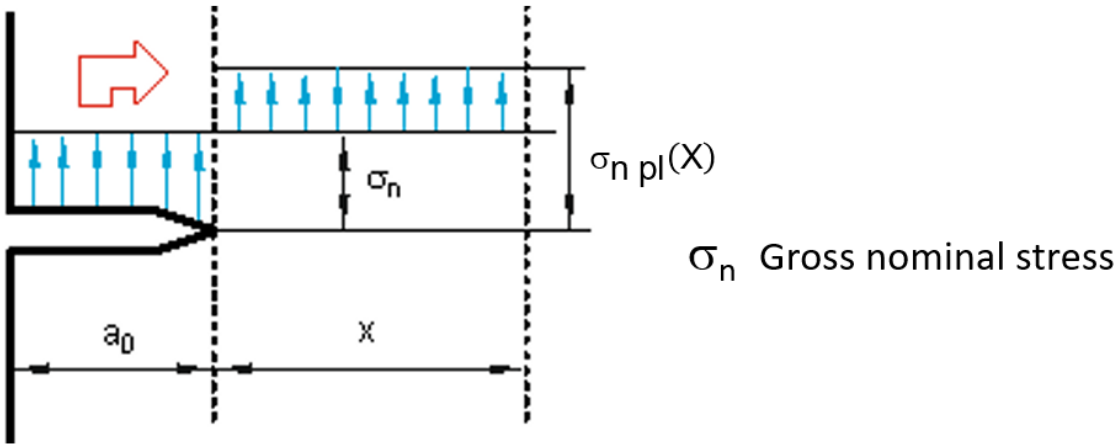

$\sigma_{n\,pl}(X) = (1 + a_o/X)\cdot\sigma_n$, nominal stress within the stress distribution length X

Figure 2.14: Evaluation of net section stress within the stress distribution length X

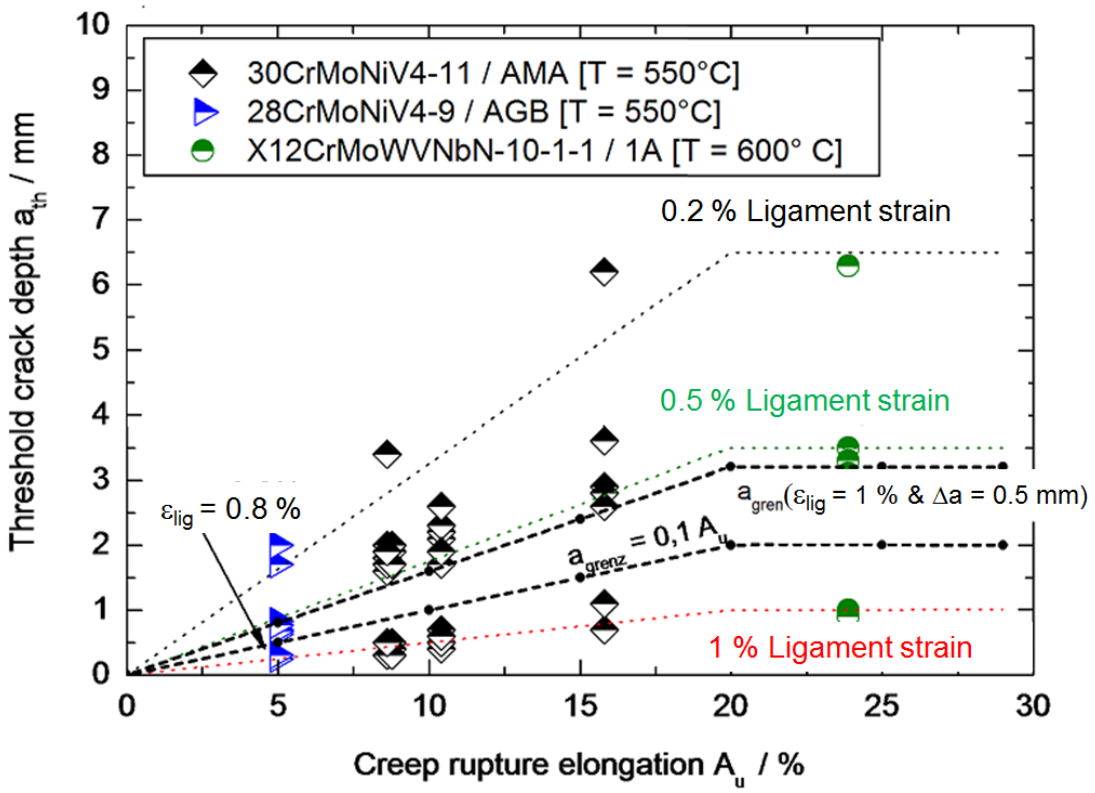

Figure 2.15: Crack size threshold a_{th} to avoid creep crack initiation in dependence on creep rupture elongation

3 Part B - Description of Crack initiation in creep ductile materials by Two-Criteria-Diagram (2CD)

3.1 Introduction

On the application of a steady load to a pre-cracked structure (not service induced defect) at high temperature, creep crack initiation occurs at about 40 - 60 % of total life [3.1], [3.6], [3.12]. In this case the remaining ligament can no longer support the applied load without crack initiation. Practically, initiation time is very dependent on the increment of crack extension Δa adopted for the definition of crack initiation. In contrast to a physical interpretation, which is based on cavity coalescence and formation of grain boundary microcracks, a more engineering view will be highlighted here. The use of an engineering-size initial crack with Δa_i = 0.5 mm is of relatively common practice in Germany [3.1], [3.8], [3.12], [3.13]. Besides this definition formerly a size dependent crack initiation length was considered as more suitable to assess the initiation time for a variety of different specimens and components. In Refs. [3.6], [3.11], [3.16], [3.17] $\Delta a_i = 0.004 \cdot W$ for CT-specimens and $\Delta a_i = 0.01 \cdot W$ for DENT-specimen (W specimen width) is proposed. Thus, for different small and large specimens different size dependent crack initiation depths even were considered.

3.2 Assessment of creep crack initiation

For the description of creep crack initiation and growth broadly three different parameters have been proposed [3.2]:

- the stress intensity factor K_I, which will now be designated as $K_{I\,id}$, where $K_{I\,id}$ is the fictitious, elastic K-value of the initial defect, calculated with the commonly used linear elastic formulas
- the path independent integral C*
- the nominal stress in the far field/ligament, which corresponds in a simplified manner to a general yield model in a creeping body.

To determine C*, most researchers use the C^*_2-formula, which is a function of load line displacement rate due to creep, [3.3], [3.4], [3.5], [3.6]:

$$C^*_2 = \dot{V}_c \cdot \sigma_{net} \cdot \eta \tag{3.1}$$

With

$\dot{V}_c$ load line displacement rate

σ_{net} net section stress

η factor depending on specimen geometry and creep exponent n

If this formula is used to analyse creep crack growth test results from specimens with different size and shape, the scatter band of this data is less than that from evaluation with $K_{I\,id}$, and other C* definitions. For practical application to components, a solution for η as well as a measurement of $\dot{V}_c$ on components surface is necessary. Such measurement for real existing cracks in components loaded to a low stress level for a long service period is rather difficult or even impossible because of the small displacement rates involved. To overcome this problem, for components C* has to be evaluated by FE-calculations, but this is time consuming and the comparability of C^*_2 and C* from FE is not directly given [3.7].

Therefore, from the beginning it has been attempted to determine the creep crack initiation by the fictitious, ideally elastic initial stress intensity parameter $K_{I\,id}$. It characterises only the crack tip geometry and not the real timely redistributed stress field at the crack tip. Solutions for K_I are available for a wide range of geometries, they are used here similar as stress intensification factors K_t in high temperature design rules.

However, in terms of considering bodies under creep, in which both stress redistribution at the crack tip and damage accumulation in the far field occurs in a time dependent manner, it is not sufficient to use $K_{I\,id}$ as the only parameter to describe the crack tip behaviour in the component. This means that in the creep regime two criteria are needed to describe creep crack initiation and growth. These parameters are $K_{I\,id}$ for the description of the crack tip situation and σ_n (nominal stress) for the consideration of the stress state in the far field / ligament. Such a Two-Criteria-Diagram for creep crack initiation was first proposed in 1984 [3.8][3.9].

The significance of the two parameters $K_{I\,id}$ and σ_n can be explained by means of a model, Figure 3.1 [3.8][3.9] distinguishes between ligament damage (related to low $K_{I\,id}/\sigma_n$-ratios) and crack tip damage (related to high $K_{I\,id}/\sigma_n$-ratios).

In Figure 3.1 the creep rupture strength of smooth specimen and the creep crack initiation resistance in terms of $K_{I\,id}$ are plotted independently as a function of loading time. If a component with a large flaw (high $K_{I\,id}$) is approaching the end of life (say at 100,000 h) due to a nominal stress σ_n, then Figure 3.1 shows that creep crack initiation would be caused relatively early in life with subsequent creep crack growth into a low pre-stressed, i.e. practically undamaged far field. This $K_{I\,id}/\sigma_n$-situation would lead to a failure mode of crack tip damage, promoting leak before fracture.

If the same component had a relatively small flaw (low $K_{I\,id}/\sigma_n$), Figure 3.1, right side, creep crack initiation with subsequent crack growth into a highly pre-stressed, partly pre-damaged far field would formally only occur at a very late stage in life. In reality a creep crack would be initiated earlier in life because of the pre-damage of the ligament by the nominal stress, leading to a ligament damage mode because the $K_{I\,id}/\sigma_n$-ratio is low. When this mode of ligament damage is dominant, the first indication of failure of the component would be given by the overall component deformation. The final failure could, however, occur in a sudden manner.

3.3 Two-Criteria-Diagram (2CD)

3.3.1 Two-Criteria–Diagram (2CD - early version)

An example of such a diagram is shown in Figure 3.2. The diagram in this early version was proposed in the 1980's [3.6], [3.8], [3.9]. It is only valid for creep ductile (no notch weakening) materials.

In the diagram the component loading parameters ($K_{I\,id}$, σ_n) are normalized by the respective time and temperature dependent data, which indicate material strength/resistance:

- $R_\sigma = \sigma_n/R_{u/t/T}$ the stress-(far field-)ratio and
- $R_K = K_{I\,ido}/K_{Ii}$ the stress intensity-(crack-tip-)ratio.

The derivation of these ratios is explained in Figure 3.3, where $\sigma_{n\,pl}$ (σ_n) indicates the nominal stress in the far field of a cracked body. But the definition of the nominal stress which should be used needs some more explanation (details see section 3.6 and Appendix B1).

For components with larger ligaments and cracks (crack tip damage mode $R_\sigma/R_K \leq 0.45$) the component nominal stress σ_n can be used (see section 3.6). For specimens the nominal stress is the net section stress in which bending portions are included as completely redistributed, this stress is designated as $\sigma_{n\,pl}$ (see Figure 3.4).

For small cracks in large components/specimen (i.e. ligament damage mode $R_\sigma/R_K \geq 1.25$) the gross nominal stress σ_n can be applied.

In the mixed mode regime, a technical stress distribution length X must be considered, which length is smaller than the total ligament of a larger component. This depth depends on the rupture ductility of the material ($X = 0.5 \cdot A_u$, see Part A, section 2.4.2).

- $R_{u/t/T}$ is the creep rupture strength of smooth tensile specimen,
- $K_{I\,ido}$ is the initial fictitious elastic K_I-value at time zero (Index "o") at the crack tip within the component or a specimen, simply designated as K_{Iid} and
- K_{Ii} is used as a kind of material characteristic. It denotes the creep crack initiation value of the material in pure crack tip damage mode. K_{Ii} depends on the shape and size of the specimens as well as on temperature. Therefore, it has to be determined from a specimen with high $K_{I\,id}/\sigma_n$-ratio. Cs25-(CT1-)specimens with a $K_{I\,id}/\sigma_{n\,pl}$-ratio of about 4.5 $\sqrt{mm}$ (see Table 3.1) are adequate and the most economic type for the determination of K_{Ii}-t_i-curves.

The Two-Criteria-Diagram distinguishes between three fields of damage mode, separated by ratio lines R_σ/R_K:

- ligament damage, $R_\sigma/R_K \geq 2$ (corresponds to $K_{I\,id}/\sigma_n >\approx 1.5\ \sqrt{mm}$),
- crack tip damage, $R_\sigma/R_K \leq 0.5$ (corresponds to $K_{I\,id}/\sigma_n >\approx 4.5\ \sqrt{mm}$) and
- mixed mode damage.

Looking at the different areas of the diagram, such a diagram enables to estimate the failure mechanisms to be expected at each time. Crack initiation can only be expected outside of the crack / no crack-boundary (Figure 3.2), according to the respective damage mechanism. Inside the boundary line different stages of exhaustion and increasing microscopic damage are expected. This crack / no crack boundary line was defined based on the following assumptions:

- For crack tip and mixed mode damage, crack initiation is defined if crack attains a size of engineering relevance (crack depth Δa_i = 0.5 mm) related to experimental results in CT1-specimen -> K_{Ii}-values
- For ligament damage situation 1 % creep strain should not be exceeded in the ligament ($R_{p1/t/T} \approx 0.75 \cdot R_{u/t/T}$ -> $R_\sigma \approx 0.75$). This 1 % creep strength limit is defined in most Codes as a damage border for ferritic steels.

The validity of ratio lines in Figure 3.2 is restricted to materials with sufficient high creep deformation capability. Only no notch weakening materials, i.e. materials with at least about 7 % creep rupture elongation, A_u, will be described in this type of diagram. For lower rupture ductility the shape of the diagram changes, see Part C.

Under the condition of high creep ductility, the specimen thickness B increases the constraint and thus has a positive impact on crack resistance. In those cases, crack initiation in large components will occur later than expected from the data for CT1-specimens, which have a thickness of only 25 mm. For specimens/components with a greater thickness (B > 50 mm) the boundary line for crack initiation can be moved to a value R_K = 1.1, as shown in Figure 3.2.

Basically, the 2CD can be applied for all creep strength limits below 1 %. Recently the shape of the 2CD has been improved by implementation of the results of the research program "Ductility" [2.1], see Part A. This in 2015 newly designed diagram will be designated as 2CD15.

3.3.2 Size of new Two-Criteria–Diagram 2015 (2CD15)

In Part A the crack initiation threshold values a_{th} for 1 % ligament- or far field-strain dependent on rupture elongation A_u were evaluated. In a 2CD the R_σ- and R_K-values from a_{th} represent the corner point B between Ligament- and Mixed-mode damage on the crack /no crack borderline. The Table 3.3 shows the values which can be deducted to optimize the 2CD in the ligament area:

With the results of Table 3.3 the following modifications of the 2CD are indicated, see Figure 3.5:

- The corner point B between ligament- and mixed-mode damage is shifted to R_K = 0.6. But with this respect it should be realized that not only the a_{th}-values depend on creep rupture

ductility A_u, but even the crack initiation characters K_{Ii}, as indicated in Table 3.3. The dependence of K_{Ii} from A_u is explained in Part C. Because of this decrease of the K_{Ii}-values with A_u the R_K ratio of corner Point B remains almost unchanged [with decreasing A_u the $K_{I\,id}(a_{th})$ is reduced due to lower a_{th}-values; K_{Ii} is reduced due to lower creep ductility. That means earlier crack initiation]. Thus, the no-crack-ligament-damage-area in the 2CD15, which is larger than in the earlier diagram (see section 3.3.1) does not mean that tolerable crack depth (a_{th}) for lower A_u-values have become deeper.

- As consequence of the new position of point B even the ratio line between ligament- and mixed-mode damage is changed to $R_\sigma/R_K = 1.25$.

This 2CD15, Figure 3.5, can be applied for all materials with no notch weakening behaviour, that means for materials with $A_u \geq\approx 7$ %. The 2CD15 has the following coordinates[4]:

- Point A: $R_\sigma = 0.75$; $R_K = 0$
- Point B: $R_\sigma = 0.75$; $R_K = 0.6$
- Point C: $R_\sigma = 0.45^{*)}$; $R_K = 1$ ($^{*)}$ this point is valid for $A_u = 8$ %, see Part C, Figure 4.4)
- Point D: $R_\sigma = 0$; $R_K = 1$

Loading conditions which are situated in the no-crack-ligament-damage-area of the diagram 2CD15 need no further considerations. These deal with situations according to Part A with $a_o \leq a_{th}$ and ligament strains, $\varepsilon_{lig} = 1$ % and corresponding stress ratio $R_\sigma = 0.75 \cdot R_{u/t/T}$.

Loading situations with ligament strain $\varepsilon_{lig} = 0.5$ % and the belonging a_{th}-value lie on the no crack / crack borderline of the mixed mode regime, because of the larger a_{th}-value ($a_{th} = 1.7$ mm, for $A_u = 10$ %).

Loading situations with ligament strain $\varepsilon_{lig} = 0.2$ % and the belonging a_{th}-value ($a_{th} = 3.3$ mm, for $A_u = 10$ %) lie also on the borderline, if corrected with the stress redistribution length X, see Section 3.6.1.

3.4 Requirements for the application of Two-Criteria-Diagram

The following requirements should be fulfilled for the prediction of creep crack initiation in components by means of 2CD:

- The considered material creep strength data $R_{u/t/T}$, obtained from uniaxial tests on smooth specimens, must be available
- Crack initiation data K_{Ii} from specimens with high $K_{I\,id}/\sigma_n$-ratio (Cs25-specimens see Table 3.1) in time- and temperature-dependent manner must be prepared
- The material must meet the requirement of creep ductility mentioned above, $A_u \geq\approx 7$ %. In general, boiler and tube materials of type CMn, 1%CrMo, 1%CrMoV, 2.25%CrMoV and 9-12%CrMoV, delivered and used according to German specification, fulfil this requirement.

3.5 Determination of K_{Ii}-values

The experimental results of K_{Ii} vs. time as a basis for the application of 2CD have been prepared with pre-cracked or spark eroded specimens of type Cs25. Based on the definition of engineering crack initiation with $\Delta a_i = 0.5$ mm, there are no significant differences between crack initiation results of spark eroded or pre-cracked specimens [3.17].

Experimental data of more than 35,000 h for 1%CrMoV-steels at 530 °C and 550 °C have been obtained by Siemens, and predominantly by IfW Darmstadt and MPA Stuttgart and the German

[4] The R_K-Value to point B can be furthermore numerically determined as shown in Appendix B3.

Creep Committee (Forschungsvereinigung Warmfeste Stähle und Hochtemperaturwerkstoffe, FVWHT) from several German research programs [3.10], [3.11], [3.12], [3.13], [3.16], [3.17], [3.21], [3.22], [3.23]. An example of such data shows Figure 3.6. Investigations on martensitic 10-12%CrMo(WNb)V-steels at 550 °C and 600 °C are extended up to 25,000 h (Two Cs25-specimens of 10%Cr-steel at 600 °C reached recently an individual testing time of 100,000 h).

Experimental K_{Ii}-data are not generally available for all temperatures needed. To assist in this situation, it has been proposed that an extrapolation to higher or lower temperatures can be made using the Arrhenius-formula [3.11]:

$$\frac{\Delta a}{\Delta t} \sim K_{Ii}^{\,n} \cdot e^{\frac{-Q}{R \cdot T}} \qquad (3.2)$$

(for 1%CrMoV: n = 9, Q/R = 30,000 K).

It is estimated, that an extrapolation range of ±30 K should be tolerable, see Figure 3.6. Another possibility is to use the Larson-Miller-Parameter (P_{LM}) from creep tests on smooth specimen, P_{LM}, for the determination of K_{Ii}-data at other temperatures [3.7]

$$P_{LM} = T \cdot [C + \log 10(t)]/1000 \qquad (3.3)$$

T: absolute temperature [K]

From such a K_{Ii}-P_{LM}-plot of existing data, K_{Ii}-t_i-curves for other temperatures can be estimated, when the values of the constant C, derived from plain bar creep rupture tests are applied:

- 1%CrMoV and other ferritic steels: C = 20,000,
- 10-12%CrMoV steels: C = 25,000.

The P_{LM}-method should not be used to extrapolate K_{Ii}-data to longer times, because the K_{Ii} depends on both, creep rupture strength and creep rupture elongation.

3.6 Application of Two-Criteria-Diagram for static (creep) loads

To answer the question whether crack initiation has to be expected after given service times $t_1, t_2 \cdots t_n$, an assessment consisting of the steps according to the flow chart of Figure 3.7 has to be carried out [3.7], [3.14], [3.15]:

Initial stress intensity, $K_{I\,id}$: Determine the initial stress intensity of the initial flaw with the initial load/stress, (the stress intensity factor $K_{I\,id}$ has to be determined by common equations of linear elastic fracture mechanics).

Nominal stress, $\sigma_{n\,pl}$: The nominal stress in the far field/ligament behind the flaw is the completely redistributed nominal stress $\sigma_{n\,pl}$, see Figure 3.4, or the time derivative for a solution via Finite Element calculation respectively. The nominal stress is always the principal stress perpendicular to the crack plane and not an equivalent stress, see Appendix B2.

As explained under section 3.3.1, the determination of the nominal stress needs special consideration:

Situations with dominant crack tip damage ($R_\sigma/R_K \leq 0.45$): $K_{I\,id}$ is decisive and the nominal stress is of minor influence. This means that for components with large ligaments the nominal stress, σ_n, can be used. For specimen with large cracks the net section stress with completely redistributed bending portion (acc. to Figure 3.4) must be applied. This stress is designated as nominal stress according to Siebel $\sigma_{n\,pl}$.

Situations with dominant ligament damage ($R_\sigma/R_K \geq 1.25$): The gross nominal stress σ_n can be used. If this stress is below $R_{p1/t/T}$, no crack initiation will occur, see Part A.

Situations with dominant mixed-mode damage ($R_\sigma/R_K = 0.45 - 1.25$): For components or specimen with larger ligament dimensions it is essential to remember that stress redistribution

will only be concentrated over a stress distribution length X, i.e. that stress redistribution cannot occur over an unlimited range of a cross-section[5], see section 2.4.2 of Part A and Part B, Appendix B1.

Situations with R_σ/R_K = 0.45 - 0.7: The area for which an increase of the gross nominal stress $\sigma_{n\,pl}(X)$ within the technical stress distribution length X has to be considered, lays between the lines for R_σ/R_K = 0.45 - 0.7 - hatched zone in Figure 3.8. This means that for an R_σ/R_K point within that part of the no crack area a $\sigma_{n\,pl}(X)$-stress has to be determined and used in the 2CD15. Figure 3.8 shows the resulting points in the 2CD15 for the a_{th}-value for A_u = 10 % and 0.2 % ligament stress. The evaluation of these points for 200,000 h is as follows:

ε_{lig} = 0.2 %; a_{th} = 3.1 mm; X = 0.5·A_u = 5 mm,

see Part A, Figure 2.15 and Table 2.1 [$R_{p0.2/t/T}$(200,000 h) ≈ 40 MPa]

$\sigma_{n\,pl}(X) = (1+a_o/X)\cdot\sigma_n$ (see

Figure 3.19, Part B)

$\sigma_{n\,pl}(X) = (1+3.1/5)\cdot R_{p02/t/T}$ = 65 MPa

$R_\sigma = \sigma_{n\,pl}(X)/R_{u/t/T}$ = 65/100 = 0.65

$R_K = K_{I\,id}/K_{Ii}$ = 0.77

R_σ/R_K = 0.84

The R_σ- and R_K-values without consideration of the stress distribution length X (see Table 3.3) are:

$R_\sigma = R_{p0.2/t/T}/R_{u/t/T}$ =40/100 = 0.40

R_K = 0.77

R_σ/R_K = 0.52

and lie within the hatched zone, Figure 3.8. This indicates the application of the distribution length X.

Situations with R_σ/R_K = 0.7 - 1.25: The gross nominal stress as well as the net section stress can be used.

3.7 Validation of the method

Figure 3.9 and Figure 3.10 are earlier examples of 2CD with crack initiation data of two 1%CrMoNiV-steels at 530 °C and 550 °C and 10-12%CrMo(WNb)V-steels at 600 °C with higher rupture elongation, see Part A[6]. Unfortunately the initiation time of the plotted data points was evaluated with the so called "size dependent crack initiation length", which leads for the smaller DENT- und C(NT)-specimen to shorter initiation times compared to the larger specimen. With a constant crack initiation criteria the smaller specimen would be positioned at larger R_K-values and therefore consist with the borderline of the new 2CD15.

[5] The use of the British reference stress σ_{ref} gives no solution of the problem, because σ_{ref} depends only on the a/W of a specimen/component and not on the absolute value of the crack depth a.
[6] Material data, see Table 3.2

In Figure 3.9 (1%CrMoV-steel) the small-scale specimen tests lasted up to 35,000 h, large scale specimens were tested up to 10,000 h. A survey of size and geometry of tested fracture mechanics specimen gives Table 3.1[7].

None of the more than 100 specimens with crack initiation are located inside the bordered area. Only 6 data points out of 9, determined on real casings after very long service times, showing no crack initiation [3.20], lie inside the no-initiation area. Thus the diagram is able to characterize a large variety of geometries in a successful manner.

Figure 3.10 shows the crack initiation results of 10-12%CrMo(WNb)V-steels. Most of the data points lie higher with stress ratios about 1, which indicates ligament damage with reduced crack tip damage influence, even for deeper cracked specimen. This results from the higher creep rupture elongation A_u of the 10%Cr-steels. (The 12%Cr steels have partly lower A_u-values.)

Due to this and to the higher constraint of large specimen, in the crack tip damage area a more conservative appearance for steels with higher creep rupture elongation can be expected, see Figure 4.3 in Part C.

Recent evaluations in all case supported the applicability of the 2CD. Therefore, the method can be said to have been proven for the above-mentioned types of (creep ductile) steels and may be used in the creep temperature range of about 450 °C - 600 °C. The findings with respect to specimen size, shape and ductility can be transferred even to other ferritic steels such as CMn-, 0.5%Cr0.5%Mo0.25%V-, 1%CrMo- and 2.25%CrMo steels when K_{Ii}-initiation data from CT1-specimens are available. The methodology to use $K_{I\,id}$ and σ_n resp. $\sigma_{n\,pl}$, as the crack tip parameter and far field parameter is basically proven in terms of steels given above.

(All tests were done in air ambient condition; the results represent surface cracks under air. A simulation of internal cracks in an oxygen free atmosphere of argon with 3 % hydrogen gas revealed insignificant differences compared to air tests [3.23][3.24], the 2CD15 needs no change.)

3.8 Proposal to consider slow stress changes (cyclic creep crack initiation) in creep ductile materials with 2CD15

3.8.1 Basic considerations with respect to the applicability of 2CD15 to cyclic creep crack initiation

To get some indications to the more typical situation of cyclic creep loading and its influence to the crack initiation behaviour, cyclic hold time tests (see Figure 3.11) on small and large specimens (D15, Cs25, Cs50, D60) of 30CrMoNiV4-11/AMA and X12CrMoWVNbN10-1-1/1A at 550 °C and 600 °C have been done at IfW Darmstadt and MPA Stuttgart [3.17], [3.18], [3.19], [3.21], [3.22], [3.25]. An overview of test procedure and results is presented in [3.18].

The aim was to use the 2CD even for cyclic hold time loadings, thus it was looked on the influence of the load cycles on the K_{Ii} value derived from static tests with Cs25-specimen.

For loading situations with long service periods at maximum stresses and lower loading / unloading frequencies, which are characterized by dominant creep damage processes it makes sense to plot the data points in the form $K_{I\,max} = f(t_i)$. This is done in Figure 3.12 for the 30CrMoNiV4-11/AMA and in Figure 3.13 and Figure 3.14 for forged and cast 10%CrMoWVNbN steel for all specimen with deeper cracks ($K_{I\,id}/\sigma_n > 4$). The few small D15-

[7] Testing of specimen with rather small cracks, $a_o < a_{th}$ in ductile materials, $A_u >\sim 7$ %, make no sense, because they experience no crack initiation, but pure ligament damage.

specimen with $K_{I\,id}/\sigma_n \approx 2$ suffer ligament damage and therefore must be rated with $\sigma_{n\,pl}$ and not with $K_{I\,id}$ (see Figure 3.15).

The parameter $K_{I\,max}$ used here is the value for the maximum load of the cycle. The diagrams (Figure 3.12, Figure 3.13, Figure 3.14) show, that all data points from hold time tests reach or surpass the static crack initiation curve $K_{Ii} = f(t_i)$. Only some short time results with hold times $t_h < 1$ h have slender shorter initiation times. The large (thick) specimens, Cs50, D60, have for all frequencies larger initiation times than Cs25-specimen under pure static creep load, Figure 3.12, Figure 3.13, Figure 3.14. The ratio L_{ic} of creep fatigue initiation time t_{icf} to creep crack initiation time t_i delivers - for the same K_{Ii}-value - in all cases ratios

$$L_{ic} = \frac{t_{icf}}{t_i} \geq 1\,, \tag{3.4}$$

which expresses no influence of frequencies resp. unloadings on the time of crack initiation with hold times $t_h > 0.3$ h.

Crack initiation time was defined for creep as well as creep fatigue loads for $\Delta a_i \approx 0.5$ mm. This $\Delta a_i \approx 0.5$ mm for the creep-fatigue loaded specimen is a definition to provide a practicability to compare creep and creep fatigue specimen, though fatigue damage starts from the first cycles.

The transition between frequency and time dependent fracture behaviour for Cs25-specimen was estimated to about 10^{-3} Hz (≈ 0,3 h hold time). This estimation is supported by microscopic investigations of fracture mode (trans- vs. inter-crystalline) and observations of crack growth rate da/dt vs. frequency and hold time respectively [3.17], [3.19].

For the large specimen (D60 and Cs50) the factor L_{ic} is always higher than for the smaller specimen. This is due to the retarded creep crack initiation time t_i, which is a consequence of the specimen size and lateral constraint (see section 3.3, Part B). This means, that the fatigue influence is minor for the large specimen as compared to the “master curve” of creep crack initiation for the small Cs25(CT1)-specimen.

But for small scale specimen/components with smaller thickness resp. dimension and hold times $t_h < 1$ h, which have less lateral constraint, for safety reasons, the static crack initiation curve according Figure 3.12, Figure 3.13, Figure 3.14 should be time wise reduced (shifted to shorter initiation times).

For specimen with B-dimensions < 20 mm (dimension parallel to crack front) and hold times 0.32 – 1 h, it is therefore proposed to shift the material´s resistance curve $K_{Ii} = f(t_i)$ in the 2CD15 diagram in time-direction for 40 % to shorter times:

$$t_{icf} = 0.6 \cdot t_i\,. \tag{3.5}$$

The static K_{Ii} value at each time is than reduced and denominated as K_{Iicf}.

Hence, all details concerning the 2CD-method remain unchanged; the flow chart in Figure 3.7 **can be used.** (With special consideration of loading situation with hold times 0.32 h - 1.0 h and small dimensions, B < 20 mm, with minor lateral constraint.)

The modified 2CD15 with the cyclic creep results of the 2 steel grades are shown in Figure 3.15, Figure 3.16, Figure 3.17. The validity of the proposed method is confirmed by the results of cyclic creep crack initiation tests. Only some points for Cs25-specimens at hold times 0.32 h are close to or just inside the no crack area.

3.8.2 Consideration of additional loading conditions with the Two-Criteria-Diagram

Influence of other fatigue stress ratios R: In the section above only experimental results with fatigue stress ratio of R = 0.1 were considered. In [3.22] some results with $R = F_{min}/F_{max} = 0.6$ on 12%CrMoWVNbN steels, up to about 3,000 h with $t_h = 0.3$ h are shown, Figure 3.16, Figure 3.17. Due to the smaller fatigue amplitude a smaller damage portion is effective. Figure 3.18 shows a reduction scheme for Cs25-specimens which indicates that for hold times $t_h > 0.3$

h and R = 0.6 the use of K_{Imax} is conservative. This procedure is not yet widely proven, it is a proposal.

Influence of Argon/3% Hydrogen protective atmosphere on cyclic creep behaviour: In [3.23], [3.24] tests on Cs25-specimen in Argon/3 % H-atmosphere on 1%CrMoV- and 10%CrMoWVNbN- steels at 550 °C and 600 °C respectively were performed to simulate internal cracks without air atmosphere. These tests revealed an earlier cyclic creep crack initiation compared to tests in air, example Figure 3.16, Figure 3.17 [3.24]. The reason is the absence of an oxide layer on the crack flanks, which - especially on the stronger oxidizing 1%CrMoV steels - increases the effective range of ΔK_I.

This influence is acceptable by allowance of a certain bigger $\Delta(\Delta a_{icf})$-value (up to about 1 mm) for hold times below 1 h for the creep ductile steels described in this section. Therefore, the described procedure (Figure 3.7) with the 2CD15 for cyclic creep crack initiation must not be changed [3.24].

3.9 Conclusions - Part B

As a general result it has been shown that the application of the 2CD15 for Creep-Crack Initiation can be said to be validated for creep ductile materials. Crack initiation time under static as well as cyclic creep load ($t_h > 0.32$ h) is easy to determine if $K_{Ii} = f(t_i)$ data are available [3.7]. The method describing the crack tip- and far-field-geometry is a way to transfer directly the initiation data from specimens to components with the same crack tip- and far-field-situation. It is therefore irrelevant whether the application of K_I as a crack tip parameter is correct or not. Applicability of Two-Criteria-Diagram is proven by more than 100 validation experiments with natural and artificial defects.

The method explained here for Crack initiation (2CD) and in [3.7] explained procedures for crack growth were able to explain the failure (leakage) after 155,000 h of an elbow from 12%CrMoV steel at 530 °C in a German base load power plant. Especially the expectation, that deeper cracks fail by crack tip damage mode, which means in the end by leakage, was proven [3.26].

Loading conditions within the newly revised Ligament Damage Area ($R_\sigma/R_K > 1.25$, $a_o \leq a_{th}$) need no further consideration if the far-field strain remains in maximum at 1 % (see Part A).

Small defects (low $K_{I\,id}$), situated in the ligament damage area evolve only microscopic crack extension below the initiation threshold size a_{th}. The behaviour of such small cracks is described in (see [2.4], Part A).

For easier application a computer-based calculation program is available at MPA-Stuttgart [3.7].

3.10 References - Part B

[3.1] Holdsworth, S.R.: Initiation and early growth of creep cracks from pre-existing defects. Mat. at high temp, Vol. 10, No. 2, 127-37, (1992).

[3.2] Ainsworth, R.A. et al.: Assessment procedure for defects under steady loading. Vol. 4 of R5 Procedure for the high temperature response of structures, (1990).

[3.3] Riedel, H.; J.R. Rice: ASTM STP 700. 112-130 (1980).

[3.4] Nikbin, K. M.; D.J. Smith, G.A. Webster: Proc. ASME, Int. Conf. on Advances in Life Prediction Methods, Albany, pp. 249-58, (1983).

[3.5] Hollstein, R.; R. Kienzler: Numerical simulation of creep crack growth experiments. COST 505-D22, 127-137, Institut für Werkstoffmechanik Freiburg, FRG, January (1987).

[3.6] Kloos, K.-H.; K. Kussmaul, J. Granacher, K. Maile, R. Tscheuschner, W. Eckert: Kriechrisseinleitung und Kriechrisswachstum warmfester Kraftwerksbaustähle unter Berücksichtigung des Größeneinflusses. Schlussbericht AiF-Nr. 6038 des Instituts für Werkstoffkunde der TH Darmstadt und der Staatlichen Materialprüfungsanstalt der Universität Stuttgart (1988), comp. Granacher, J.; R. Tscheuschner, K. Maile and W. Eckert. Kriechrissverhalten typischer Kraftwerksbaustähle. steel research vol. 11, 514-521 (1989).

[3.7] Mao, T.; F. Müller, A. Scholz, M. Machalowska, A. Klenk: Programmgestützte fortschrittliche Kriech- und Kriechermüdungsbeschreibung für typische langzeit-beanspruchte Kraftwerksbauteile, Abschlussberichtes zum AVIF Vorhaben Nr. 202, FKM Heft 287 - 2005, MPA Stuttgart und IfW Darmstadt.

[3.8] Ewald, J.; K.-H. Keienburg, K. Maile: Estimation of manufacturing defects in the creep range. Nucl Eng and Design vol. 87, 389-398 (1985).

[3.9] Ewald, J.; K.-H. Keienburg: A Two-Criteria-Diagram for creep crack initiation. Int. Conf on Creep, Tokyo, pp. 173-178, 14 -18 April (1986).

[3.10] Kloos, K.-H.; K. Kussmaul, J. Granacher, K. Maile, R. Tscheuschner: Rissverhalten warmfester Kraftwerksbaustähle im Kriech- und Kriechermüdungsbereich. Schlussbericht AiF-Nr. 7251 des Instituts für Werkstoffkunde der TH Darmstadt und der Staatlichen Materialprüfungsanstalt, Universität Stuttgart (1987 bis 1992), see also Granacher, J.; R. Tscheuschner, K. Maile, W. Eckert: Langzeitiges Kriechrissverhalten kennzeichnender Kraftwerksstähle. Mat.-wiss. und Werkstofftechnik 24, 367-376 (1993).

[3.11] Tscheuschner, R.: Anriss- und Rissfortschrittsverhalten zeitstandbeanspruchter warmfester Schmiedewerkstoffe. Dissertation TH Darmstadt (D17) (1988).

[3.12] Ewald, J.; T. Hollstein, G.A. Webster, F. Djavanroodi, S.R. Holdsworth: High-temperature crack growth in steam turbine materials. European Commission, physical sciences, Report EUR 14678 EN, Editor: J. B. Marriott, COST 501 and 505 secretariat (1994).

[3.13] Ewald, J.; C. Berger, H. Brachvogel: Investigation of crack initiation and propagation under static and combined load. COST 505-D20/21 (Siemens Proj. No.: 03K05110, Final Report, June (1989).

[3.14] Ewald, J.: Handling instruction for the assessment of creep crack initiation under static load by means of the Two-Criteria-Diagram. HIDA-doc. 1702/TG1/2/PMB22 (translation from Siemens TW-PA 10.95).

[3.15] Ewald, J.; S. Sheng: The Two-Criteria-Diagram for creep crack initiation and its application to an IP-turbine. Mat at high temp, vol. 15, 281-288 (1998)

[3.16] Berger, C.; J. Granacher, Y. Kostenko, E. Roos, K. Maile, G. Schellenberg: Kriechrissverhalten ausgewählter Kraftwerksstähle in erweitertem, praxisnahen Parameterbereich. Schlussbericht AVIF-Nr. A78 des Instituts für Werkstoffkunde der TU Darmstadt und der Staatlichen Materialprüfungsanstalt, Universität Stuttgart (1999).

[3.17] Berger, C.; J. Granacher, M. Tramer, E. Roos, K. Maile, G. Schellenberg: Rissverhalten typischer warmfester Kraftwerksbaustähle im Kriechermüdungsbereich. Schlussbericht AiF-Nr. 10 395 des Instituts für Werkstoffkunde der TU Darmstadt und der Staatlichen Materialprüfungsanstalt, Universität Stuttgart (1999), see also Berger, C.; J. Granacher, M. Tramer, K. Maile, G. Schellenberg. Conference Advanced heat resistant steels for power generation, San Sebastian, Spain (1998).

[3.18] Granacher, J.; F. Müller, A. Klenk, G. Schellenberg, J. Ewald: Creep fatigue crack behaviour of two power plant steels. 2nd Int. Hida-Conference, Stuttgart, 4-6. Oct. 2000,S4-2-1 to S4-2-20.

[3.19] Maile, K.; A. Klenk, J. Granacher, G. Schellenberg, M. Tramer: Creep and creep fatigue crack behaviour of 1%Cr and 9%Cr steels. Creep and fracture of engineering materials and structures, CFEMS-8, National Institute for Metals (NRIM), Japan, (1999).

[3.20] Ewald, J.; K.-H. Keienburg, G. Röttger: Beitrag zur Abschätzung der Kriechrisseinleitung in fehlerhaften Bauteilen, Archiv f. d. Eisenhüttenwesen, 55 (1984), Vol. 11, 549 - 555.

[3.21] Berger, C.; A. Scholz, E. Roos, K. Maile, F. Müller, W. Stadtmüller: Hochtemperaturverhalten der neuen 600 °C Stähle für Wellen und Gehäuse von Dampfturbinen, Abschlussberich, AVIF-Forschungsvorhaben Nr.127 des Instituts für Werkstoffkunde der TU Darmstadt (IfW) und der Staatl. Materialprüfungsanstalt, Universität Stuttgart (MPAS), 2002.

[3.22] Berger, C.; E. Roos, A. Scholz, A. Klenk, F. Müller, T. Gengenbach: Kriech- und Kriechermüdungsrissverhalten moderner Kraftwerksstähle im Langzeitbereich, Abschlussbericht AVIF 178, IfW Darmstadt und MPA Stuttgart, 2005.

[3.23] Berger, C.; E. Roos, A. Scholz, A. Klenk, F. Müller, G. Schellenberg: Einfluss inerter Atmosphäre auf das Rissverhalten warmfester Stähle im Kriech- und Kriechermüdungsbereich Abschlussbericht zum AiF-Forschungsvorhaben Nr. 11722 des IfWD und der MPAS, 2002.

[3.24] Müller, F.: Einfluss der Rissflächenoxidation auf das Kriechermüdungsrissverhalten warmfester Stähle, Dissertation 2004, Fortschritt-Berichte VDI Reihe 5, Nr. 715, 2005.

[3.25] Schellenberg, G: Beschreibung des Risseinleitungsverhaltens v. warmf. Stählen unter Kriech- und Kriechermüdungsbeanspruchung, Diss. Univ. Stuttgart, 2003.

[3.26] Speicher, M.; A. Klenk, E. Roos, K. Maile: Creep crack assessment of components at high temperatures, ICF12, Ottawa 2009, Volume 8, p. 6278.

[3.27] Sheng, S.: Anwendung von Festigkeitshypothesen im Kriechbereich bei mehrachsigen Spannungs-Formänderungszuständen, Diss. (MPA) Univ. Stuttgart 1992.

[3.28] Ewald, J.: Verminderung des Verformungsvermögens bei mehrachsigen Spannungszuständen unter Kriechbeanspruchung, Mat. wiss. u. Werkstofftechnik 22. 359-369 (1991).

[3.29] Roos, E.; C. Weichert: Gruppenfehlstellen unter mehrachsiger Beanspruchung, Abschlussbericht AVIF-Vorhaben A143/99, FVV-Heft 278-2004, FVV Frankfurt.

3.11 Tables and figures - Part B

Table 3.1: Size and geometry of tested fracture mechanic's specimen dimensions

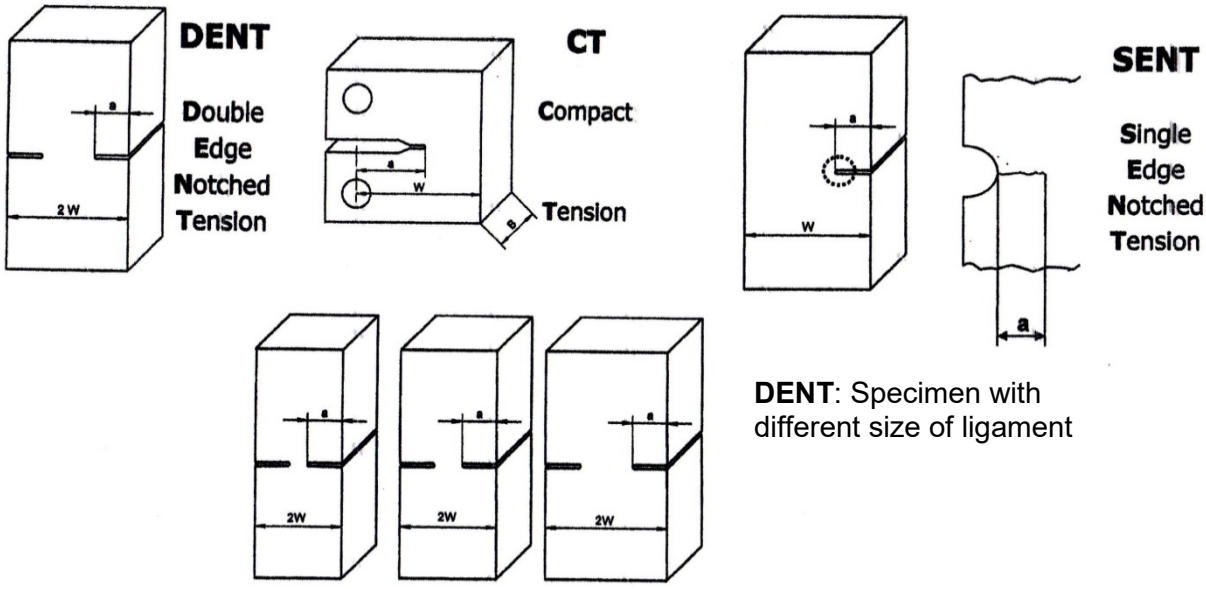

DENT: Specimen with different size of ligament

Type	CT						CNT		DENT			
	Cs12	Cs20	Cs25	Cs50	Cs55	CT100	C15		D9	D15	D30	D60
Width W (mm)	25	40	50	100	110	200	10		5	10	22	50
a_0/W	0.4 to 0.55						0.2 to 0.4		0.05 to 0.6			
K_{IId0} / σ_{npl}	3,2	4,1	4,5	7,7		9	1,8	2,2	1,7	2,2	3,4	5
a/W	0,55	0,55	0,55	0,55		0,55	0,2	0,4	0,2	0,4	0,2	0,2

Table 3.2: Chemical composition and yield strength ($R_{p0.2}$) of six forged steels and one cast steel

Materials \ Chemical Composition	C	Si	Mn	P	S	Cr	Mo	Ni	V	W	Nb	N	$R_{p0,2}$ (MPa)
30CrMoNiV4-11, 217am/AMA	0,30	0,24	0,73	0,009	0,018	1,04	1,05	0,58	0,30				610
X22CrMoV12-1, 220ta/AMB	0,22	0,41	0,68	0,022	0,001	11,3	0,90	0,69	0,29				713
X20CrMoV 12-1, 220sa/AMD	0,20	0,27	0,49	0,012	0,003	11,3	0,86	0,78	0,30				500
28CrMoNiV4-9, 216k/AGB	0,28	0,17	0,69	0,005	0,012	1,04	0,85	0,68	0,31				620
X12CrMoWVNbN10-1-1/AXN	0,12	0,10	0,45	0,008	0,002	10,4	1,06	0,74	0,18	0,81	0,045	0,055	620
X12CrMoWVNbN10-1-1/1A	0,12	0,10	0,42	0,007	0,001	10,7	1,04	0,76	0,16	1,04	0,050	0,056	801
GX12CrMoWVNbN10-1-1/2A	0,13	0,29	0,82	0,014	0,005	9,51	1,02	0,52	0,19	1,02	0,059	0,041	605

Table 3.3: R_K and R_σ values at crack depth a_{th} for 1%CrMoV- and 10%Cr-steels, creep rupture ductility A_u = 5 % - 20 %

AMA, 1%CrMoV, 550 °C, ε_{lig} = 1%

A_u / t_u	a_{th} (mm) Δa_i=0.1mm	a_{th} (mm) Δa_i=0.5mm	$K_{I\,id}$ [N/mm$^{3/2}$]	K_{Ii} [N/mm$^{3/2}$]	$K_{I\,id}/R_{p1\%}$ ($K_{I\,id}/\sigma_n$)	R_K $K_{I\,id}/K_{Ii}$	R_σ	R_σ/R_K	$R_{p1/t/T}$ [MPa]	$R_{u/t/T}$ [MPa]
8% 200,000 h	-	0,8	125	200	1,8	0,62	0,73	1,18	70	100
10% 200,000 h	-	1,0	140	223	2	0,63	0,73	1,16	70	100
15% 30,000 h	-	1,5	280	408	2,4	0,68	0,78	1,15	»120	»150

AMA, 1%CrMoV, 550 °C, ε_{lig} = 0.5%

A_u / t_u	a_{th} (mm) Δa_i=0.1mm	a_{th} (mm) Δa_i=0.5mm	$K_{I\,id}$ [N/mm$^{3/2}$]	K_{Ii} [N/mm$^{3/2}$]	$K_{I\,id}/R_{p0,5\%}$ ($K_{I\,id}/\sigma_n$)	R_K $K_{I\,id}/K_{Ii}$	R_σ	R_σ/R_K	$R_{p0.5/t/T}$ [MPa]	$R_{u/t/T}$ [MPa]
10% 200,000 h	1,7	-	158	188***	2,6	0.8 (0.78-0.84)	≈0.58	≈0.72	55-61	100

AMA, 1%CrMoV, 550 °C, ε_{lig} = 0.2% *

A_u / t_u	a_{th} (mm) Δa_i=0.1mm	a_{th} (mm) Δa_i=0.5mm	$K_{I\,id}$ [N/mm$^{3/2}$]	K_{Ii} [N/mm$^{3/2}$]	$K_{I\,id}/R_{p0,2\%}$ ($K_{I\,id}/\sigma_n$)	R_K $K_{I\,id}/K_{Ii}$	R_σ	R_σ/R_K	$R_{p0.2/t/T}$ [MPa]	$R_{u/t/T}$ [MPa]
10% 200,000 h	3,1	-	144	188***	3,6	0,77	0,4	0,52	≅ 40	100

AGB, 1%CrMoV, 550 °C, ε_{lig} = 0.8%

A_u / t_u	a_{th} (mm) Δa_i=0.1mm	a_{th} (mm) Δa_i=0.5mm	$K_{I\,id}$ [N/mm$^{3/2}$]	K_{Ii} [N/mm$^{3/2}$]	$K_{I\,id}/R_{p0,8\%}$ ($K_{I\,id}/\sigma_n$)	R_K $K_{I\,id}/K_{Ii}$	R_σ	R_σ/R_K	$R_{p0.8/t/T}$ [MPa]	$R_{u/t/T}$ [MPa]
5%** 200,000 h	0,3	-	93	170***	1,1	0,54	0,61	1,13	85	141

1A, 10%Cr, 600 °C, ε_{lig} = 1%

A_u / t_u	a_{th} (mm) Δa_i=0.1mm	a_{th} (mm) Δa_i=0.5mm	$K_{I\,id}$ [N/mm$^{3/2}$]	K_{Ii} [N/mm$^{3/2}$]	$K_{I\,id}/R_{p1\%}$ ($K_{I\,id}/\sigma_n$)	R_K $K_{I\,id}/K_{Ii}$	R_σ	R_σ/R_K	$R_{p1\%t}$ [MPa]	$R_{u/t/T}$ [MPa]
20% 200,000 h	-	2,0	143	248	2,8	0,58	0,74	1,27	51	69
20% 100,000 h	-	2,0	188	284	2,8	0,66	0,79	1,19	67	85

* Stress redistribution length X should be considered, see Fig. 3.8

** Steel AGB is too "Brittle" for 2CD ($A_u \geq 7\%$)

*** Δa_i = 0.1 mm for K_{Ii}

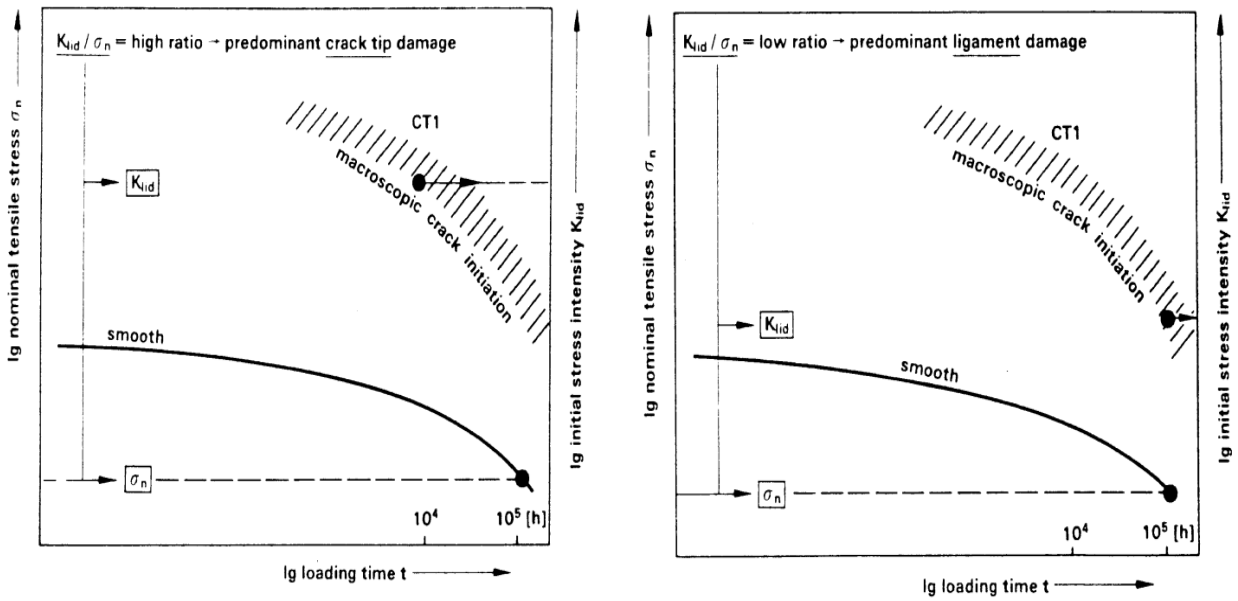

Figure 3.1: Creep loading with predominant crack tip damage (left) and predominant ligament damage respectively (right), schematic

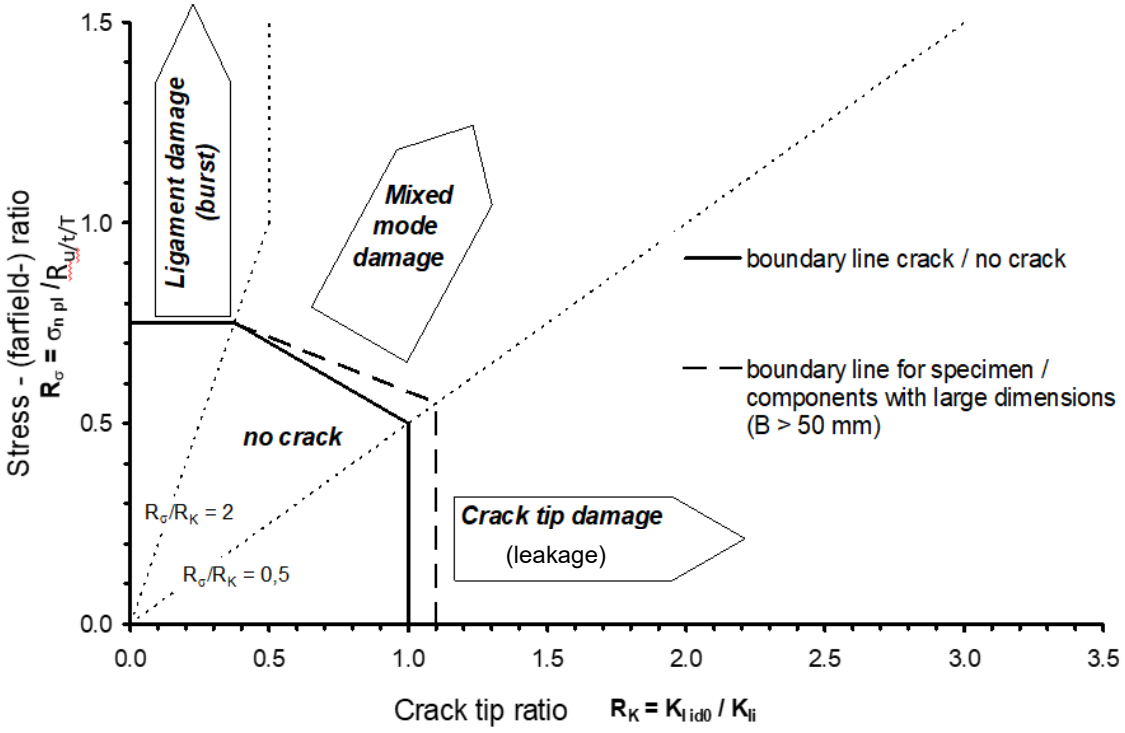

Figure 3.2: Two-Criteria-Diagram for creep crack initiation (creep ductile, early version, [3.8], [3.9], $R_{mt} = R_{u/t/T}$)

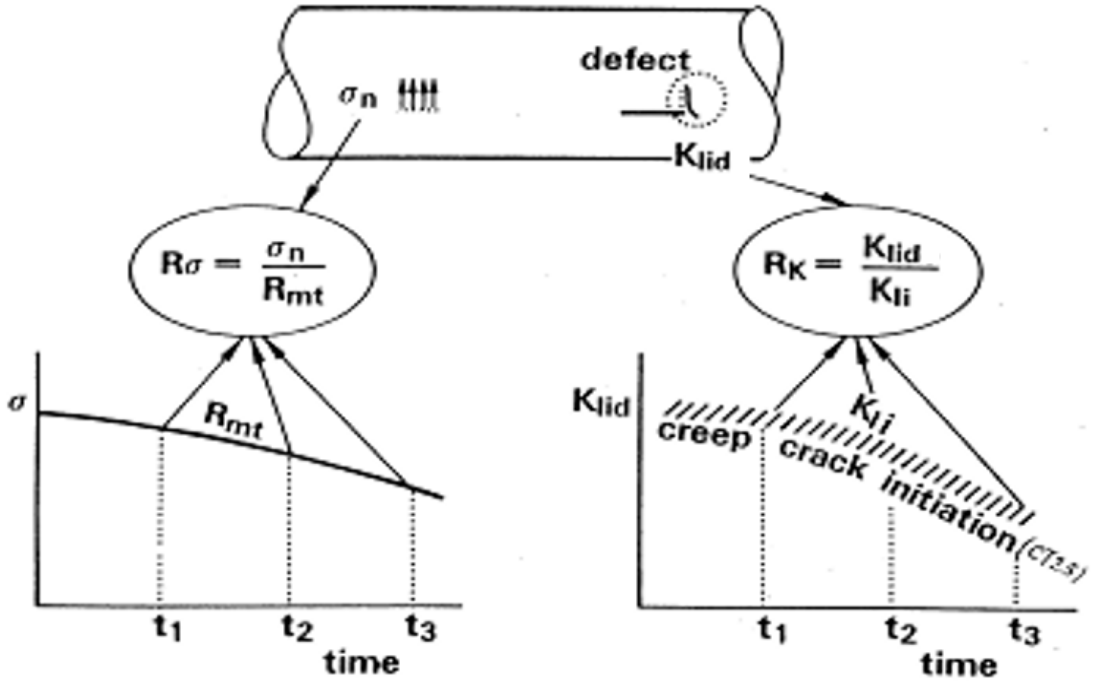

Figure 3.3: Explanation of the normalized values R for stress and stress intensity

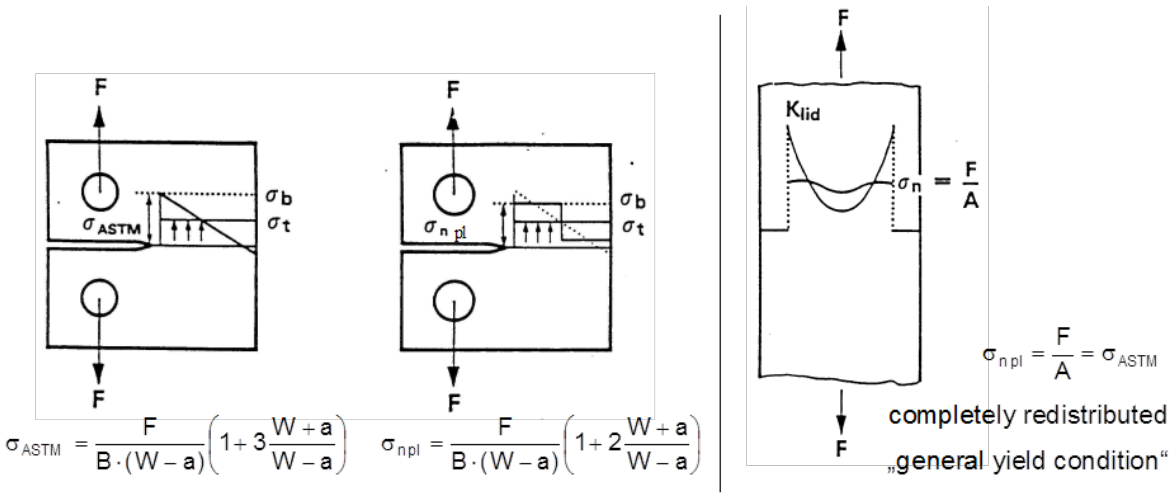

Figure 3.4: Determination of stress in fracture mechanic’s specimens

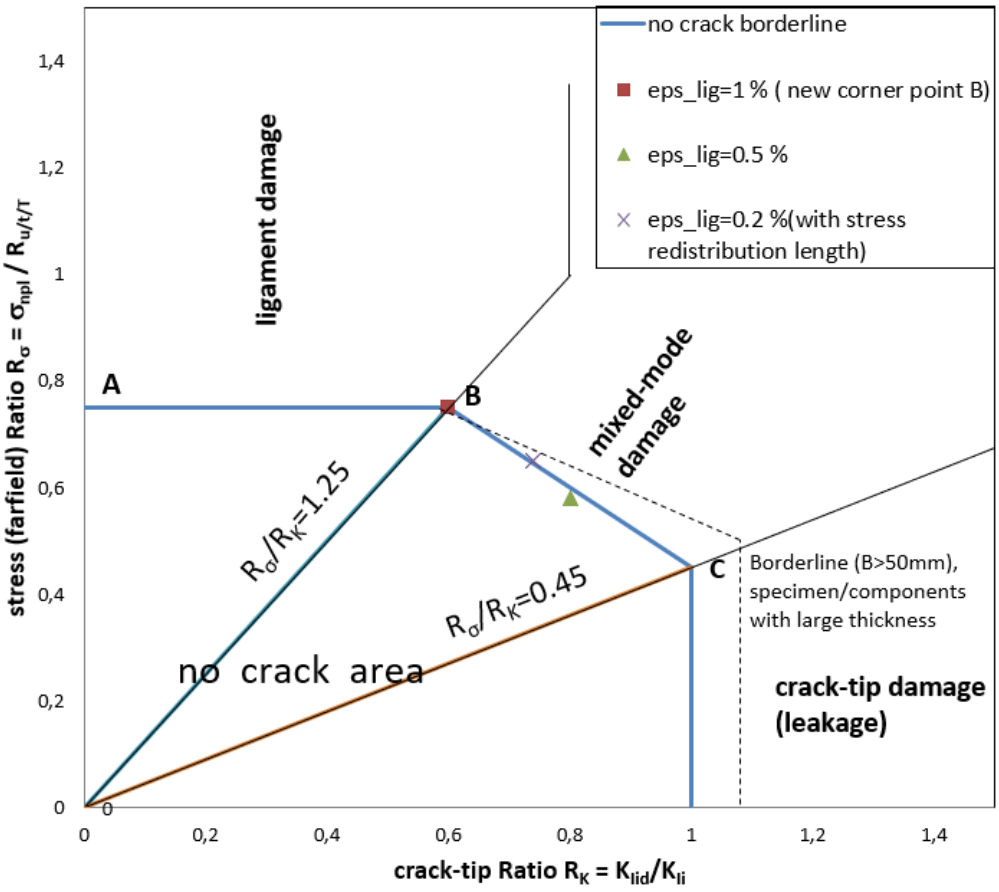

Figure 3.5: Two-Criteria-Diagram 2015 (2CD15), creep rupture ductility A_u = 7 - 10 %, 1%CrMoV-steel, 550 °C

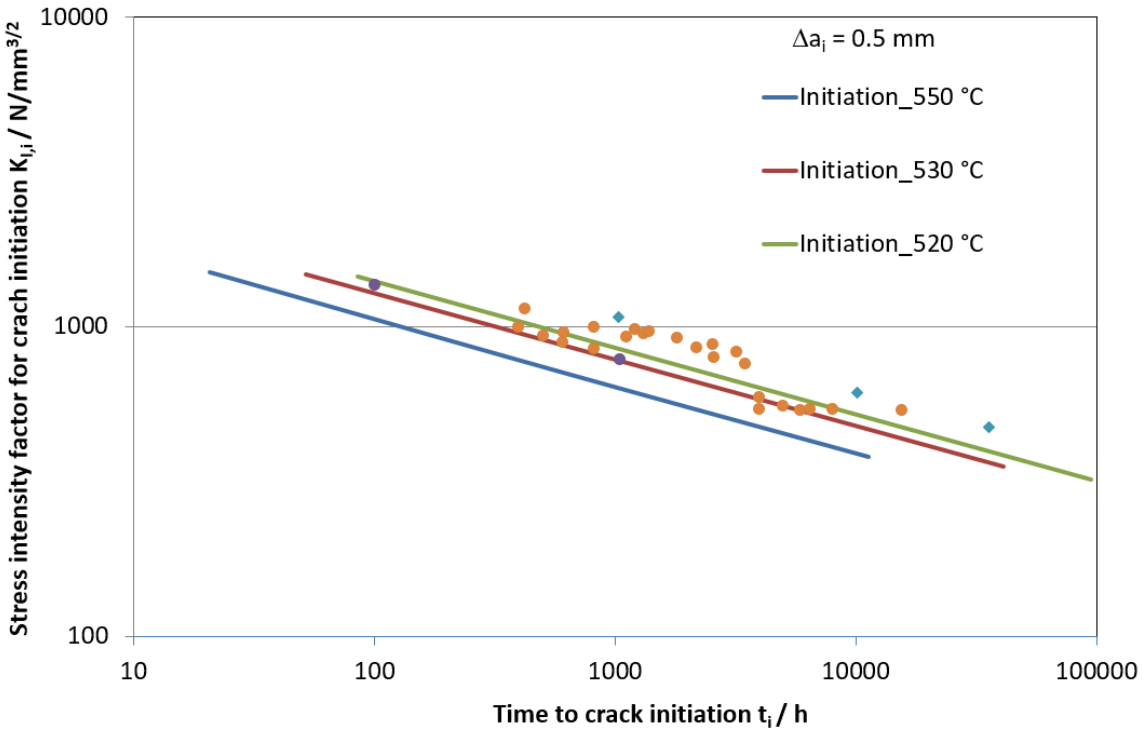

Figure 3.6: Creep crack initiation curve for 1%CrMoV-steel (ductile, lower bound curves)

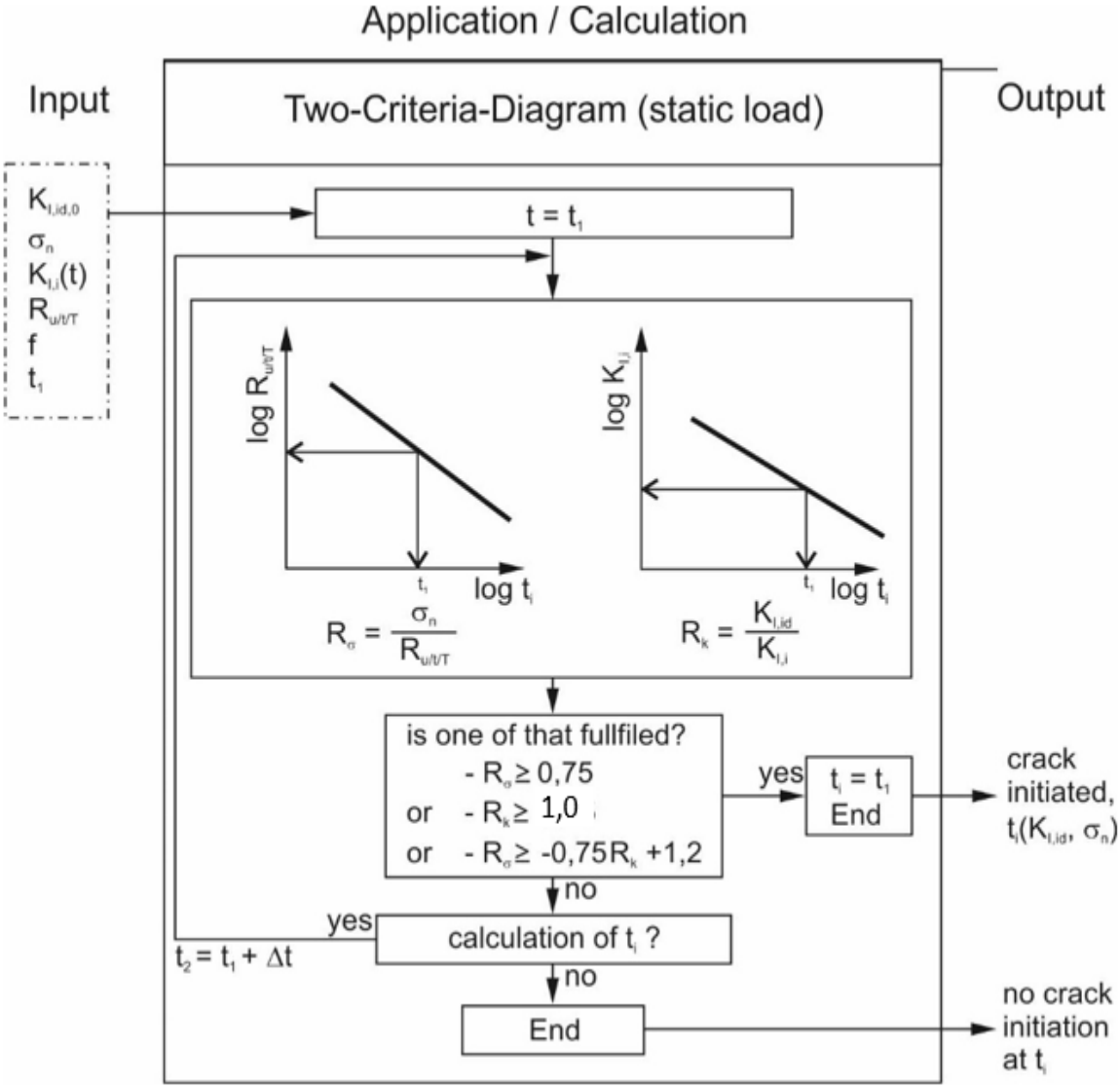

Figure 3.7: Flow chart for assessment of crack initiation time by 2CD

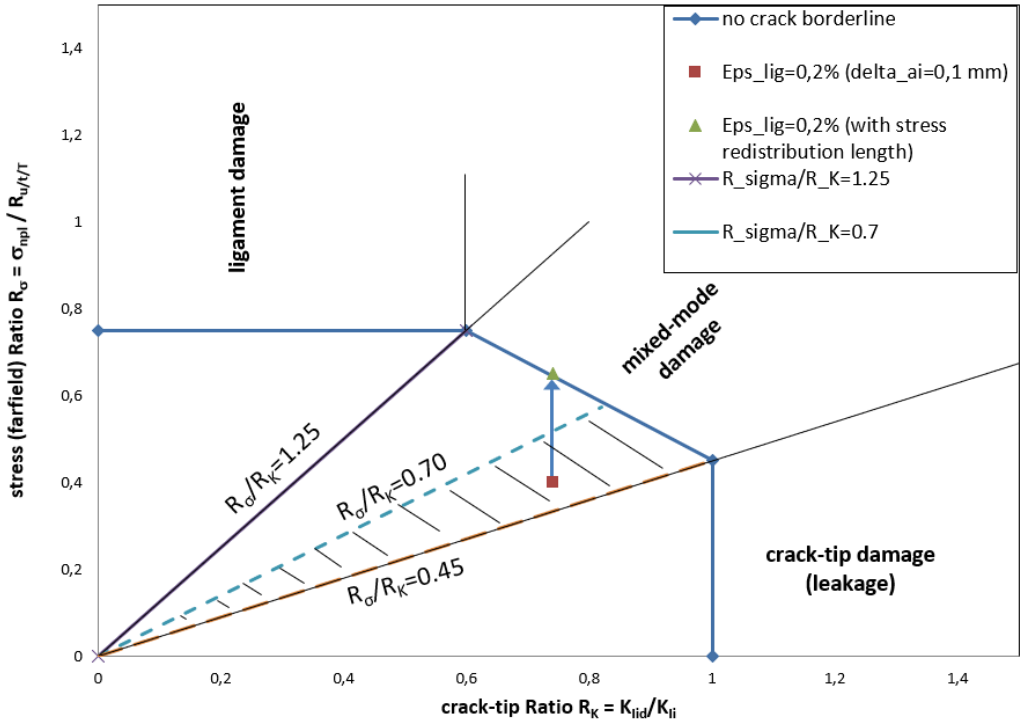

Figure 3.8: Two-Criteria-Diagram (2CD15), 1%CrMoV-steel, creep rupture ductility A_u = 7 - 10 %, with consideration of technical stress redistribution length X (see section 3.6)

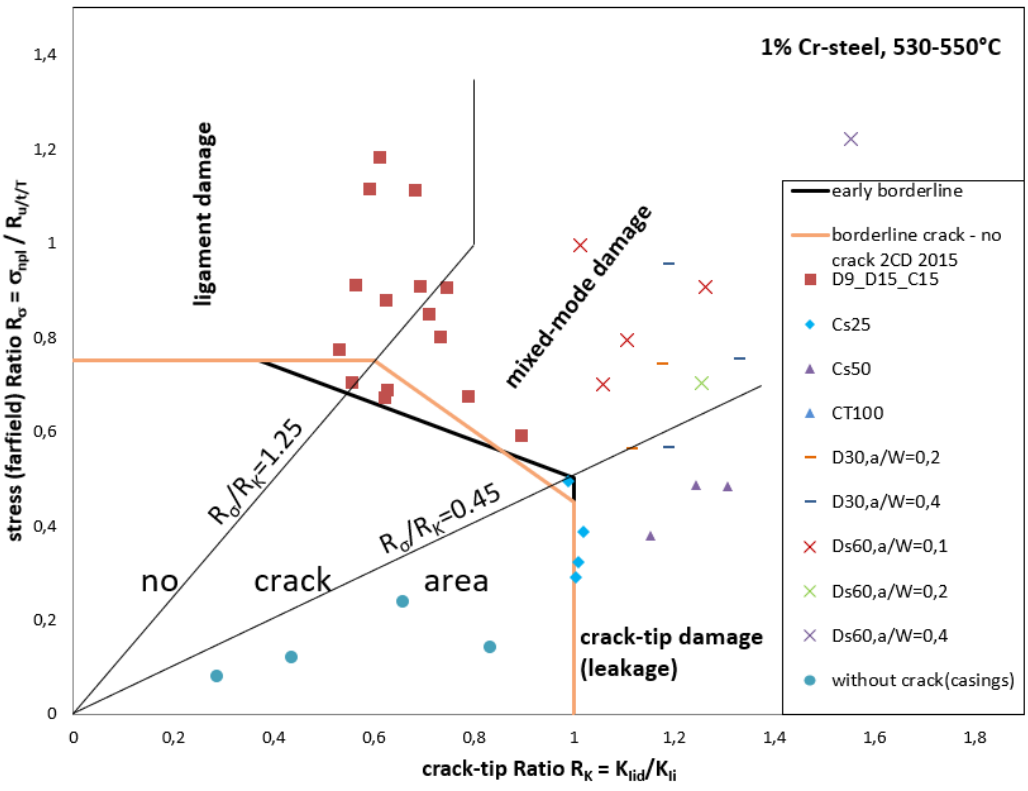

Figure 3.9: Diagram with formerly evaluated specimens, with earlier borderline and 2CD15

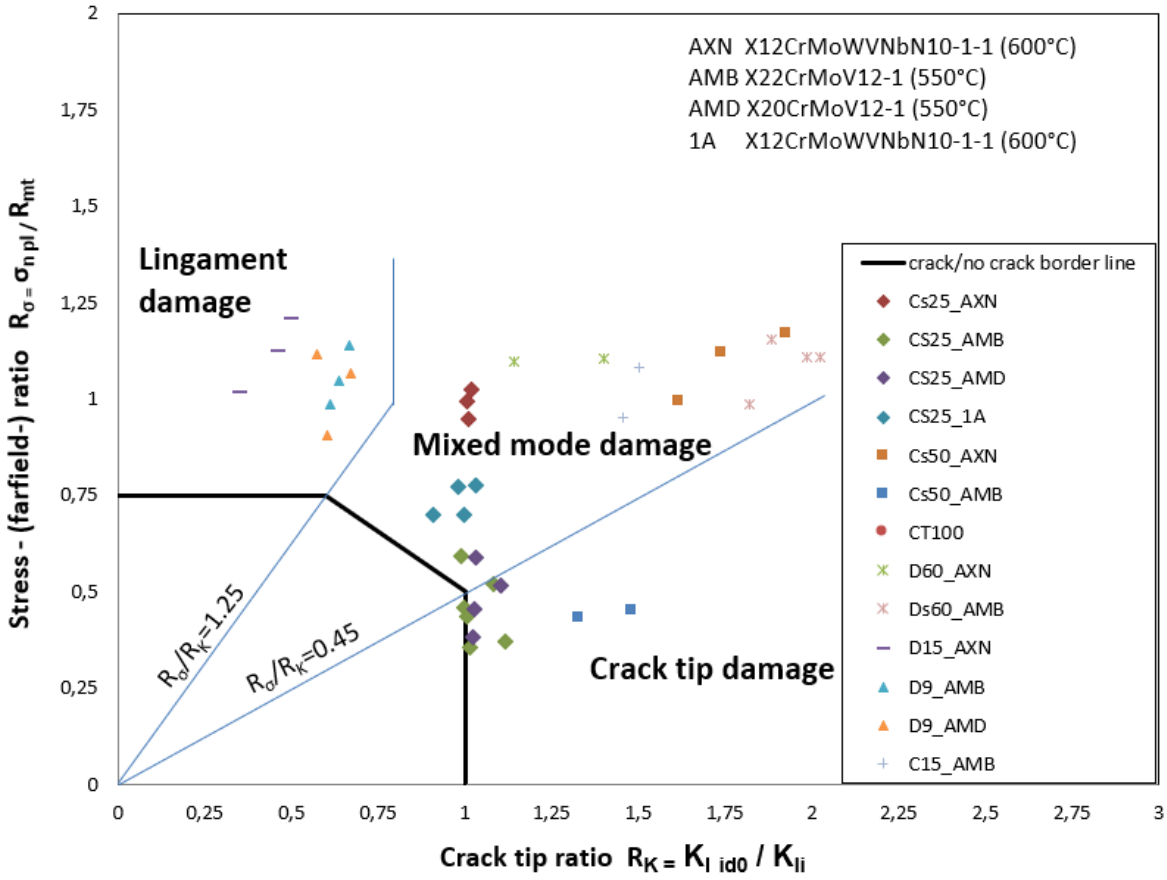

Figure 3.10: Data approving the Two-Criteria-Diagram for 10 %CrMoNiWV-steel

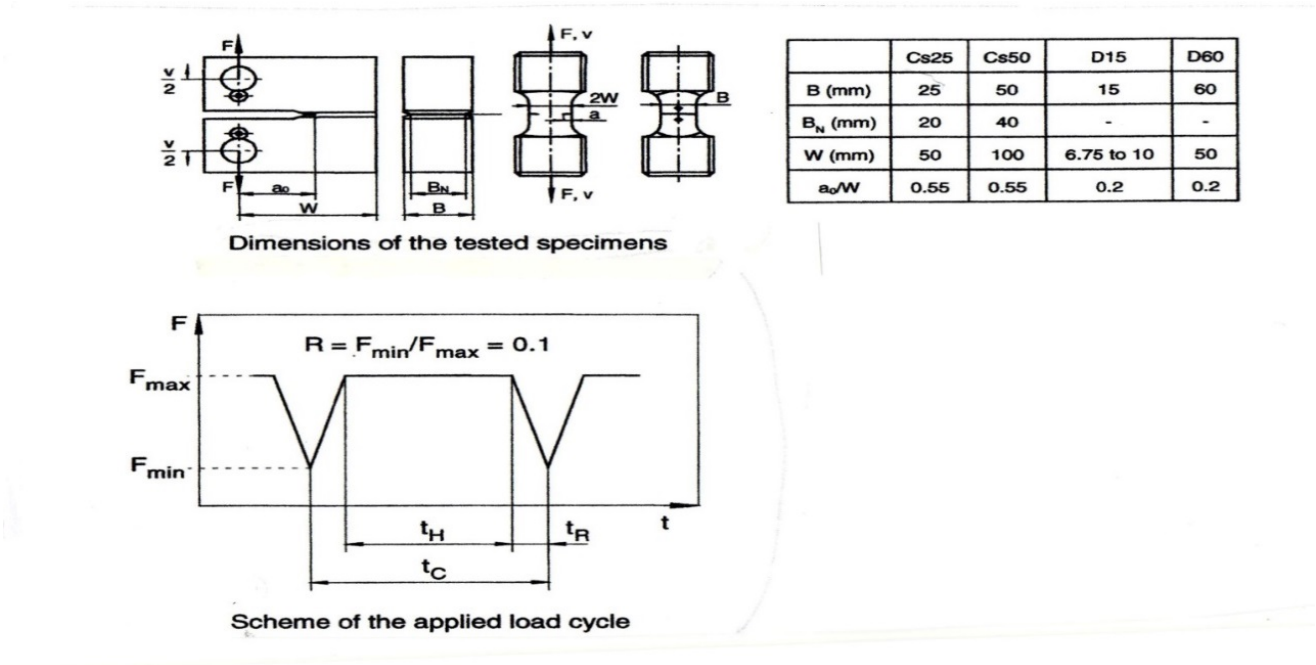

	Cs25	Cs50	D15	D60
B (mm)	25	50	15	60
B_N (mm)	20	40	-	-
W (mm)	50	100	6.75 to 10	50
a_0/W	0.55	0.55	0.2	0.2

Figure 3.11: Dimensions of specimens and scheme of the applied load cycle

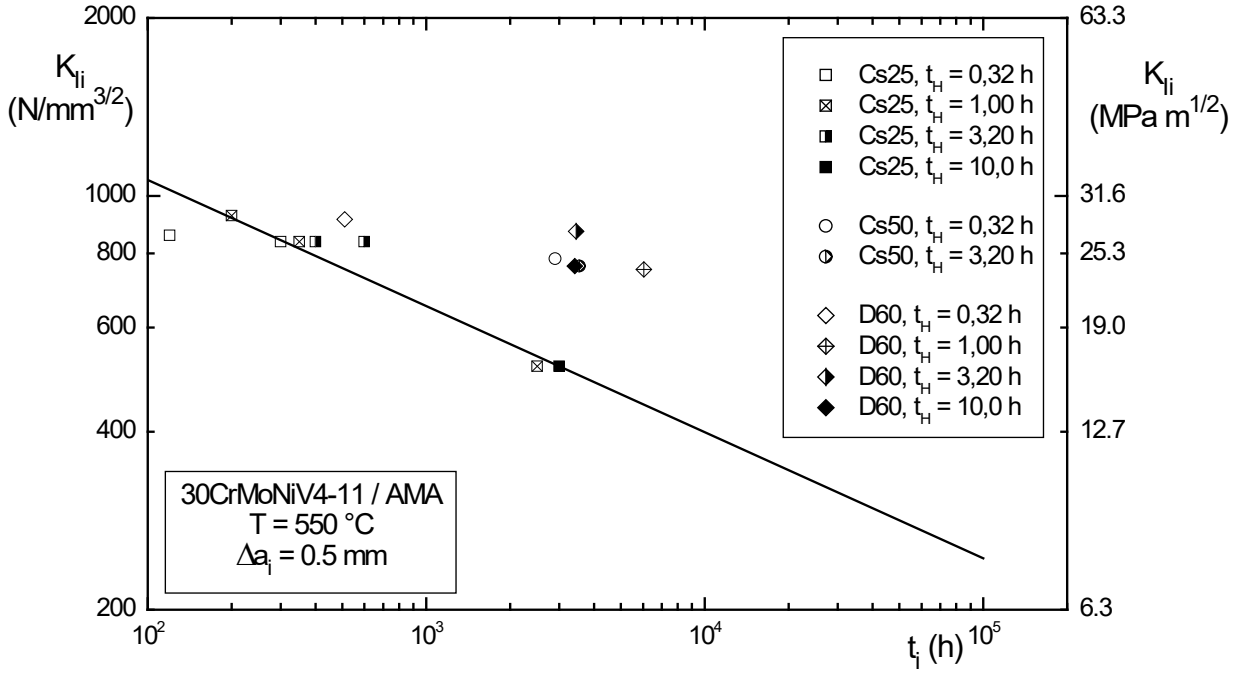

Figure 3.12: Creep crack initiation curve (lower bound) and crack initiation time t_{icf} for hold time tests data points (Δa_i = 0.5 mm) for Cs- and DENT-specimens of steel 30CrMoNiV4-11/AMA, T = 550 °C

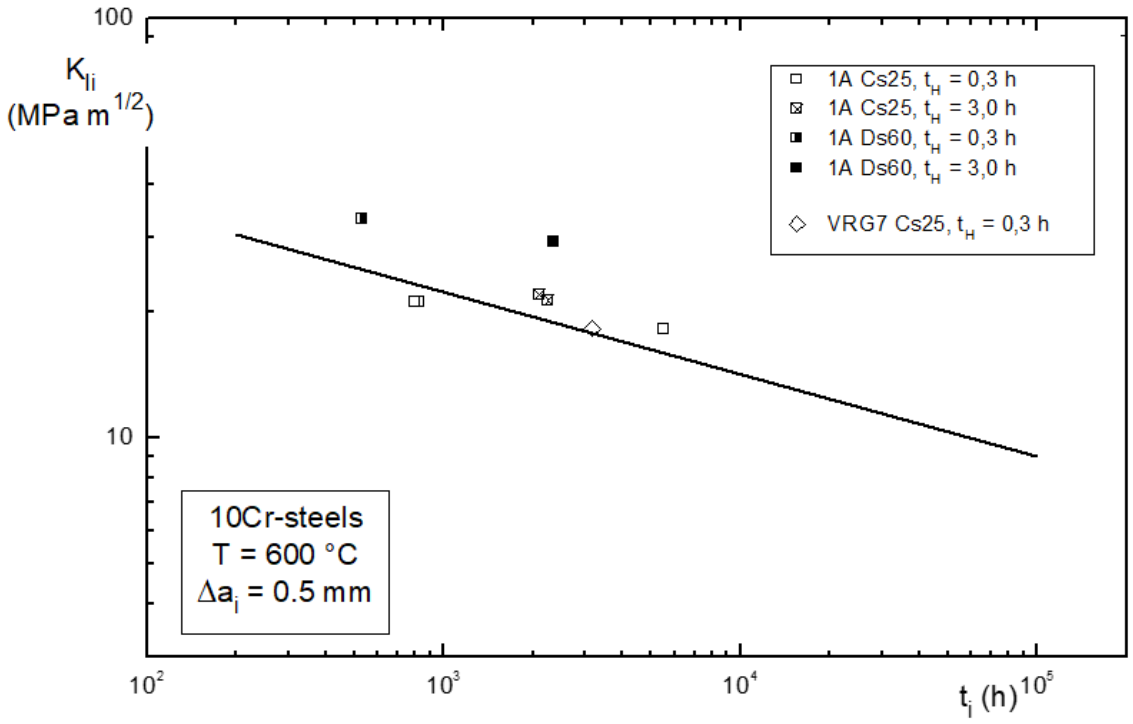

Figure 3.13: Creep crack initiation curve (lower bound) and crack initiation time t_{icf} for hold time tests data points (Δa_i = 0.5 mm) for Cs25- and DENT60-specimens of forged steel 10CrMoWV, T = 600 °C

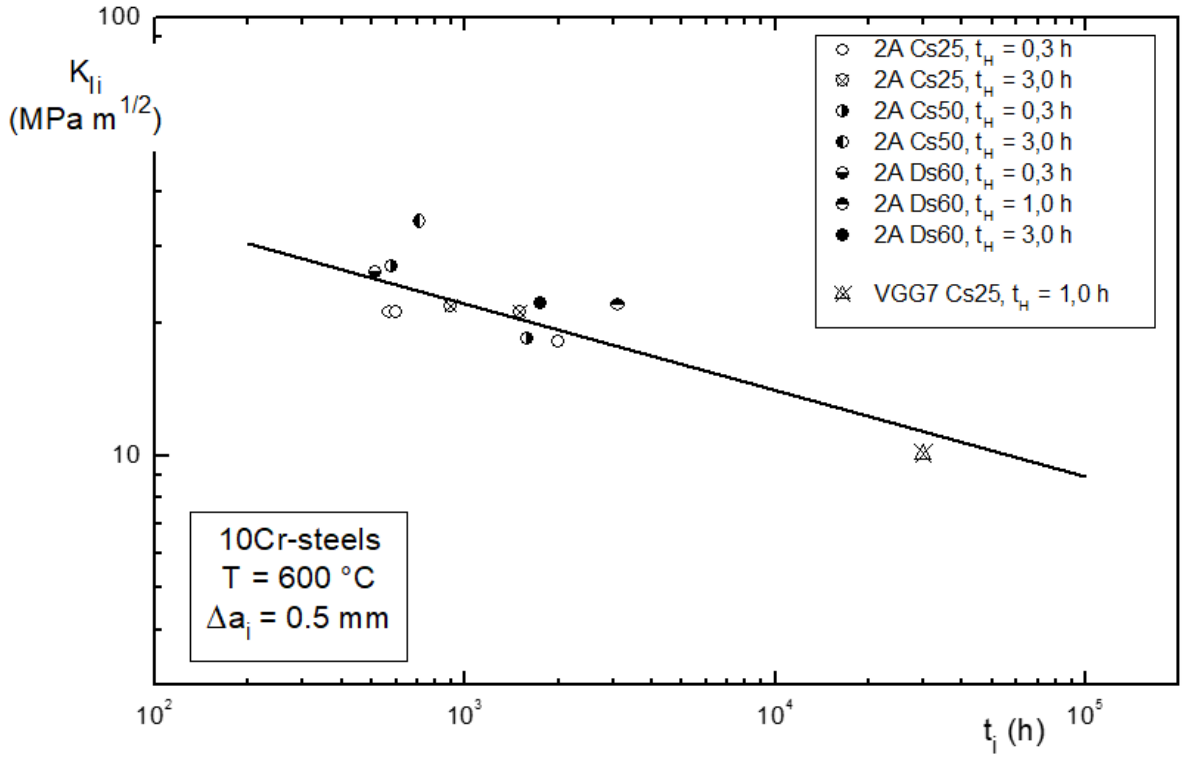

Figure 3.14: Creep crack initiation curve (lower bound) and crack initiation time t_{icf} for hold time tests data points (Δa_i = 0.5 mm) for Cs- and DENT60-specimens of 10%Cr cast steel

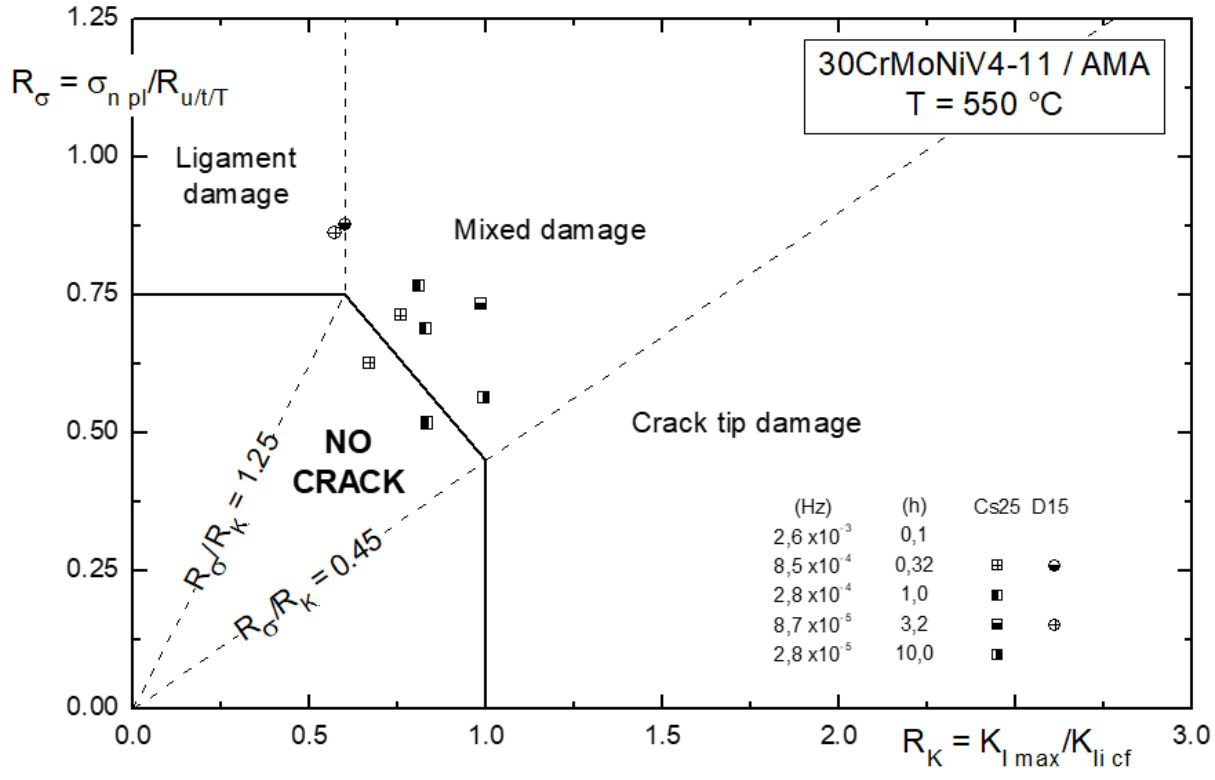

Figure 3.15: Two-Criteria-Diagram for crack initiation under creep fatigue condition, 30CrMoNiV4-11/AMA, 550 °C

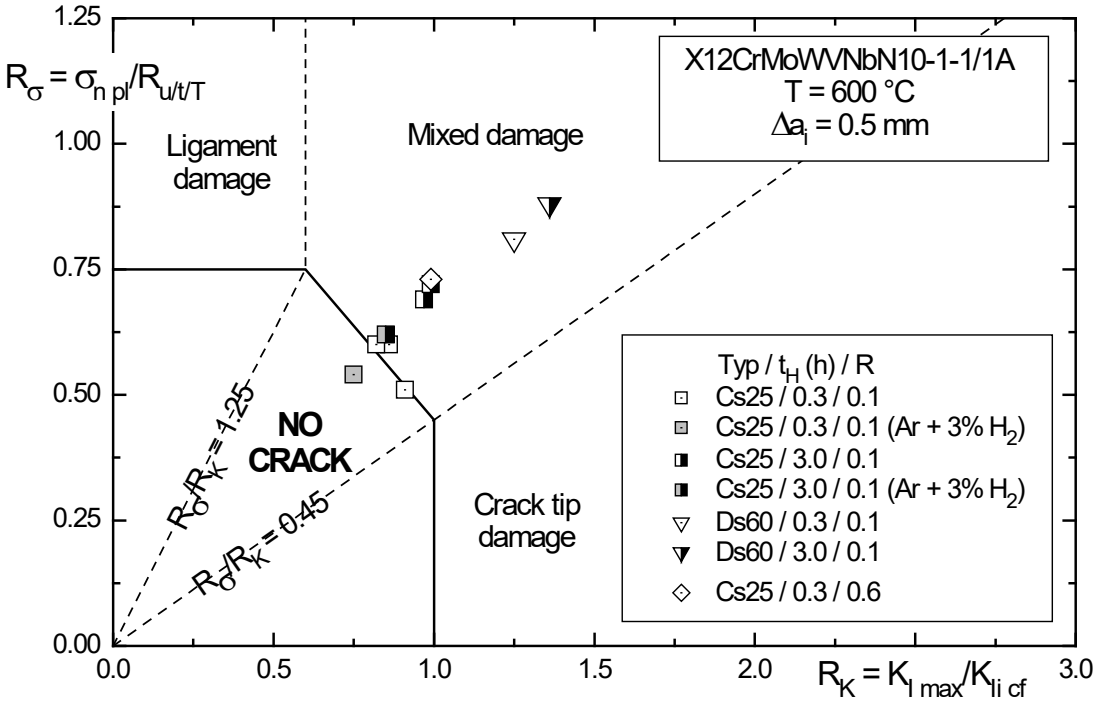

Figure 3.16: Two-Criteria-Diagram for crack initiation under creep fatigue condition, X12CrMoWVNbN10-1-1/1A, 600 °C

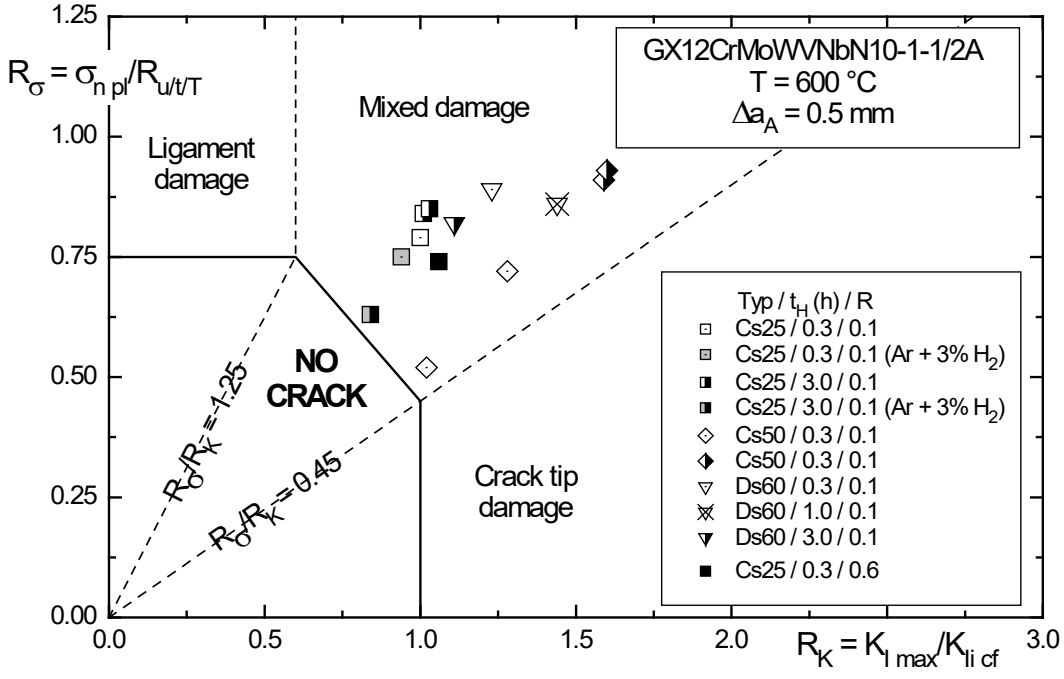

Figure 3.17: Two-Criteria-Diagram for crack initiation under creep fatigue condition, cast steel GX12CrMoWVNbN10-1-1/2A, 600 °C

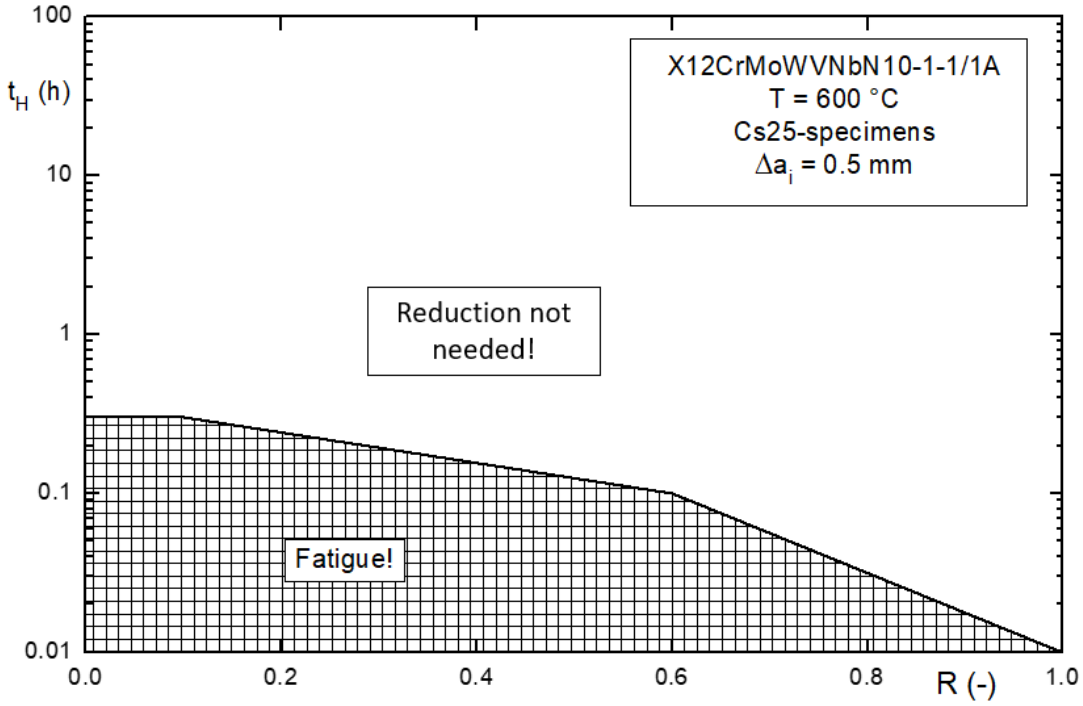

Figure 3.18: Diagram showing the change in hold-time depending on transition from creep fatigue to dominant fatigue load conditions for X12CrMoWVNbN10-1-1/1A, 600 °C

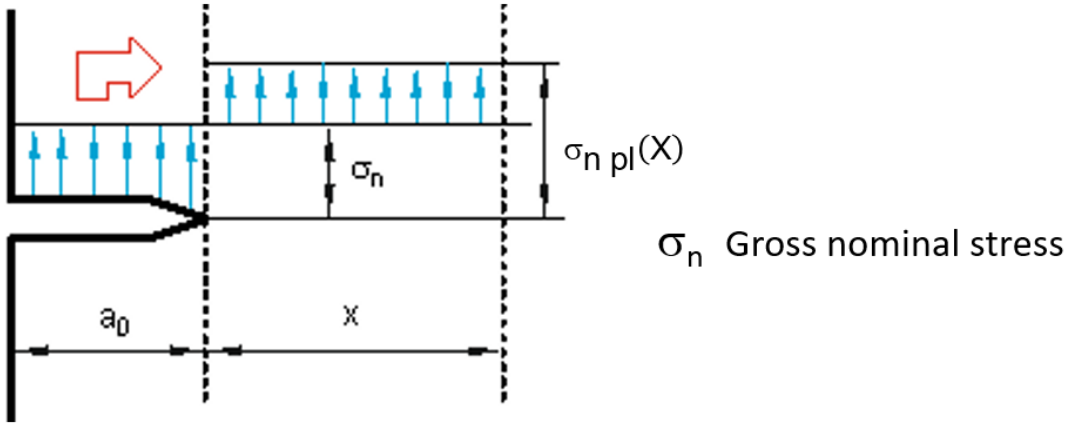

$\sigma_{n\,pl}(X) = (1 + a_o/X)\cdot\sigma_n$, nominal stress within the stress distribution length X

Figure 3.19: Increase of σ_n within the technical stress distribution length X

3.12 Appendix B1 - Calculation of nominal stress

For the calculation of nominal stress σ_n the following comments will be given: For fracture mechanics specimens the stress must be determined for the moment of engineering crack initiation (crack depth a_o). For specimens with additional bending stresses (type SENT or CT) the value will be calculated, in contrast to ASTM E616, as a completely redistributed one, designated as $\sigma_{n\,pl}$ see Figure 3.4.

Thus, it must be kept in mind that all "deep crack specimen" with which the approval of the Two-Criteria-Diagram was done, are assessed with the completely redistributed net section stress within the ligament of the specimens.

Situation with $R_\sigma/R_K \leq 0.45$: For components with deep cracks (low ratio R_σ/R_K, resp. high ratio $K_{I\,id}/\sigma_{n\,pl}$), i.e. load conditions with relatively large net section areas, the problem needs no special consideration, because the prevailing damage mode is crack tip damage ($K_{I\,id}$ is of importance) and in addition the tested DENT and CT specimens had large ligament dimensions. Therefore, the influence of the stress distribution length X was covered by the test itself and is of minor relevance. Thus, for specimen or components with $R_\sigma/R_K \leq 0.45$ it is sufficient to use the redistributed net section stress $\sigma_{n\,pl}$ or the (gross) nominal stress σ_n in a component with a large ligament/ far field-depth.

Situation with $R_\sigma/R_K \geq 1.25$: For components with large ligament dimensions but small cracks ($a \leq 0.5$ - 3 mm), this means ligament damage is dominating, the findings according to Part A show that even the gross nominal stress can be used, because multi-axiality in the crack tip area und the size of the 2CD15 cover the smaller differences between gross and net section stress $\sigma_{n\,pl}$.

Situation with $R_\sigma/R_K = 0.45$ - 1.25: For Components at mixed mode damage with medium crack depths, it must be considered that stress redistribution could only be expected over a technical stress distribution length, X. The value of X depends predominantly on creep ductility of the material (creep rupture elongation A_u). From Part A we know that $X = 0.5 \cdot A_u$.

Situation with $R_\sigma/R_K = 0.70$ - 1.25: In this area with smaller cracks and ratios between $R_\sigma/R_K = 0.70$ - 1.25 it is estimated that it is sufficient to work with the gross nominal stress σ_n or the net section stress $\sigma_{n\,pl}$, if the component width is at least W = 20 mm (small difference gross nominal- and net section-stress).

Situation with $R_\sigma/R_K = 0.45$ - 0.70: In the remaining area of the mixed mode damage area, $R_\sigma/R_K = 0.45$ - 0.70, the technical stress distribution length X must be considered, Figure 3.8 and section 3.6.

Figure 3.19 shows which increase of the gross normal stress σ_n within the technical stress distribution length X should be taken into consideration. The stress within the depth X is increased to the level of $\sigma_n(X)$ (an example for application of the nominal stress $\sigma_n(X)$ is shown in section 3.6)

However, in addition to this, it is important to hold the nominal stress $\sigma_n(X)$ within the depth X below the 1 % creep strength limit, $R_{p1/t/T}$. This means that with ligament damage mode for $R_\sigma = \sigma_{n\,pl}/R_{u/t/T}$ it is precluded that $\sigma_{n\,pl} = \sigma_n(X) \leq R_{p1/t/T}$. Furthermore, the ligament of a component should have a width W-a > X.

In summary the 2CD15 for creep ductile materials ($A_u >\approx 7$ %) works, depending on the crack depth a_o, with 3 different types of nominal stresses:

crack depth a_0	$R_K = K_{Iid} / K_{Ii}$	Incline of ratio line R_σ/R_K	type of nominal stress
small	< 0.6	1.25 (ligament/mixed)	gross nominal-, σ_n
medium	0.6 - 1	1.25 - 0.7	gross or net section-stress
		0.7 – 0.45	Stress redistributed over X, $\sigma_{n(X)}$ (Fig. 3.19)
larger	≥ 1	0.45 (mixed/crack tip)	σ_{npl}, see Fig. 3.4, Part B

3.13 Appendix B2 - Consideration of multi-axial stress states for dominant ligament damage conditions

For ligament damage situations the stress state within the ligament is decisive. A multi-axial state of stress reduces with increasing rigidity

- the creep rate (which depends on the von Mises stress [3.27]) and
- rupture deformation [3.27], [3.28] (in the direction of the primary principal stress)

These influences of the multi-axial stresses are considered for the calculation of the stress-ratio $R_\sigma = \sigma_{n\ pl}/R_{u/t/T}$, in using the nominal stress which is determined as the principal stress perpendicular to the crack plane. The principal stress is always higher than a three-axial tensile von Mises stress which in turn means that with the principal stress the creep rate is higher and reaches the creep-rupture in the ligament earlier than the lower von Mises stress reaches the reduced rupture ductility [3.29].

For crack-tip damage situations the multi-axial stress state in the crack tip area is decisive (i.e. $K_{I\ id}$ is decisive). This means that a multi-axial stress state in the ligament is less important.

Also for mixed-mode situations with higher influence of the ligament-stress-state the use of the principal stress compensates the reduction in the rupture deformation capacity.

3.14 Appendix B3 - Determination of R_K-value of point B in 2CD

According to the definition, R_K is equal to

$$R_K = \frac{K_{Iid}}{K_{Ii}} \tag{3.6}$$

With

$$K_{Iid} = \sigma \cdot \sqrt{\pi \cdot a_{th}} \cdot Y = R_{p1/t/T} \cdot \sqrt{\pi \cdot a_{th}} \cdot Y = R_{p1/t/T} \cdot \sqrt{\pi \cdot 0.1 \cdot A_u} \cdot Y \tag{3.7}$$

($a_{th} = 0.1 \cdot A_u$, see eq. 5, Part A)

and

$$K_{Ii} = R_{u/t/T} \cdot \sqrt{0.163 \cdot \pi \cdot A_u} \tag{3.8}$$

(see Appendix C, Part C)

Therefore,

$$R_K = \frac{R_{p1/t/T}}{R_{u/t/T}} \cdot \frac{\sqrt{\pi \cdot 0.1 \cdot A_u}}{\sqrt{0.163 \cdot \pi \cdot A_u}} \cdot Y \cong 0.75 \cdot \frac{\sqrt{0.1}}{\sqrt{0.163}} \cdot 1.1 \cong 0.65 \tag{3.9}$$

This result of the numerical calculation conforms with the outcome from Table 3, Part B. The point B abscissa coordinate was conservatively pint to $R_K = 0.6$.

4 Part C - Consideration of the influence of the creep deformation capability on the shape of the Two-Criteria-Diagram, 2CD15

4.1 Influence of the creep (rupture) elongation on the shape of the Two-Criteria-Diagram

The Two-Criteria-Diagram (2CD), Figure 4.1, [4.1] (older version) is only valid for steels which are not subjected to the notch weakening effect. In notched specimen according to DIN EN ISO 204 ($K_t \approx 4.5$) for 1%CrMoV-steels notch weakening can be avoided if the creep rupture elongation A_u is higher than ≈ 7 %. In case of lower creep rupture elongation values, the shape of the 2CD must be changed. An example of the possible shape of a 2CD for creep brittle materials is shown in Figure 4.2 [4.2], whereas Figure 4.3 show the 2CD with data points of a creep ductile material, for which the borderlines of the crack initiation seems to be in a rather conservative position. In the following, it is suggested to modify the 2CD depending on the creep ductility level, A_u [4.5]. For every heat or specified steel grades the lowest A_u-value must be taken.

The 2CD has been adapted to varying A_u-values of steels by changing the corner-points A, B, C, and the inclination of the ratio-lines R_σ/R_K, which surround the areas of the ligament damage and the crack tip damage mode, respectively, see Figure 4.4.

4.2 Changes in the shape of the 2CD

Figure 4.4 shows the changes of the diagram subjected to changes in creep ductility. The improvements related to the ligament and mixed mode area (point B) are already explained in Part B. For the crack tip area, which relates to deeper cracks, the situation is as follows:

- The position of point B changes to $R_K = 0.6$. The slope of the ratio-line $R_\sigma/R_{K\ Ligament}$ consequently moves to $R_\sigma/R_K = 1.25$ (Figure 3.5, Part B).
- Point C remains per definition at $R_K = 1.0$ for all ductility levels, but the values of K_{Ii} for creep brittle materials are lower (see Appendix C). The decline of the ratio-line $R_\sigma/R_{K\ crack\ tip}$ (0-C) is influenced by rupture ductility of the steel.

The respective changes of the ratio-lines depend on the extent of stress redistribution (depth of the plastic zone) due to the level of creep ductility. The plastic zone depth d_{pl} can be estimated by a modified Dugdale formula [4.3], (proposed in 1984 [4.4]) for the determination of the plastic zone, d_{pl}, in CT1-specimen, see Figure 4.6.

For an applicability in creep the following adjustments are introduced in the Dugdale formula [4.4], [4.5]:

- K_I is substituted by $K_{Ii}(t_i)$ (which is the fictitious elastic stress intensity of the CT1-specimen for creep crack initiation at time t_i)
- Yield strength, $R_{p0.2}$, is substituted by $R_{u/t/T}$ (R_{mt}) for the corresponding initiation time t_i
- $R_{u/t/T}$ stands for the time dependent (true) creep stress in the stress redistribution zone d_{pl},

$$d_{pl} = \frac{1}{\pi} \cdot \left(\frac{K_{Ii}}{R_{u/t/T}} \right)^2 \qquad (4.1)$$

which is now time dependent.

In Figure 2.13, Part A, it was shown that L_{pl} (resp. d_{pl} for CT-specimen) which is proportional to $(K_{Ii}/R_{u/t/T})^2$ is influenced by the creep ductility. Therefore, an evaluation was performed to show the dependence of d_{pl} according to formula (4.1) on creep rupture elongation, A_u, for available CCI-test data of CT1-specimen.

The result is a Master curve $d_{pl} = f(A_u)$, shown in Figure 4.7. There is a linear dependence of d_{pl} on A_u up to ≈ 25 % creep rupture elongation. For higher value of creep rupture elongations, where local reduction of area dominates, no further increase in K_{Ii} can be expected, except when $R_{u/t/T}$ increases (see also Figure 2.4, Part A).

The following relationship is proposed between creep rupture elongation A_u and the inclination of the ratio-line for crack tip damage, which crosses point C (Figure 4.4). From the Master curve in Figure 4.7 we obtain:

$$A_u \sim d_{pl} \sim \left(\frac{K_I}{R_{u/t/T}}\right)^2 \tag{4.2}$$

and with

$$\frac{R_\sigma}{R_K} = \left(\frac{\sigma_{n\,pl}}{R_{u/t/T}}\right) \cdot \left(\frac{K_{Ii}}{K_{Iid}}\right) = \left(\frac{\sigma_{n\,pl}}{K_{Iid}}\right) \cdot \left(\frac{K_{Ii}}{R_{u/t/T}}\right) \tag{4.3}$$

and (4.1)

$$\left(\frac{K_{Ii}}{R_{u/t/T}}\right)^2 = d_{pl} \cdot \pi$$

it results

$$\frac{R_\sigma}{R_K} = \frac{\sigma_{n\,pl}}{K_{Iid}} \cdot \sqrt{d_{pl} \cdot \pi}\,. \tag{4.4}$$

The 2CD and the Master curve $d_{pl} = f(A_u)$ are both based on data of CT1-specimen, which have for an a/W-ratio of about 0.55 a fix, only geometry dependent ratio of $K_{I\,id}/\sigma_{n\,pl} = 4.5\ \sqrt{mm}$. With this fix ratio-value (4.4) gives:

$$\frac{R_\sigma}{R_K} = \frac{1}{4.5} \cdot \sqrt{d_{pl} \cdot \pi} \sim A_u \tag{4.5}$$

and with

$$d_{pl} = 0.163 \cdot A_u \tag{4.6}$$

(from Master curve - solid line, Figure 4.7), it results in the relationship

$$\frac{R_\sigma}{R_K} = 0.16 \cdot \sqrt{A_u}\,. \tag{4.7}$$

This is now the creep ductility dependent slope of the ratio-line $R_\sigma/R_{K\,crack\,tip}$ through point C in Figure 4.4 (Results are given in Table 4.1). Taking into account steps given above, the shape of the 2CD in dependence of the creep ductility can be changed.

For materials with low creep ductility, $A_u <\approx 7$ %, formula (4.7) can also be applied see Figure 4.4 and Table 4.1. But only few results from creep brittle material are available. As soon as a crack initiates in a component body of low creep ductility (A_u = 2 % - 5 %) the nominal stress in the ligament must be lower than $R_{p1/t/T}$.

Figure 4.9 shows a numerical result for a more creep brittle 1%CrMoV-steel with $A_u \approx 5$ %, (Table 2.1, Part A, heat AGB). The calculation revealed that only with 0.8 % creep strain [$R_\sigma = R_{p0.8/t/T}/R_{u/t/T} \approx 0.6$] in the far field a measurable small $a_{th} \approx 0.3$ mm can be tolerated. For lower A_u-values the tolerable R_σ-ratios for a small crack will be still lower. Hence, the sustainable nominal stress, (1st principal stress) for every small crack or notch decreases with creep ductility.

Thus, the main alterations of the 2CD shape result from changes in point B and C, resp. the inclination of the ratio-line through point C.

4.3 Shape of the 2CD15 for different creep rupture ductility

Table 4.1 shows the inclination of the ratio-line $R_\sigma/R_{K\,crack\,tip}$ in dependence of the creep rupture ductility. In Figure 4.4 and Figure 4.8, the different ductility dependent slopes of the crack tip

ratio-lines are drawn into the revised 2CD15. For a creep rupture ductility of A_u = 8 % the crack tip ratio-line has an inclination of $R_\sigma = 0.45 \cdot R_K$, which is near to the earlier 2CD, which had $R_\sigma = 0.5 \cdot R_K$.

For high creep rupture ductility (for example A_u = 20 %) the slope of the crack tip ratio line could be steeply rising and the mixed-mode area becomes smaller. This is in accordance with experimental findings, see Figure 4.3. But it is recommended to use the change of the 2CD15 for more ductile materials with care, because high creep ductility is often temporary. The increased ductility provides a higher conservatism.

For lower creep rupture ductility (below 8%) the requested flatter slopes are shown in Figure 4.9. But the reader should remember that not only the inclination of the ratio-lines flattens, but the K_{Ii}-values are also lower than for creep ductile materials (an idea of how much the values may be reduced can be obtained from formula (4.2) and the Master-curve in Figure 4.7, see Appendix C).

As mentioned before, the shape of the ligament damage area and of the crack-tip damage area must be changed as well. In the ligament damage area, the horizontal upper borderline to the no crack situation line, between point A and B, decreases with diminishing creep rupture elongation A_u, Figure 4.9.

Below A_u = 5 % the height of the lines is not yet clear. Because there are no numerical evaluations and the number of experimental data points for creep brittle materials is limited or less. The available data are shown in Figure 4.9. They are provided by [4.6] and [4.7] for creep rupture elongations between 2 and 5 % for deeply cracked specimens. All data points with Δa_i = 0.2 mm crack initiation criteria support basically the new shape of the diagram. Only the data points from [4.7] which have Δa_i = 0.1 mm as crack initiation criteria are partly positioned inside the no crack area. Generally, the data base is scarce and needs wide extrapolations.

4.4 Conclusions - Part C

Materials with high creep rupture ductility: These are materials with A_u >≈ 7 %, which do not tend to notch weakening. For such materials the position of point B was changed. This means the ligament damage area was enlarged to $R_K = K_{I\,id}/K_{Ii} = 0.6$, but it should have kept in mind that K_{Ii} diminishes with less rupture ductility, what in turn gives lower tolerable $K_{I\,id}$ resp. a_{th} values.

It was explained which influence higher A_u-values have on the position of point C. This influence is now understood, but implies no general need to change the 2CD15. Even in case of rather high creep rupture ductility and the need to exploit this, it should be done with care, because:

- the exact amount of rupture elongation for each specific melt is not known,
- creep rupture elongation changes with time.

Hence, an exploitation of the potential of higher creep rupture ductility with respect to crack initiation needs a good data base and an engineering judgement.

Materials with low creep rupture ductility: The shape of the present 2CD15 changes significantly. In the ligament-damage area the defect tolerance (a_{th}) is strongly reduced because the sustainable gross nominal stress in a component body - with even a small crack - is significantly reduced. The situation in the mixed-mode damage area is unclear and cannot be rated, due to lack of data.

The draft of the "brittle" 2CD enlightens the influence of creep rupture ductility on crack initiation behaviour. Materials with low creep rupture ductility have generally low crack tolerance and technical application should be considered with great care; the better way is to avoid the use of such materials.

4.5 References - Part C

[4.1] Ewald, J.; S. Sheng, A. Klenk, G. Schellenberg: Engineering Guide to Assessment of Creep Crack Initiation on Components by Two Criteria Diagram, 2. HIDA Conference, Stuttgart, 4.-6.10.2000, Tagungsband MPA-Stuttgart, Beitrag p.5-2. resp.: Int. Journal of Press. Vessel + Piping 78 (2001), 937-949.

[4.2] Ewald, J.: Beurteilung von Risseinleitung und Risswachstum im Kriechbereich mit Hilfe eines Rissspitzen-Fernfeld-Konzeptes, Mat.-Wiss u. Werkstofftechn. 20 (1989) S.195 - 206.

[4.3] Knott, J.F.: Fundamentals of Fracture Mechanics, Butherworths, London, 1973, p66.

[4.4] Ewald, J.; K.-H. Keienburg, G. Röttger: Beitrag zur Abschätzung der Kriechrisseinleitung in fehlerhaften Bauteilen, Archiv f. d. Eisenhüttenwesen, 55 (1984), Vol. 11, S. 549 – 554.

[4.5] Ewald, J.: Zwei-Kriterien-Diagramm für Kriechrisseinleitung – Berücksichtigung des Kriechverformungsvermögens für ferritische Werkstoffe, 26. Vortragsveranstaltung, Arbeitsgemeinschaft für warmfeste Stähle (AGW), 28.11.2003, 87 - 97.

[4.6] Tscheuschner, R.: Anriss- und Rissfortschrittsverhalten zeitstandbeanspruchter warmfester Schmiedewerkstoffe, Dr.-Ing. Dissertation 1988 (D17), TU Darmstadt.

[4.7] Holdsworth, S.R.: Initiation and early growth of creep cracks from pre-existing defects, Mat. at High.Temp., Vol.10, No. 2, May 1992, 127 - 137.

4.6 Tables and figures - Part C

Table 4.1: Ratio-line R_σ/R_K in dependence of the creep rupture ductility A_u for steels from formula 4.8

A_u [%]	R_σ / R_K
< 30	0,71
20	0,71
10	0,51
8	0,45
5	0,36
2,5	0,25
1,5	0,2

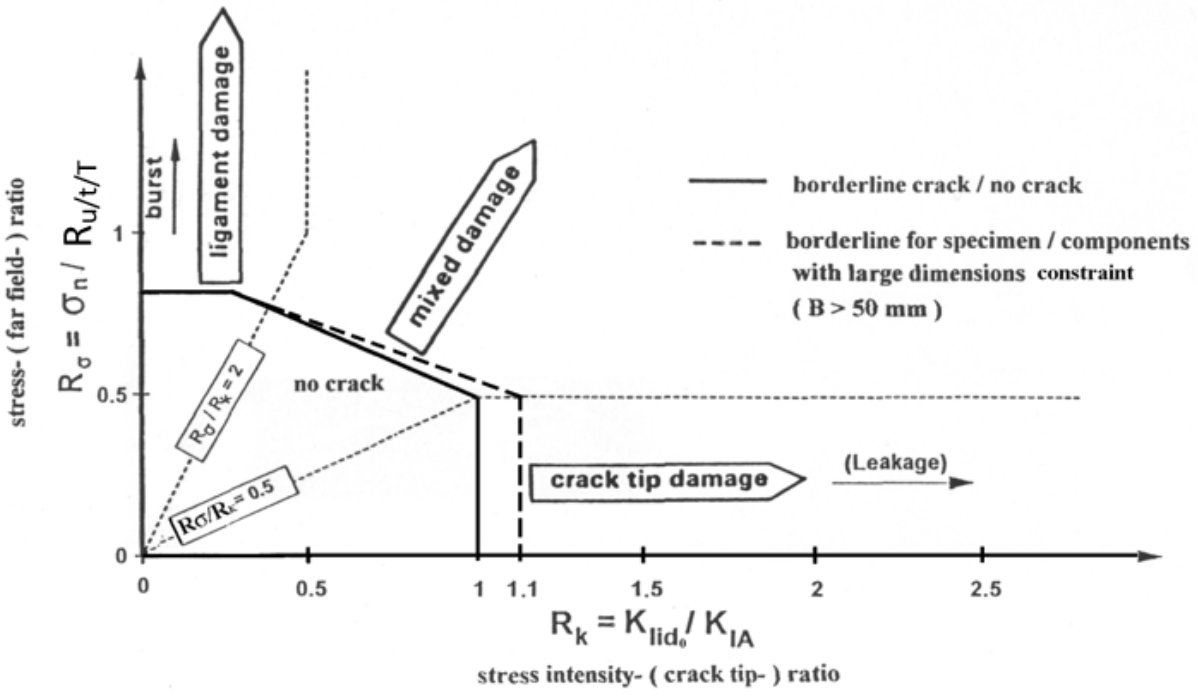

Figure 4.1: Two-Criteria-Diagram for creep ductile steels, status 1998

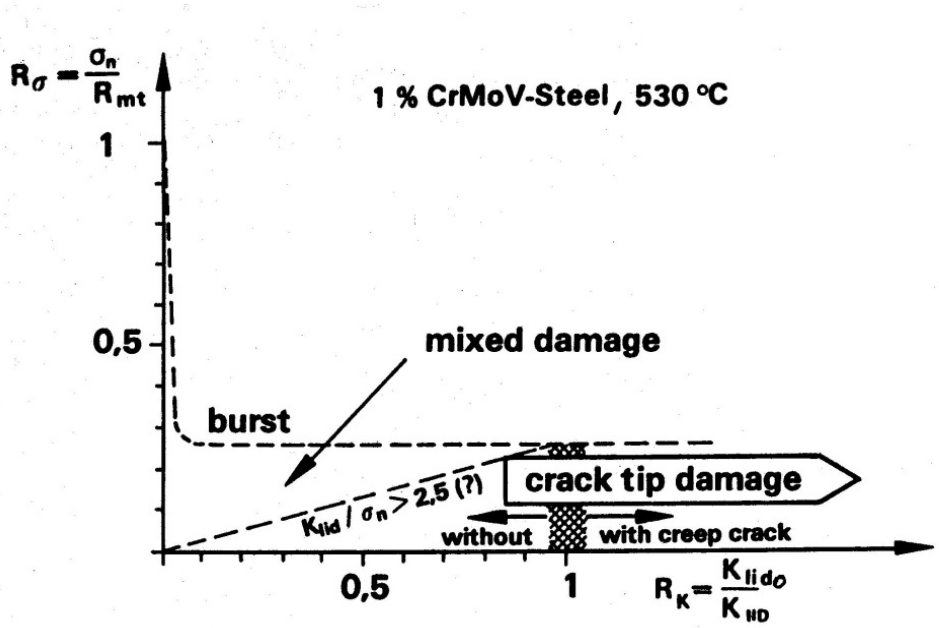

Figure 4.2: Former draft for a Two-Criteria-Diagram for creep crack initiation for creep-brittle (notch weakening) steels [4.2]

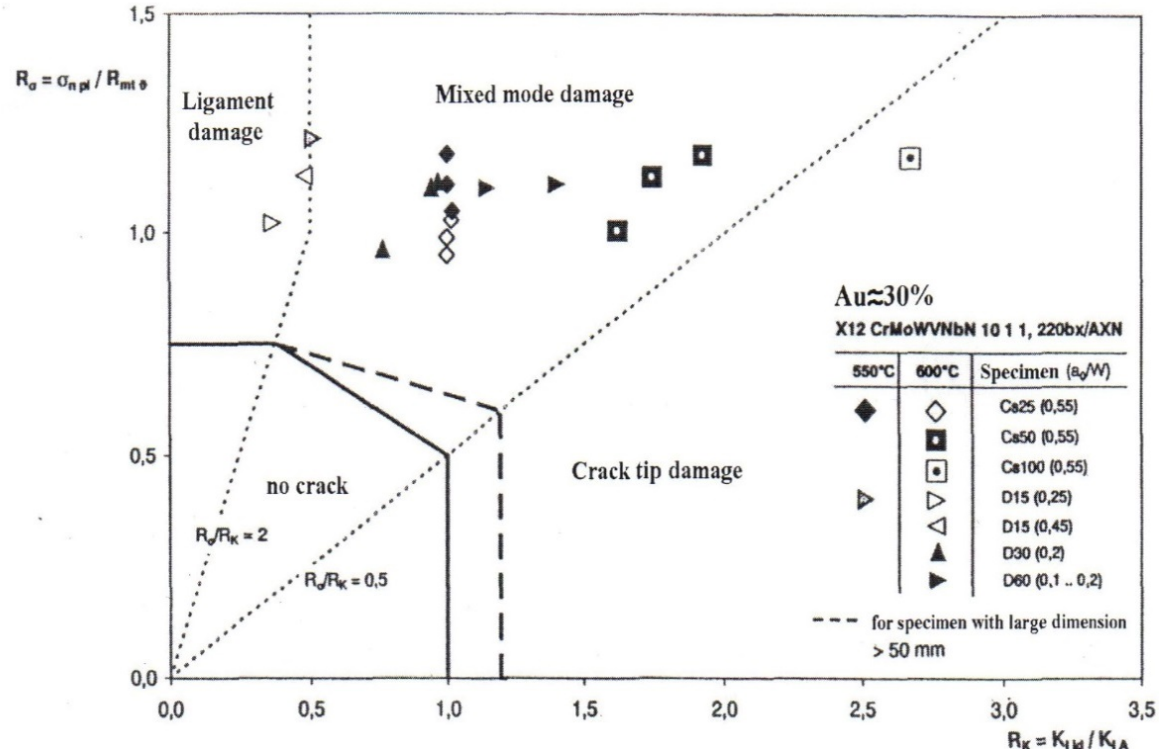

Figure 4.3: Former Two-Criteria-Diagram wit data points of a forged steel with high creep rupture ductility

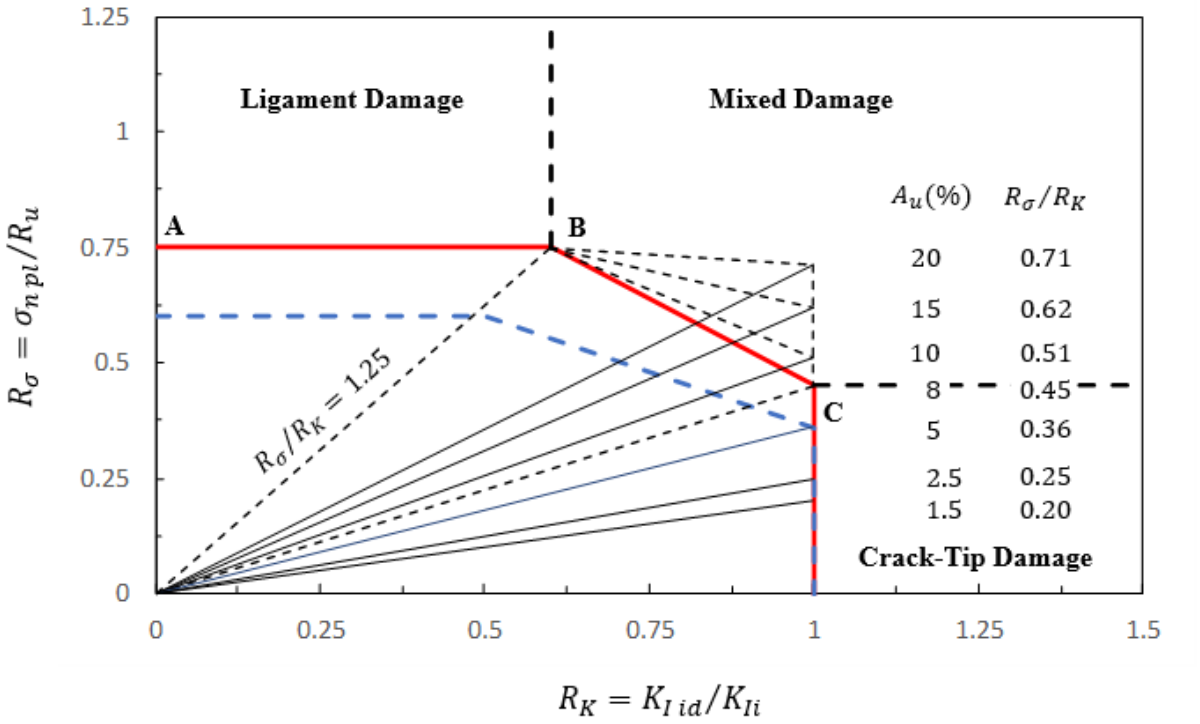

Figure 4.4: Two-Criteria-Diagram, influence of creep rupture ductility on specimen with predominant crack tip damage for steels

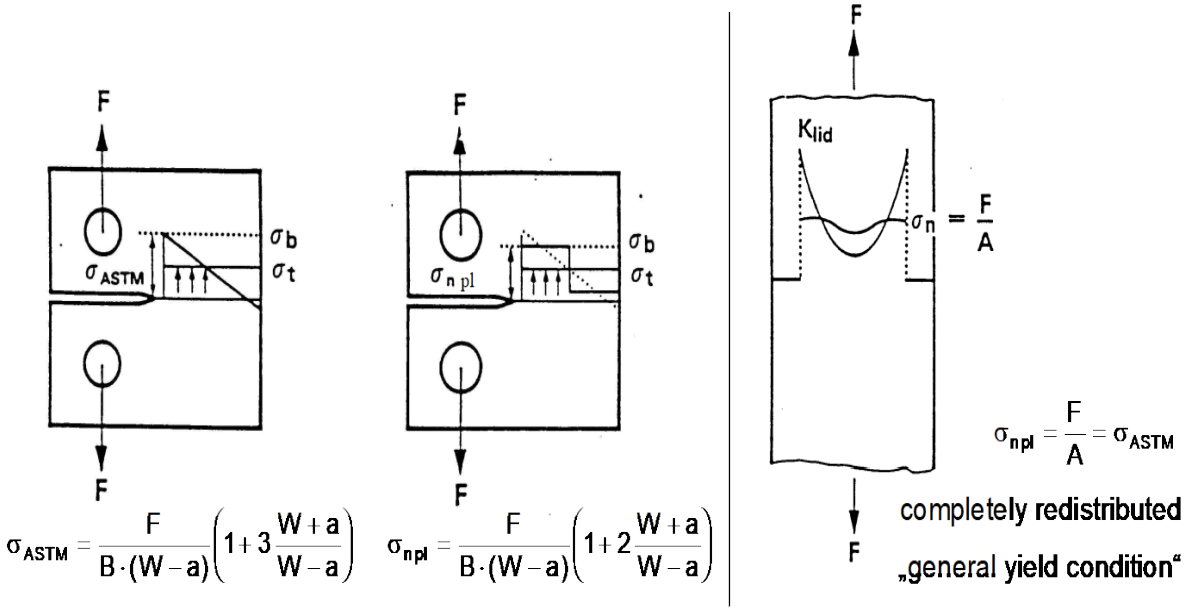

Figure 4.5: Determination of the nominal stress, $\sigma_{n\,pl}$, in creep loaded fracture mechanic specimen

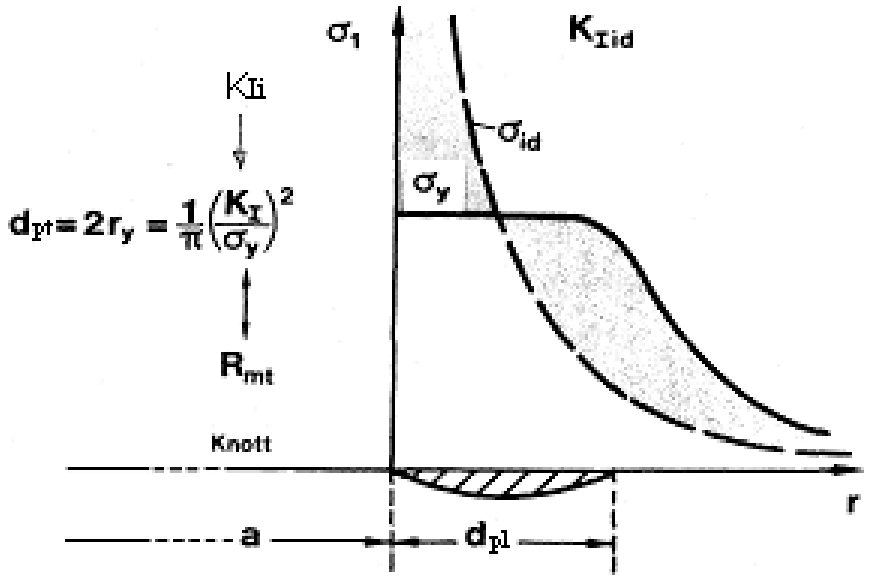

Figure 4.6: Adjustment of the Dugdale formula to time-dependent creep crack initiation

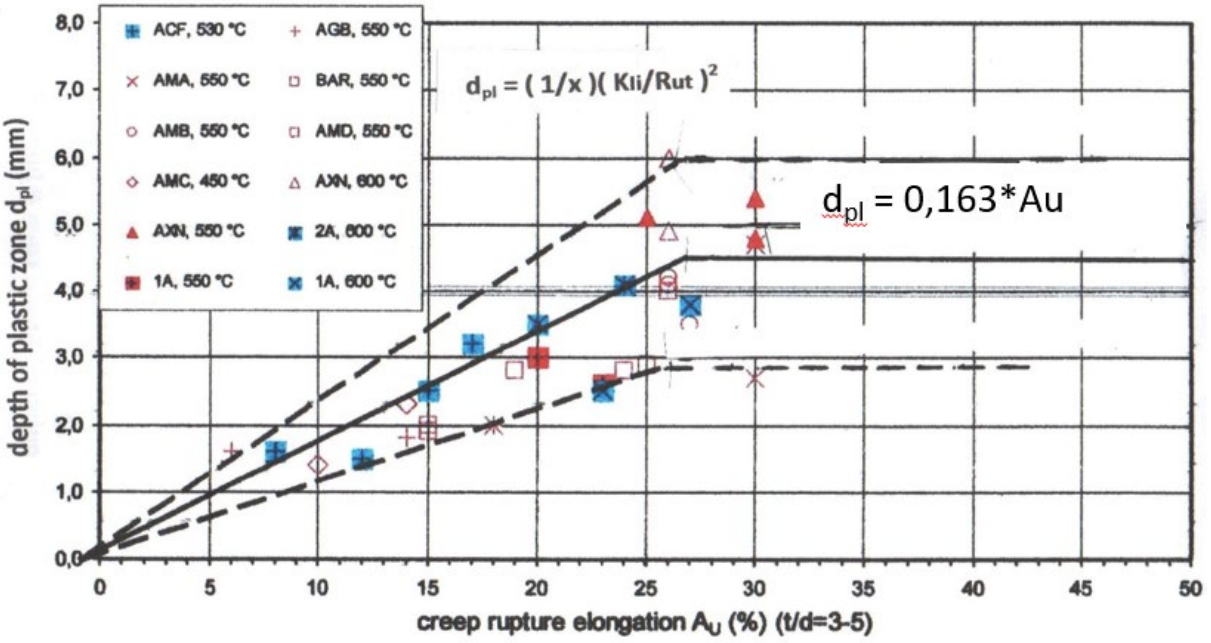

Figure 4.7: Depth of plastic zone in CT1-specimens as function of creep rupture elongation in smooth tensile specimens for different types of steels

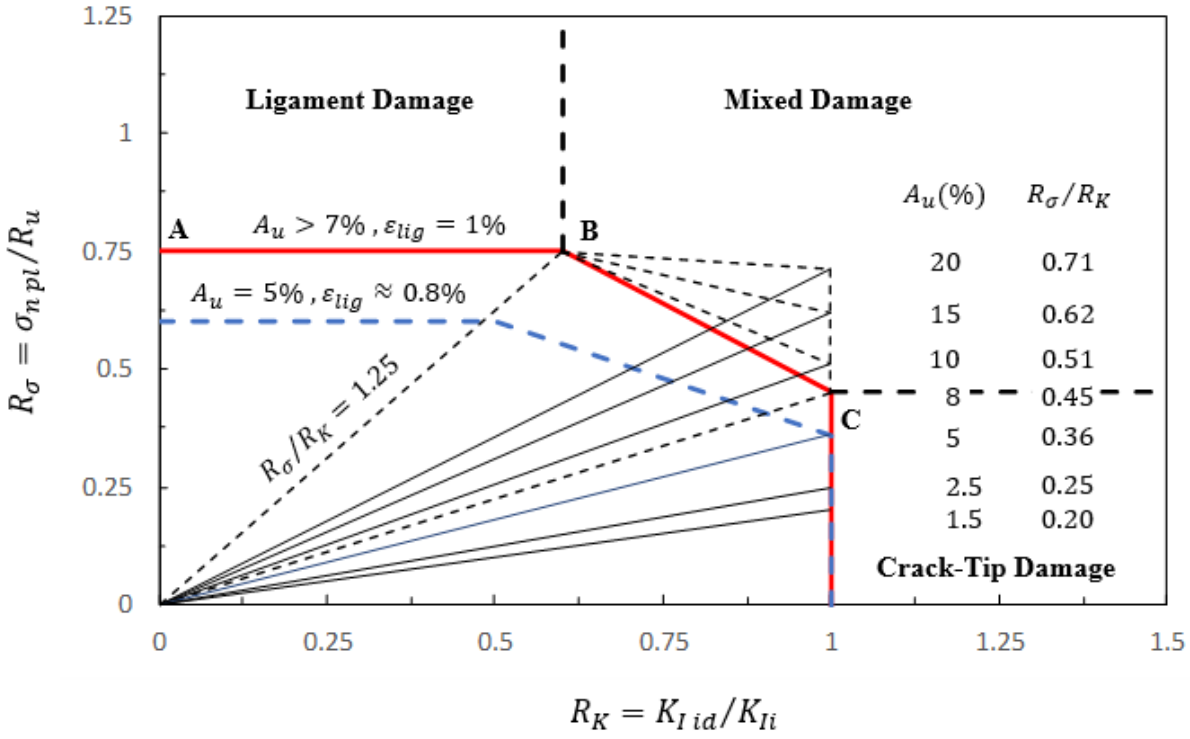

Figure 4.8: Two-Criteria-Diagram 2015 (2CD15) for steels A_u > 5 %

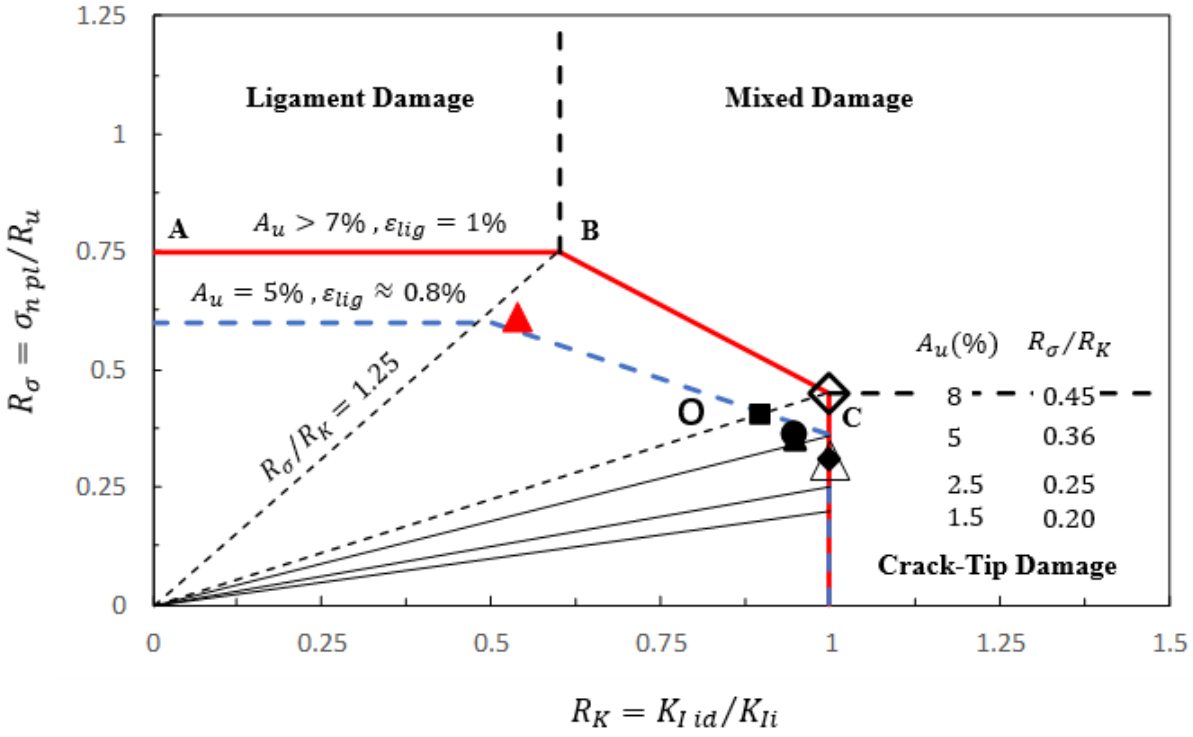

		R_k	R_σ
	Holdsworth [6] Steel, $A_u \approx 5\%, 550°C$		
◆	CT25	1	0.31
▲	CNT25	0.95	0.35
■	SENT25	0.9	0.4
	$\Delta a_i \approx 0.1mm, t_i \approx 10^4h$		
	Tscheuschner [7]		
◇	CS25, $\Delta a_i \approx 0.2mm$	1	0.45
○	CS12, $\Delta a_i \approx 0.2mm$	0.8	0.42
	AGA, $A_u \leq 5\%, 550°C, > 3000h$		
●	CS12, $\Delta a_i \approx 0.1mm$	0.95	0.36
△	CS25, $\Delta a_i \approx 0.2mm$	1	0.31
	AGC, $A_u \approx 2-3\%, 550°C, 1-10^4h$		
▲	DENT, $\Delta a_i \approx 0.1mm$	0.54	0.61
	Analytical, $A_u = 5\%, \varepsilon_{lig} = 0.8\%$		
	numerical calculations [1] Part A		

Figure 4.9: Two-Criteria-Diagram for 1%CrMoV steels with low creep rupture ductility A_u < 5 %

4.7 Appendix C - Method to estimate the decline of K_{Ii} values with decrease of creep rupture elongation A_u

According to formula (4.1) the plastic zone is written as follows:

$$d_{pl} = \frac{1}{\pi} \cdot \left(\frac{K_{Ii}}{R_{u/t/T}} \right)^2 \tag{4.8}$$

and from Figure 4.7 results in:

$$d_{pl} = m \cdot A_u \tag{4.9}$$

with m as value of the slope.

This means

$$m \cdot A_u \sim \left(\frac{K_{Ii}}{R_{u/t/T}} \right)^2 \tag{4.10}$$

and

$$\sqrt{m} \sim \frac{1}{\sqrt{A_{u1}}} \cdot \left(\frac{K_{Ii1}}{R_{u/t/T1}} \right) \sim \frac{1}{\sqrt{A_{u2}}} \cdot \left(\frac{K_{Ii2}}{R_{u/t/T2}} \right) \tag{4.11}$$

if $R_{u/t/T1} = R_{u/t/T2}$

$$\frac{A_{u2}}{A_{u1}} = \left(\frac{K_{Ii2}}{K_{Ii1}} \right)^2 . \tag{4.12}$$

With this parabolic proportionality it is possible to estimate the decline of K_{Ii} if the creep ductility is reduced. But values A_u > 20 % should not be applied, because for such high rupture elongations no benefit in terms of uniform strain, which is the decisive value for the deformation capability, Figure 2.4, Part A, can be expected. In case that the rupture strength of the two materials is not equal, then the following relationship can be postulated:

$$\frac{K_{Ii2}}{R_{u/t/T2}} = \frac{K_{Ii1}}{R_{u/t/T1}} \cdot \sqrt{\frac{A_{u2}}{A_{u1}}} \tag{4.13}$$

The K_{Ii}-values for the materials in Table 2.13 of Part B were estimated with formula (4.14). In addition, it is possible with formula (4.1) together with Figure 4.7 to estimate K_{Ii}-values of CT1-specimen, when $R_{u/t/T}$- and A_u-values are available. With (4.1):

$$K_{Ii} = R_{u/t/T} \cdot \sqrt{m \cdot \pi \cdot A_u} \qquad m = 0.163, \text{ see Figure 4.7} \tag{4.14}$$

The K_{Ii}-values estimated in this way are here called "Dugdale"-values.

5 Nomenclature

Name	UNIT(S)	SYMBOL
Stress exponent in Norton or Norton-Bailey creep equations	-	n
Time exponent in Norton-Bailey creep equation	-	p
Yield strength	MPa	$R_{p0.2}$
0.2 % creep (plastic strain) strength at time, t, and temperature, T	MPa	$R_{p0.2/t/T}$
1 % creep (plastic strain) strength at time, t, and temperature, T	MPa	$R_{p1/t/T}$
Rupture strength for time, t, and temperature, T	MPa	$R_{u/t/T}$
Elastic strain	%	ε_e
Creep strain	%	ε_c
Initial plastic strain	%	ε_i
Plastic strain	%	ε_p
Creep strain in the ligament far field	%	ε_{lig}
Creep strain at point q_{min}, strain transformed to a primary strain by Cooks & Ashby factor (q_{min} -> q at point of highest multi-axiality)	%	$\varepsilon_{c\ qmin}/\varepsilon^*_{ref}$
Quotient of multi-axiality by Clausmeyer, $q = \sigma_{vM}/(\sqrt{3}\cdot\sigma_h)$	-	q
Uniform (rupture) elongation	%	ε_{gl}
Creep rupture elongation for time, t, and temperature, T Creep rupture ductility	%	A_u ($A_{u/t/T}$)
Creep rupture reduction of area for time, t, and temperature, T	%	Z_u ($Z_{u/t/T}$)
Creep Crack Initiation	-	CCI
Creep Crack Opening displacement	-	CTOD

Test results, Name	UNIT(S)	SYMBOL
Crack size threshold to avoid CCI	mm	a_{th}
Initial crack depth	mm	a_o
Final crack length	mm	a_f
Crack extension	mm	Δa
Crack initiation criterion (e.g. Δa_i = 0.5 mm)	mm	Δa_i
Crack growth rate (per unit time)	mm/h	da/dt $\dot{a}$
Time to rupture	h	t_u
Time to creep crack initiation for crack extension Δa_i = 0.5 mm	h	t_i

Parameters, Name	UNIT(S)	SYMBOL
A line or surface integral based parameter used to characterize the local stress-strain rate fields at any instant around the crack front in a body deforming due to creep. The parameter characterizes crack-tip stress-strain rate fields under conditions of steady-state large-scale creep.	MPa·m/h	C*
Crack tip opening displacement	μm	CTOD, δ
diameter of the cross-section of the parallel length of a cylindrical specimen	mm	d_o
diameter of cross-section of a cylindrical specimen after creep fracture	mm	d_u
diameter of cylindrical specimen close to threaded end after fracture	mm	d_{u1}
diameter of cylindrical specimen close to necking after fracture	mm	d_{u2}
Plastic zone, stress redistribution zone in CT1-specimen (Dugdale method, see Figure 4.6, Part C)	mm	d_{pl}
Elastic-plastic crack tip characterizing parameter	N/mm	J
Stress intensity factor	$MPa \cdot m^{1/2}$	K_I
Time dependent stress intensity factor for crack initiation at initial crack length (experimental with CT1-specimen)	$MPa \cdot m^{1/2}$	K_{Ii}
Fictitious ideal elastic, instantaneous stress intensity factor in a component/specimen	$MPa \cdot m^{1/2}$	$K_{I\,id}$
Limit length in specimen with dominant ligament damage, ductility dependent depth of stress redistribution zone behind crack tip $L_{pl} = 2(r_{pl} - r_{plo})$	mm	L_{pl}
Stress intensity ratio in Two-Criteria-Diagram	-	R_K
Stress ratio in Two-Criteria-Diagram	-	R_σ
Two-Criteria-Diagram	-	2CD
Technical stress redistribution length	mm	X
Specimen width resp. component thickness, wall thickness	mm	W
CTOD at creep crack initiation	μm	δ_i
Gross nominal stress	MPa	σ_n
Net section stress	MPa	σ_{net}, σ_{lig}
Nominal stress according to Siebel (see Figure 3.4, Part B)	MPa	$\sigma_{n\,pl}$
Nominal stress within stress redistribution length X (see Figure 2.14, Part A)	MPa	$\sigma_{n\,pl}(X)$
Reference stress	MPa	σ_{ref}
von Mises stress	MPa	σ_{vM}
Hydrostatic stress	MPa	σ_h
0.2 % proof strength (at temperature T)	MPa	$R_{p0.2}$

Parameters, Name	UNIT(S)	SYMBOL
Tensile strength	MPa	R_m
Tensile fracture reduction of area	%	Z

Specimens, Name	UNIT(S)	SYMBOL
Centre Cracked Tension	-	CCT
C-Ring	-	CS(T)
Compact Tension (with side grooves)	-	CT (Cs)
Double Edge Notched Tension, (with side grooves)	-	DENT (Ds)
Round Notched Bar	-	RNB(T)
Single Edge Notched Bend	-	SENB
Single Edge Notched Tensile	-	SENT

FVV

Bundesministerium für Wirtschaft und Energie

Forschungsnetzwerk Mittelstand

FÖRDERGEBER
FUNDING ORGANISATIONS

Bundesministerium für Wirtschaft und Energie
Federal Ministry for Economic Affairs and Energy

Arbeitsgemeinschaft industrieller Forschungsvereinigungen
Federation of Industrial Research Associations

FKM Forschung im VDMA

VDMA

KOOPERATIONEN
PARTNER ASSOCIATIONS

Forschungskuratorium Maschinenbau
Mechanical Engineering Research Federation

Verband Deutscher Maschinen- und Anlagenbau
Mechanical Engineering Industry Association

Forschungsvereinigung
Verbrennungskraftmaschinen e.V.
Research Association
for Combustion Engines

Lyoner Strasse 18
60528 Frankfurt am Main, Germany

T +49 69 6603 1345
F +49 69 6603 2345
info@fvv-net.de

www.fvv-net.de